Chapter I.

General Introduction

I-1. *Bacillus cereus*

Bacillus cereus is a spore-forming, opportunistic Gram-positive bacterium that is widely distributed in the environment. It is classified as the *Bacillus cereus* group, comprising *B. thuringiensis*, *B. anthracis*, *B. mycoides*, *B. weihenstaphanensis*, *B. pseudomycoides* and *B. cytotoxicus,* based on their genetic similarity (Guinebretiere et al., 2013; Zwick et al., 2012). *B. cereus* grows well after cooking and cooling (< 48℃) since the heat treatment induces spore germination while inhibiting other competing flora (Granum and Lund, 1997). Because *B. cereus* produces emetic toxin and enterotoxins, it causes food poisoning, including vomiting and diarrhea, particularly after the consumption of rice-based dishes. The Centers for Disease and Control and Prevention (CDC) reported that *B. cereus* outbreaks account for 2 to 5% of foodborne diseases in the United States (Centers for Disease and Prevention, 2011). *B. cereus* outbreaks can be underreported as both types of illness are relatively mild and usually last for less than 24 h (Granum and Lund, 1997). Occasionally, *B. cereus* food poisoning are misdiagnosed due to symptomatic similarities to *Staphylococcus aureus* intoxication (*B. cereus* vomiting type) or *Clostridium perfringens* food poisoning (*B. cereus* diarrheal type) (Bennett et al., 2013). In addition to food poisoning, *B. cereus*

is also associated with potentially fatal non-gastrointestinal tract infections due to the various types of toxins, including phospholipases, proteases, and hemolysins, produced during growth (Drobniewski, 1993). For these reasons, there is an urgent need to control *B. cereus*. Since *B. cereus* is generally resistant to beta-lactam antibiotics and several strains of *B. cereus* are also resistant to erythromycin, tetracycline, and fluoroquinolones (Bottone, 2010; Simm et al., 2012), the demand for alternative methods to control *B. cereus* has grown (Drobniewski, 1993).

I-2. Bacteriophage and its endolysin as biocontrol agents

Bacteriophages, natural killers of bacteria, are viruses that target and replicate within bacteria. Frederick Twort first discovered most of the essential features of bacteriophages in 1915 (Twort, 1915), and in few years later Felix d'Herelle discovered and isolate bacteriophages independently (d'Herelle, 1917). Since then, many knowledgeable scientists like d'Herelle, used phages as a natural antimicrobial agent against bacterial infections and the phage therapy met significant success, only to be rejected due to the emergence of antibiotics (Keen, 2012). However, they have regained increasing attention in the past few decades, particularly in light of emerging antibiotic resistance (Garcia et al., 2008; Lu and Koeris, 2011). Bacteriophages are much more specific than antibiotics, so they have minimal impact on commensal bacteria other than the host. In addition, phages can amplify themselves when it infects the host bacteria, releasing hundreds of progeny phages, which in turn, allows infecting adjacent bacteria. Although bacteria can develop resistance to their viral predators, finding a new phage that can kill resistant bacteria is not difficult because the phage itself continually evolves against the mutated bacteria. Furthermore, phage cocktails, containing different kinds of phages, can efficiently prevent

bacteria from developing phage resistance (Chan et al., 2013; Gu et al., 2012). For these reasons, several phage cocktail products (ListShield from Intralytix and LISTEX^{TM} from MICREOS) were designed to protect food from *Listeria monocytogenes*, and were approved by the US Food and Drug Administration (FDA) as GRAS (Generally Recognized as Safe) (Sharma, 2013). However, safety concerns, such as potential transfer of toxin genes, bacterial virulence factors, or antibiotic resistance genes, should be considered before widely using phages as therapeutic agents (Sulakvelidze et al., 2001).

Endolysin is a peptidoglycan hydrolase of bacteriophage that lyses its bacterial host at the end of the phage life cycle (Fischetti, 2010). Since endolysins show species- or genus-specific strong lytic activities, the use of purified phage endolysins generates interest as an alternative to antibiotics (Loessner, 2005). Exogenous addition of endolysins can lyse the peptidoglycan of target bacteria resulting in rapid osmotic lysis and cell death. This endolysin-mediated "lysis from without" phenomenon is restricted to Gram-positive bacteria as the outer membrane of Gram-negative bacteria shields the peptidoglycan from the access of endolysins. To circumvent this problem, many researchers have used outer membrane

permeabilizers, such as ethylene diamine tetraacetic acid (EDTA), detergent, organic acids, to combat Gram-negative infections (Briers et al., 2011; Oliveira et al., 2014; Walmagh et al., 2012). Recombinant fusion endolysins or chemical modification of endolysin has also been an alternative method to transport an endolysin across the outer membrane. Recently, one group developed outer membrane-penetrating endolysins by attaching lipopolysaccharide (LPS)-destabilizing peptides, and confirmed 4 to 5 log reduction of Gram-negative pathogens within 30 min (Briers et al., 2014). Another group designed a novel hybrid endolysin by fusing T7 lysozyme and the FyuA binding domain of pesticin (Lukacik et al., 2012).

In contrast to typical single-domain globular endolysins from Gram-negative host, endolysins from Gram-positive bacteria infecting phages generally show a modular structure with at least two clearly separated functional domains: one or more catalytic domains and a cell wall binding domain (Nelson et al., 2012). The catalytic domain, also called enzymatic active domain (EAD), of endolysin provides peptidoglycan degrading activity. According to their different target bonds within the peptidoglycan, endolysins can be classified into three different groups: those that hydrolyze the linkages of sugar moieties (i.e., glycosidases and lytic transglycosylases),

those that cleave between a sugar residue and an amino acid (i.e. N-acetylmuramoyl-L-alanine amidase), and those that cleave within the peptide moieties (i.e. endopeptidase) (Hermoso et al., 2007). The cell wall binding domain (CBD) confers enzymatic specificity to endolysins by recognizing epitopes on the cell wall surface. These epitopes include species- or even strain-specific carbohydrates, teichoic acids, or peptide moieties of the peptidoglycan (Schmelcher et al., 2011). The same enzymatic activities and similar modular architectures are also found in bacterial enzyme, so-called autolysins, which hydrolyze the peptidoglycan of its own or closely related bacteria. Bacterial autolysins are involved in cell wall remodeling, cell division, transformation, or as virulence factors (Hermoso et al., 2007). Both phage-derived endolysins and bacterial autolysins show high homologies between their distinct domains, suggesting that they share common ancestry and co-evolved by interchange of functional domains (Lopez and Garcia, 2004).

Endolysins against Gram-negative pathogens have been studied extensively for half a century, particularly their role in the phage replication cycle rather than a therapeutic agent. For endolysins from Gram-positive infecting phages, on the other hand, studies have been focused on medical

and biotechnological applications. Since the capacity of an endolysin to kill bacteria was first reported in 1957 (Krause, 1957), numerous researchers have studied *in vitro* lytic activities of endolysins (Hermoso et al., 2007). It has only been since 2001 that scientists have begun evaluating the use of purified recombinant endolysins in animal infection models of human disease (Hermoso et al., 2007). Nelson et al. firstly proved that endolysins can be used as therapeutic agents to prevent or reduce the colonization of mucosal surfaces with group A streptococci in mice (Nelson et al., 2001). One year later, Schuch et al. demonstrated that intraperitoneal injections of *Bacillus anthracis* and PlyG, an endolysin isolated from the *B. anthracis* γ phage, cured most of infected mice (Schuch et al., 2002). Rashel et al. investigated the efficacy of *Staphylococcal* phage endolysin MV-L, and confirmed ~3 log reduction of methicillin-resistant *S. aureus* (Rashel et al., 2007). Some endolysins were shown to be synergistic with other antimicrobials, such as lysostaphin (Becker et al., 2008), antibiotics (Daniel et al., 2010), or nisin (Garcia et al., 2010).

Endolysins are globular proteins that can trigger immune responses when administrated mucosally or systemically, which may render endolysins inactive or hinder their therapeutic development. To address this issue,

rabbits and mice were hyperimmunized to various endolysins (Pal, Cpl-1) specific to *Streptococcus pneumonia* (Jado et al., 2003; Loeffler et al., 2003). Although antibodies were readily raised to the treated endolysins, these antibodies did not effectively neutralize the corresponding enzymatic activities of endolysins *in vivo*. It is also believed that high purity and removal of Gram-negative lipopolysaccharide are required for minimizing a host immune response.

Resistance development is another obvious concern about the therapeutic use of endolysins. To date, however, no endolysin-resistant strains were isolated after repeated exposure of endolysins (Hermoso et al., 2007). In one study, *S. pneumonia*, *S. pyogenes*, and *B. anthracis* cells were exposed to sublethal doses of endolysins. Surviving colonies were then challenged with lethal doses and there was no notable change in susceptibility (Fischetti, 2005). In a separate study, chemical mutagen was employed to increase the chance of spontaneous resistance, but none endolysin-resistant strains were detected (Schuch et al., 2002). Under same conditions, the frequency of resistance to the antibiotics novobiocin and streptomycin increased 3 to 4 logs, indicating that the probability of bacteria developing endolysin resistance seems to be very low. It is possible that

phages have evolved to target a unique, and essential conserved bonds in the peptidoglycan, making resistance to endolysins a rare event (Fischetti, 2005).

For successful application of phage endolysins as biocontrol agents, endolysins should have strong antibacterial activities. Several reports for the purpose of making a better antimicrobial activity have been conducted. In one study, site-directed or random mutagenesis of endolysin improved its antibacterial activity against group B streptococci (Cheng and Fischetti, 2007). Resch et al. reported the construction of endolysin Cpl-1 dimer by introducing specific cysteine residues to increase antipneumococcal activity and plasma half-life (Resch et al., 2011). In another study, inverting the net charge of cell wall binding domain of the Cpl-7 improved lethal effect of the endolysin (Diez-Martinez et al., 2013). Thermostability is also an important factor for endolysins to be used in food application. Heselpoth and Nelson designed a new screening method for the directed evolution of thermostable endolysin (Heselpoth and Nelson, 2012). The Loessner group demonstrated that *Listeria* endolysins featured high thermoresistance and increased activity after divalent metal cations substitution (Schmelcher et al., 2012). Some researchers produced chimeric or truncated endolysins with improved lytic activity (Becker et al., 2009; Mao et al., 2013), enhanced solubility

(Manoharadas et al., 2009) and altered host spectra (Croux et al., 1993).

I-3. CBD as a novel detection bioprobe

Bacteriophages have been used as alternative probes for pathogenic bacteria sensing because they have extreme host specificity and strong resistance to heat, pH, and chemicals (Arya et al., 2011; Mahony et al., 2011; Tawil et al., 2014). Recently, bacteriophage-derived proteins have received more attention than whole bacteriophages since it is easy to modify the affinity and binding properties of these proteins by protein engineering (Brzozowska et al., 2015; Chibli et al., 2014; Javed et al., 2013; Poshtiban et al., 2013). One of the examples of these phage-derived bioprobes is the receptor binding protein (RBP) of bacteriophage. RBPs, which are usually tail spike proteins or tail fiber proteins, confer host specificity of the phages (Singh et al., 2011; Singh et al., 2010). Due to their highly specific binding properties and relatively smaller size than whole phages, they offer significant advantages over phage-based approaches. However, RBPs usually bind to the host receptor (capsular polysaccharide, LPS) reversibly and possess hydrolytic activity to allow efficient phage DNA injection (Singh et al., 2012). In addition, many RBPs function as an oligomer or in concert with other adjacent phage tail proteins. These characteristics of RBPs might be barriers that should be addressed for the development of RBPs as a detection

agent.

Endolysins from Gram-positive bacteria-infecting phages consist of modular proteins including N-terminal catalytic domain and C-terminal cell wall binding domain (CBD) as described previously. CBDs feature high specificity and strong binding affinity (K_d values of pico- to nanomolar range) to bacteria (Schmelcher et al., 2010; Schmelcher et al., 2011). Typical CBDs are relatively small (10 ~ 15 kDa), act as a monomer, and have no lytic activity. These characteristics of CBDs can be advantageous over the RBPs, and several recent studies have exploited the CBDs as novel probes for the detection of bacteria. Recombinant CBDs fused to different fluorescent proteins allowed multiplex detection and serotype differentiation of *L. monocytogenes* (Schmelcher et al., 2010). The high affinity and specificity of the CBD was also harnessed for immobilization and separation of *Listeria* cells. Kretzer et al. firstly designed CBD-based magnetic separation (CBD-MS) scheme, and demonstrated that more than 90% *Listeria* cells from suspensions were recovered within 20-40 minutes (Kretzer et al., 2007). In this paper, they also observed that CBD-coated magnetic beads did not lead to agglutination of cell-bead mixtures, whereas antibody-coated magnetic beads showed strong agglutination. Using this CBD-MS techniques, Walcher

et al. reported that 10^2 to 10^3 CFU/ml of *L. monocytogenes* cells in milk can be detected in combination with plating or quantitative real-time PCR analysis (Walcher et al., 2010). Sainathrao et al. proved that only a 10 amino-acid motif of the CBD from *B. anthracis* endolysin PlyG was sufficient for binding, and allowed sensitive detection of *B. anthracis* cells when it combined with fluorescent quantum dots (Sainathrao et al., 2009). More recently, Tolba et al. developed an CBD-based electrochemical impedance biosensor for the rapid detection of *Listeria* cells (Tolba et al., 2012).

I-4. Purpose of this study

B. cereus is an opportunistic human pathogen responsible for food poisoning and other, nongastrointestinal infections. Due to the emergence of multidrug-resistant *B. cereus* strains, the demand for alternative therapeutic options is increasing. In this regard, bacteriophage-based therapies have been re-introduced as an additional tool in the war against multi-drug resistant pathogens. These tools can come not only from phage itself but also from phage-encoded proteins, such as endolysins. The modular nature of endolysins encouraged me to use the functional domain as an alternative biocontrol agent against *B. cereus*. In addition, the target-specific binding activity of the CBDs of endolysins inspired me to explore the feasibility of engineering CBD to target and capture bacterial cells.

Therefore, this study aims to (i) isolate and characterize novel phages specific to *B. cereus* from various samples, (ii) recombinantly produce and characterize the phage endolysins and its functional domains, (iii) and develop the CBD-based bioprobes for the detection of pathogenic bacteria.

I-5. References

Arya, S.K., Singh, A., Naidoo, R., Wu, P., McDermott, M.T., Evoy, S., (2011) Chemically immobilized T4-bacteriophage for specific Escherichia coli detection using surface plasmon resonance. Analyst 136, 486-492.

Becker, S.C., Foster-Frey, J., Donovan, D.M., (2008) The phage K lytic enzyme LysK and lysostaphin act synergistically to kill MRSA. FEMS Microbiol. Lett. 287, 185-191.

Becker, S.C., Foster-Frey, J., Stodola, A.J., Anacker, D., Donovan, D.M., (2009) Differentially conserved staphylococcal SH3b_5 cell wall binding domains confer increased staphylolytic and streptolytic activity to a streptococcal prophage endolysin domain. Gene 443, 32-41.

Bennett, S.D., Walsh, K.A., Gould, L.H., (2013) Foodborne disease outbreaks caused by Bacillus cereus, Clostridium perfringens, and Staphylococcus aureus--United States, 1998-2008. Clin. Infect. Dis. 57, 425-433.

Bottone, E., (2010) Bacillus cereus, a volatile human pathogen. Clin. Microbiol. Rev. 23, 382 - 398.

Briers, Y., Walmagh, M., Lavigne, R., (2011) Use of bacteriophage endolysin EL188 and outer membrane permeabilizers against Pseudomonas aeruginosa. J. Appl. Microbiol. 110, 778-785.

Briers, Y., Walmagh, M., Van Puyenbroeck, V., Cornelissen, A., Cenens, W., Aertsen, A., Oliveira, H., Azeredo, J., Verween, G., Pirnay, J.P., Miller, S., Volckaert, G., Lavigne, R., (2014) Engineered endolysin-based "Artilysins" to combat multidrug-resistant gram-negative pathogens. mBio 5, e01379-01314.

Brzozowska, E., Smietana, M., Koba, M., Gorska, S., Pawlik, K., Gamian, A., Bock, W.J., (2015) Recognition of bacterial lipopolysaccharide using bacteriophage-adhesin-coated long-period gratings. Biosens. Bioelectron. 67, 93-99.

Centers for Disease, C., Prevention, (2011) Surveillance for foodborne disease outbreaks--United States, 2008. MMWR Morb. Mortal. Wkly. Rep. 60, 1197-1202.

Chan, B.K., Abedon, S.T., Loc-Carrillo, C., (2013) Phage cocktails and the future of phage therapy. Future Microbiol. 8, 769-783.

Cheng, Q., Fischetti, V.A., (2007) Mutagenesis of a bacteriophage lytic enzyme PlyGBS significantly increases its antibacterial activity against group B streptococci. Appl. Microbiol. Biotechnol. 74, 1284-1291.

Chibli, H., Ghali, H., Park, S., Peter, Y.A., Nadeau, J.L., (2014) Immobilized phage proteins for specific detection of staphylococci. Analyst 139, 179-186.

Croux, C., Ronda, C., Lopez, R., Garcia, J.L., (1993) Interchange of functional domains switches enzyme specificity: construction of a chimeric pneumococcal-clostridial cell wall lytic enzyme. Mol. Microbiol. 9, 1019-1025.

d'Herelle, F., (1917) An invisible antagonist microbe of dysentery bacillus. Cr Hebd Acad Sci 165, 373-375.

Daniel, A., Euler, C., Collin, M., Chahales, P., Gorelick, K.J., Fischetti, V.A., (2010) Synergism between a Novel Chimeric Lysin and Oxacillin Protects against Infection by Methicillin-Resistant Staphylococcus aureus. Antimicrob. Agents Chemother. 54, 1603-1612.

Diez-Martinez, R., de Paz, H.D., Bustamante, N., Garcia, E., Menendez, M., Garcia, P., (2013) Improving the lethal effect of cpl-7, a pneumococcal phage lysozyme with broad bactericidal activity, by inverting the net charge of its cell wall-binding module. Antimicrob. Agents Chemother. 57, 5355-5365.

Drobniewski, F.A., (1993) Bacillus cereus and related species. Clin. Microbiol. Rev. 6, 324-338.

Fischetti, V.A., (2005) Bacteriophage lytic enzymes: novel anti-infectives. Trends Microbiol. 13, 491-496.

Fischetti, V.A., (2010) Bacteriophage endolysins: a novel anti-infective to control Gram-positive pathogens. Int. J. Med. Microbiol. 300, 357-362.

Garcia, P., Martinez, B., Obeso, J.M., Rodriguez, A., (2008) Bacteriophages and their application in food safety. Lett. Appl. Microbiol. 47, 479-485.

Garcia, P., Martinez, B., Rodriguez, L., Rodriguez, A., (2010) Synergy between the phage endolysin LysH5 and nisin to kill Staphylococcus aureus in pasteurized milk. Int. J. Food Microbiol. 141, 151-155.

Granum, P.E., Lund, T., (1997) Bacillus cereus and its food poisoning toxins. FEMS Microbiol. Lett. 157, 223-228.

Gu, J.M., Liu, X.H., Li, Y., Han, W.Y., Lei, L.C., Yang, Y.J., Zhao, H.L., Gao, Y., Song, J., Lu, R., Sun, C.J., Feng, X., (2012) A Method for Generation Phage Cocktail with Great Therapeutic Potential. PLoS One 7.

Guinebretiere, M.H., Auger, S., Galleron, N., Contzen, M., De Sarrau, B., De Buyser, M.L., Lamberet, G., Fagerlund, A., Granum, P.E., Lereclus, D., De Vos, P., Nguyen-The, C., Sorokin, A., (2013) Bacillus cytotoxicus sp. nov. is a novel thermotolerant species of the Bacillus cereus Group occasionally associated with food poisoning. International journal of systematic and evolutionary microbiology 63, 31-40.

Hermoso, J.A., Garcia, J.L., Garcia, P., (2007) Taking aim on bacterial pathogens: from phage therapy to enzybiotics. Curr. Opin. Microbiol. 10, 461-472.

Heselpoth, R.D., Nelson, D.C., (2012) A new screening method for the directed evolution of thermostable bacteriolytic enzymes. Journal of visualized experiments : JoVE.

Jado, I., Lopez, R., Garcia, E., Fenoll, A., Casal, J., Garcia, P., Stu, S.P.I., (2003) Phage lytic enzymes as therapy for antibiotic-resistant Streptococcus pneumoniae infection in a murine sepsis model. J. Antimicrob. Chemother. 52, 967-973.

Javed, M.A., Poshtiban, S., Arutyunov, D., Evoy, S., Szymanski, C.M., (2013) Bacteriophage Receptor Binding Protein Based Assays for the Simultaneous Detection of Campylobacter jejuni and Campylobacter coli. PLoS One 8.

Keen, E.C., (2012) Phage therapy: concept to cure. Frontiers in microbiology

3, 238.

Krause, R.M., (1957) Studies on bacteriophages of hemolytic streptococci. I. Factors influencing the interaction of phage and susceptible host cell. J. Exp. Med. 106, 365-384.

Kretzer, J.W., Lehmann, R., Schmelcher, M., Banz, M., Kim, K.P., Korn, C., Loessner, M.J., (2007) Use of high-affinity cell wall-binding domains of bacteriophage endolysins for immobilization and separation of bacterial cells. Appl. Environ. Microbiol. 73, 1992-2000.

Loeffler, J.M., Djurkovic, S., Fischetti, V.A., (2003) Phage lytic enzyme Cpl-1 as a novel antimicrobial for pneumococcal bacteremia. Infect. Immun. 71, 6199-6204.

Loessner, M.J., (2005) Bacteriophage endolysins--current state of research and applications. Curr. Opin. Microbiol. 8, 480-487.

Lopez, R., Garcia, E., (2004) Recent trends on the molecular biology of pneumococcal capsules, lytic enzymes, and bacteriophage. FEMS Microbiol. Rev. 28, 553-580.

Lu, T.K., Koeris, M.S., (2011) The next generation of bacteriophage therapy. Curr. Opin. Microbiol. 14, 524-531.

Lukacik, P., Barnard, T.J., Keller, P.W., Chaturvedi, K.S., Seddiki, N., Fairman, J.W., Noinaj, N., Kirby, T.L., Henderson, J.P., Steven, A.C., Hinnebusch, B.J., Buchanan, S.K., (2012) Structural engineering of a phage lysin that targets gram-negative pathogens. Proc. Natl. Acad. Sci. U. S. A. 109, 9857-9862.

Mahony, J., McAuliffe, O., Ross, R.P., van Sinderen, D., (2011) Bacteriophages as biocontrol agents of food pathogens. Curr. Opin. Biotechnol. 22, 157-163.

Manoharadas, S., Witte, A., Blasi, U., (2009) Antimicrobial activity of a chimeric enzybiotic towards Staphylococcus aureus. J. Biotechnol. 139, 118-123.

Mao, J., Schmelcher, M., Harty, W.J., Foster-Frey, J., Donovan, D.M., (2013)

Chimeric Ply187 endolysin kills Staphylococcus aureus more effectively than the parental enzyme. FEMS Microbiol. Lett. 342, 30-36.

Nelson, D., Loomis, L., Fischetti, V.A., (2001) Prevention and elimination of upper respiratory colonization of mice by group A streptococci by using a bacteriophage lytic enzyme. Proc. Natl. Acad. Sci. U. S. A. 98, 4107-4112.

Nelson, D.C., Schmelcher, M., Rodriguez-Rubio, L., Klumpp, J., Pritchard, D.G., Dong, S., Donovan, D.M., (2012) Endolysins as antimicrobials. Adv. Virus Res. 83, 299-365.

Oliveira, H., Thiagarajan, V., Walmagh, M., Sillankorva, S., Lavigne, R., Neves-Petersen, M.T., Kluskens, L.D., Azeredo, J., (2014) A thermostable Salmonella phage endolysin, Lys68, with broad bactericidal properties against gram-negative pathogens in presence of weak acids. PLoS One 9, e108376.

Poshtiban, S., Javed, M.A., Arutyunov, D., Singh, A., Banting, G., Szymanski, C.M., Evoy, S., (2013) Phage receptor binding protein-based magnetic enrichment method as an aid for real time PCR detection of foodborne bacteria. Analyst 138, 5619-5626.

Rashel, M., Uchiyama, J., Ujihara, T., Uehara, Y., Kuramoto, S., Sugihara, S., Yagyu, K., Muraoka, A., Sugai, M., Hiramatsu, K., Honke, K., Matsuzaki, S., (2007) Efficient elimination of multidrug-resistant Staphylococcus aureus by cloned lysin derived from bacteriophage phi MR11. J. Infect. Dis. 196, 1237-1247.

Resch, G., Moreillon, P., Fischetti, V.A., (2011) A stable phage lysin (Cpl-1) dimer with increased antipneumococcal activity and decreased plasma clearance. Int. J. Antimicrob. Agents 38, 516-521.

Sainathrao, S., Mohan, K.V., Atreya, C., (2009) Gamma-phage lysin PlyG sequence-based synthetic peptides coupled with Qdot-nanocrystals are useful for developing detection methods for Bacillus anthracis by using its surrogates, B. anthracis-Sterne and B. cereus-4342. BMC Biotechnol. 9, 67.

Schmelcher, M., Shabarova, T., Eugster, M.R., Eichenseher, F., Tchang, V.S., Banz, M., Loessner, M.J., (2010) Rapid multiplex detection and

differentiation of Listeria cells by use of fluorescent phage endolysin cell wall binding domains. Appl. Environ. Microbiol. 76, 5745-5756.

Schmelcher, M., Tchang, V.S., Loessner, M.J., (2011) Domain shuffling and module engineering of Listeria phage endolysins for enhanced lytic activity and binding affinity. Microbial biotechnology 4, 651-662.

Schmelcher, M., Waldherr, F., Loessner, M.J., (2012) Listeria bacteriophage peptidoglycan hydrolases feature high thermoresistance and reveal increased activity after divalent metal cation substitution. Appl. Microbiol. Biotechnol. 93, 633-643.

Schuch, R., Nelson, D., Fischetti, V.A., (2002) A bacteriolytic agent that detects and kills Bacillus anthracis. Nature 418, 884-889.

Sharma, M., (2013) Lytic bacteriophages: Potential interventions against enteric bacterial pathogens on produce. Bacteriophage 3, e25518.

Simm, R., Voros, A., Ekman, J.V., Sodring, M., Nes, I., Kroeger, J.K., Saidijam, M., Bettaney, K.E., Henderson, P.J.F., Salkinoja-Salonen, M., Kolsto, A.B., (2012) BC4707 Is a Major Facilitator Superfamily Multidrug Resistance Transport Protein from Bacillus cereus Implicated in Fluoroquinolone Tolerance. PLoS One 7.

Singh, A., Arutyunov, D., McDermott, M.T., Szymanski, C.M., Evoy, S., (2011) Specific detection of Campylobacter jejuni using the bacteriophage NCTC 12673 receptor binding protein as a probe. Analyst 136, 4780-4786.

Singh, A., Arutyunov, D., Szymanski, C.M., Evoy, S., (2012) Bacteriophage based probes for pathogen detection. Analyst 137, 3405-3421.

Singh, A., Arya, S.K., Glass, N., Hanifi-Moghaddam, P., Naidoo, R., Szymanski, C.M., Tanha, J., Evoy, S., (2010) Bacteriophage tailspike proteins as molecular probes for sensitive and selective bacterial detection. Biosens. Bioelectron. 26, 131-138.

Sulakvelidze, A., Alavidze, Z., Morris, J.G., Jr., (2001) Bacteriophage therapy. Antimicrob. Agents Chemother. 45, 649-659.

Tawil, N., Sacher, E., Mandeville, R., Meunier, M., (2014) Bacteriophages:

biosensing tools for multi-drug resistant pathogens. Analyst 139, 1224-1236.

Tolba, M., Ahmed, M.U., Tlili, C., Eichenseher, F., Loessner, M.J., Zourob, M., (2012) A bacteriophage endolysin-based electrochemical impedance biosensor for the rapid detection of Listeria cells. Analyst 137, 5749-5756.

Twort, F.W., (1915) An investigation on the nature of ultra-microscopic viruses. Lancet 2, 1241-1243.

Walcher, G., Stessl, B., Wagner, M., Eichenseher, F., Loessner, M.J., Hein, I., (2010) Evaluation of paramagnetic beads coated with recombinant Listeria phage endolysin-derived cell-wall-binding domain proteins for separation of Listeria monocytogenes from raw milk in combination with culture-based and real-time polymerase chain reaction-based quantification. Foodborne Pathog. Dis. 7, 1019-1024.

Walmagh, M., Briers, Y., dos Santos, S.B., Azeredo, J., Lavigne, R., (2012) Characterization of modular bacteriophage endolysins from Myoviridae phages OBP, 201phi2-1 and PVP-SE1. PLoS One 7, e36991.

Zwick, M.E., Joseph, S.J., Didelot, X., Chen, P.E., Bishop-Lilly, K.A., Stewart, A.C., Willner, K., Nolan, N., Lentz, S., Thomason, M.K., Sozhamannan, S., Mateczun, A.J., Du, L., Read, T.D., (2012) Genomic characterization of the Bacillus cereus sensu lato species: backdrop to the evolution of Bacillus anthracis. Genome Res. 22, 1512-1524.

Chapter II.

B. cereus bacteriophages and their genomes

II-1. Introduction

Bacteriophages are the most abundant self-replicating units on earth, outnumbering their host bacteria by an estimated 10-fold (Rohwer, 2003). These viruses, a total population size of 10^{31} phage particles, can kill 50% of the bacteria per day, implicating their ecological importance and impact on bacterial evolution (Brussow and Hendrix, 2002). The majority (96%) of reported phages are *Caudovirales,* which possess double-stranded DNA (dsDNA) genomes in icosahedral head and tails with various lengths (Ackermann, 2003). These *Caudovirales* are divided into three families based on their tail morphologies: *Siphoviridae* (61%), having long, flexible, and noncontractile tails, *Myoviridae* (25%), with long, rigid, and contractile tails, and *Podoviridae* (14%), with short and noncontractile tails (Ackermann, 2007). Phages exhibit great diversity, with genome sizes ranging from 17 kbp to 0.5 Mbp, and present an enormous reservoir of novel genes (Comeau et al., 2008). These phage genomes are usually mosaic, reflecting horizontal and vertical genetic exchange during phage evolution (Hendrix et al., 2000).

The *B. cereus* group consists of seven closely related species: *B. cereus, B. thuringiensis*, *B. anthracis*, *B. mycoides*, *B. weihenstaphanensis*, *B. pseudomycoides, and B. cytotoxicus* (Guinebretiere et al., 2013). Of these, *B.*

anthracis, B. cereus, and B. thuringiensis are of special interest due to their capacity of causing human diseases and for their biotechnological values. *B. cereus* is the causative agent of food poisoning and opportunistic infections in humans. *B. anthracis,* a category A bio-threat agent, is causing fatal enthrax infections in humans and animals. *B. thuringiensis* is an insect pathogen commonly used as a pesticide in agriculture. Although the members of the *B. cereus* group are genetically very close, they show highly specialized lifestyles with distinct virulence spectra and ecological niches (Jensen et al., 2003). These diverse lifestyles are often associated with the acquisition of mobile genetic elements, particularly plasmids, but also insertion sequences, transposons, and phages (Gillis and Mahillon, 2014a). Since the members of the *B. cereus* group are known to be associated with species-specific phages either as prophages or as independently replicating elements, phages have recently received increasing attention in terms of their contribution to the distinctive ecotypes and pathotypes (Gillis and Mahillon, 2014b). In addition, the lytic activity and high specificity of phages provide a potential resource for medical, molecular, and biotechnological applications.

In order to understand genetic diversity of *B. cereus* phages and further develop phage-based genetic, biotechnological, and clinical tools,

isolating and characterizing new *B. cereus* phages is essential. To date, however, only a few *B. cereus* phages have been characterized in detail (Bandara et al., 2012; El-Arabi et al., 2013; Klumpp et al., 2014; Lee et al., 2013; Lee et al., 2011; Shin et al., 2011; Shin et al., 2014; Smeesters et al., 2011). Here, the results of microbiological and genomic characterization of the novel *B. cereus* phages were presented. The results described here will not only broaden our knowledge of *B. cereus* phages, but will also be useful for developing efficient biocontrol agents against the notorious human pathogen *B. cereus*.

II-2. Materials and Methods

II-2-1. Bacterial strains and growth conditions

All of the *Bacillus* strains were grown in Luria-Bertani (LB) broth at 37℃. To create agar medium, the broth medium was supplemented with 1.5% agar. All of the media used in this study were purchased from Difco and used according to the manufacturer's instructions.

II-2-2. Bacteriophage isolation and propagation

Soil and sewage samples collected from farms and the Seonam Water Reclamation Center (Seoul, South Korea) were used as sources for isolation of *B. cereus* phages. Briefly, a 25-ml sample was added to equal volumes of 2X LB broth and incubated with shaking at 37℃ for 24 h. After centrifugation (15,000 x g for 10 min), the supernatant was filtrated using 0.22-μm-pore size filter (Millipore). Then, 10 ml of the filtrate was mixed with 50 ml of LB broth and 500 μl of *B. cereus* host strains overnight cultures, and the mixture was incubated at 37℃ for 12 h with shaking. The culture was centrifuged and the supernatant was filter sterilized as described

above. The presence of phages was confirmed using a plaque forming assay with molten 0.4% LB soft agar inoculated with *B. cereus* overnight cultures. After incubation at 37℃ for 12 h, single phage plaque was picked with a sterile pipette tip and eluted in 1 ml of SM buffer (50 mM Tris-HCl (pH7.5), 100 mM NaCl, and 10 mM $MgCl_2$). These plaque isolation and elution steps were repeated at least three times to purify single phages. For purification and high-titer stock preparation of phages, phage particles were precipitated with 10% polyethylene glycol 6000 (Sigma) in the presence of 1 M NaCl at 4℃ overnight. After centrifugation (10,000 x g, 20 min, 4℃), the precipitated phages were resuspended in SM buffer, and purified by CsCl density gradient ultracentrifugation (78,500 x g, 2 h, 4℃). Separated phages were dialyzed against 1,000 volumes of SM buffer using a Spectra/Por 4 dialysis membrane tube (Spectrum) for 2 h with one buffer change.

II-2-3. Host range determination by spotting assay

Host range studies were performed by plaque-forming assays. Isolated phages (1 x 10^7 PFU/ml) were serially diluted 10-fold, and a 10-μl aliquots were spotted onto the 0.4% LB soft agar overlay containing the test bacteria

grown overnight. The plate was incubated at 37℃ overnight, and single plaque formation was monitored.

II-2-4. Morphological analysis by TEM

Purified phages (1 x 10^{10} PFU/ml) were placed on carbon-coated copper grids and negatively stained with 2% aqueous uranyl acetate (pH 4.0) for 20 s. Phages were visualized by transmission electron microscopy (LEO 912AB TEM, Carl Zeiss) at 80 kV. Images were scanned with a Proscan 1,024 x 1,024-pixel charge-coupled device camera at the National Academy of Agricultural Science (Suwon, South Korea). Phages were classified according to the guidelines of the International Committee on the Taxonomy of Viruses.

II-2-5. Genome sequencing and annotation

Phenol-chloroform extraction was used to isolate the phage's genomic DNA, and it was sequenced using the Genome Sequencer FLX Titanium by Macrogen, Seoul, South Korea. The assembly of quality filtered reads was

performed using GS De Novo Assembler (v. 2.6), and the open reading frames (ORFs) were predicted using the Glimmer 3.02 (Delcher et al., 2007), GeneMark.hmm (Besemer et al., 2001), and FgenesB (Softberry, Inc., Mount Kisco, NY) software. The prediction of ribosomal binding sites (RBS) of ORFs was conducted using RBSfinder (J. Craig Venter Institute, Rockville, MD). The ORFs were limited to those encoding proteins of more than 50 amino acids. Conserved-domain analysis of the predicted ORFs was carried out using BLASTP (Altschul et al., 1990), InterProScan (Zdobnov and Apweiler, 2001), and the NCBI Conserved Domain Database (Marchler-Bauer et al., 2007). Searches for tRNAs were conducted using the tRNAscan-SE program (Lowe and Eddy, 1997).

II-2-6. Phylogenetic analysis

To determine the phylogenetic position of the isolated phages, I made phylogenetic trees based on the alignment of the amino acid sequence from the large subunit of terminase and major capsid protein from various bacteriophages. The amino acid sequences used for phylogenetic trees are available online at NCBI nucleotide databases

(http://www.ncbi.nlm.nih.gov/nuccore). Alignment of amino acid sequences was created using the Clustal X2 program (Larkin et al., 2007). The phylogenetic tree was constructed with MEGA5 by the neighbor-joining method and bootstrap analysis (1,000 replicates) with p-distance values (Kumar et al., 2008). Average nucleotide identity (ANI) was calculated with Kalign (Lassmann and Sonnhammer, 2005).

II-2-7. Bacterial challenge test in liquid culture

An exponentially growing *B. cereus* ATCC 21786 cells (2 x 107 CFU/ml) in 50 ml LB were infected with 1 ml of PBC1 (10^{10}, 10^{9}, and 10^{8} PFU/ml, respectively) and incubated for another 10 h at 37℃ with vigorous shaking. Bacterial growth was monitored by measuring the OD600 at various time points. As a negative control, one bacterial culture was inoculated with 100 μl SM buffer instead of PBC1.

II-2-8. Inhibition of *B. cereus* growth in boiled rice

To evaluate the effect of phage PBC1 on growth of *B. cereus* cells in foods, I

chose boiled rice as a food sample because rice-based dishes are frequently involved in *B. cereus* poisoning (Grande et al., 2006). Round grain white rice was purchased at local market and boiled rice samples were prepared as described previously with slight modification (Grande et al., 2006). Briefly, rice (200 g) was boiled in water (250 ml) for 30 min, and the resulting cooked rice (10 g) was diluted in 40 ml of distilled water under vigorous shaking for 10 min. Then, the homogenous slurry samples (10 ml) were incubated at desired temperatures (25℃or 37℃) for 1 h, and the samples were artificially contaminated with *B. cereus* ATCC 21768 (10^3 CFU/ml). Next, aliquots of PBC1 (0.01 ml) were added to the samples to achieve a final concentration of 10^8 PFU/ml (Bandara et al., 2012; Guenther et al., 2009). Following phage addition, the samples were thoroughly mixed and incubated at desired temperatures (25℃or 37℃). After desired intervals of incubation, food samples were serially diluted in PBS and plated in duplicate on LB agar. Plates were incubated at 37℃ for 12 h, and the average number of colonies were determined. The experiments were carried out independently in triplicate.

II-2-9. *In vitro* phage adsorption assay

Bacterial cells (20 ml, OD_{600} = 1.0-1.5) were harvested by centrifugation (6,000 x g, 10 min, 4℃) and resuspended in 20 ml fresh LB broth. The bacterial suspension was adjusted to produce an OD_{600} of 0.1 (about 10^7 CFU/ml), and the sample was aliquoted into 15 ml falcon tubes (10-ml suspension per tubes). Cells were supplemented with 25 μg/ml of chloramphenicol to prevent the cell growth and phage multiplication (Baptista et al., 2008). Then, PBC1 was added to each tube with 10 mM $CaCl_2$ and $MgCl_2$ to achieve the final concentration of 10^4 PFU/ml and incubated at 37℃. Samples were taken at 5-min intervals, and the cells were immediately removed by centrifugation (16,000 x g, 1 min 4℃) and filtration (0.22-μM pore-size filter). The number of unbound free phage particles was determined by overlay assay. Because phages can exploit both carbohydrates and surface proteins as receptors, I treated bacteria with periodate or proteinase K and tested how these treatments affected PBC1 adsorption. For the periodate and proteinase K treatment assay, I followed the method as described previously (Kiljunen et al., 2011; Sorensen et al., 2011). Briefly, exponentially growing *B. cereus* ATCC 21768 cells were harvested and washed once with fresh LB broth. The bacterial cells were

then treated with proteinase K (0.2 mg/ml; Qiagen) at 45℃ for 2 h. For the periodate treatment group, the cells were centrifuged, and the bacterial pellet was suspended into sodium acetate (50 mM; pH 5.2) or sodium acetate containing either 10 or 100 mM periodate (Sigma) before being incubated for 2 h in a dark area. Following incubation, the samples were washed three times with fresh LB broth. Adsorption assay was performed for the various treated cells, as described above.

II-2-10. One-step growth curve

When the OD_{600} of the *B. cereus* ATCC 21768 culture reached 1.5 (10^8 CFU/ml), 50 ml of the culture was harvested. The PBC1 phage (1 ml, 5 x 10^6 PFU/ml) was added with 10 mM $CaCl_2$ and $MgCl_2$ and allowed to adsorb for 5 min. The mixture was centrifuged at 6,000 x g for 10 min and the supernatant was discarded to remove the residual phages. The cell pellet was then resuspended with the same volume of fresh LB broth, and the culture was further incubated at 37℃ with shaking. Two sets of samples were collected every 5 min before dilution and overlay onto the bacterial lawn containing 10 mM of $CaCl_2$ and $MgCl_2$ for phage titration. To determine the

eclipse period, the second set of samples was treated with 1% chloroform to release the intracellular phages before the overlay assay.

II-3. Results and Discussion

II-3-1. Isolation and morphology of bacteriophages

B. cereus phages were isolated from various environmental samples, such as sewage (PBC1, PBC2, PBC6), soils (PBC4, PBC9), and activated sludges (PBC5). TEM analysis revealed that isolated phages were classified into the *Siphoviridae* (PBC1, PBC2, PBC4, PBC5) and *Myoviridae* (PBC6, PBC9) families (**Fig. II-1**). Their capsid diameters and tail lengths are summarized in **Table II-1**. Interestingly, PBC2 exhibits a very long, flexible, and non-contractile tail with a length of approximately 500 nm, indicating that PBC2 is a giant siphovirus.

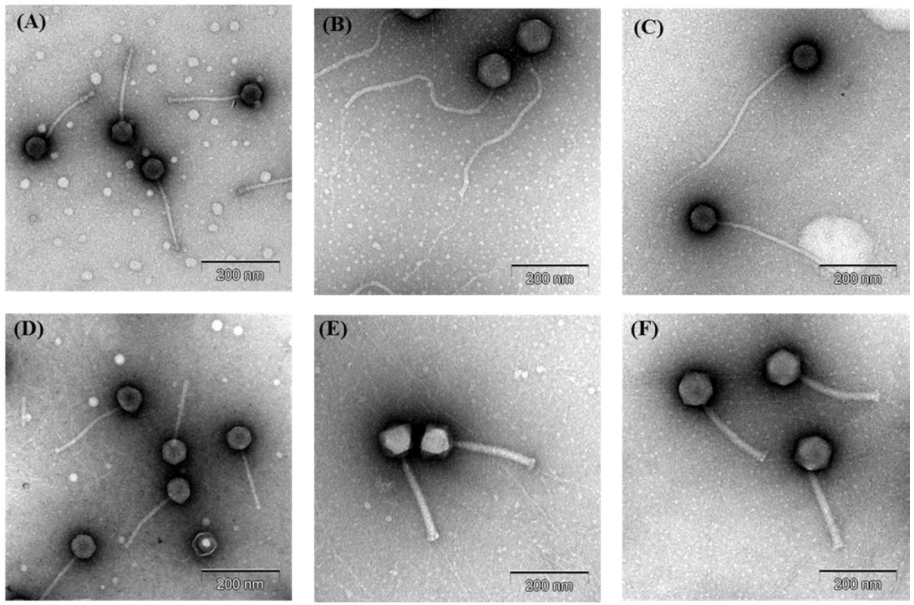

Fig. II-1. Transmission electron microscopy images of *B. cereus* phages.

(A) PBC1, (B) PBC2, (C) PBC4, (D) PBC5, (E) PBC6, (F) PBC9.

Table II-1. General characteristics and genome features of *B. cereus* phages

Phage	Family	Capsid diam (nm)	Tail length (nm)	Genome size (bp)	G+C content (mol%)	No. of ORFs predicted/no. with function assigned	Predicted lifestyle	Source
PBC1	*Siphoviridae*	70	200	41,164	41.7	50/22	virulent	Kong and Ryu, 2012
PBC2	*Siphoviridae*	80	500	168,689	34.4	251/47	temperate	This work
PBC4	*Siphoviridae*	65	369	80,647	34	94/29	temperate	This work
PBC5	*Siphoviridae*	64	169	56,332	40.3	95/29	virulent	This work
PBC6	*Myoviridae*	92	215	157,147	39.9	227/46	virulent	This work
PBC9	*Myoviridae*	80	215	156,179	39.9	229/46	virulent	This work

II-3-2. Host range determination

Since the host range of phage is an important factor for developing biocontrol agents, I performed a plaque assay with a variety of bacterial species. As shown in **Table II-2**, isolated *B. cereus* phages typically showed limited host range within the *B. cereus* group species. PBC1, PBC2, and PBC4 showed high host specificity, producing single plaques only against the certain strains of *B. cereus* out of the fourteen *B. cereus* strains tested. Other *B. cereus* group species (*B. thuringiensis*, *B. mycoides*) were resistant to those phages. Other Gram-positive or Gram-negative bacterial species were also resistant to the phages (data not shown). The myovirus PBC6 and PBC9 exhibited relatively broader host range than siphovirus, albeit limited to the *B. cereus* group species. Exceptionally, PBC5 is the only siphovirus that displayed a host range over species borders. Overall, the isolated *B. cereus* phages have high host specificity, and consequently, each phage alone would not be an efficient biocontrol agent against diverse strains of *B. cereus*. However, some phages showed unique host ranges; in the case of PBC1, the host strain (ATCC 21768) was resistant to all other phages isolated by Dr. Ryu's group (Bandara et al., 2012; Kong et al., 2012). From these results, I suspected that each phage could be a potential candidate for an effective

phage cocktail lytic for *B. cereus*. Therefore, I further characterized the phages.

Table II-2. Host range of *B. cereus* phages

Strains[a]	Plaque formation[b]					
	PBC1	PBC2	PBC4	PBC5	PBC6	PBC9
B. cereus ATCC 27348	-	-	-	-	-	-
B. cereus ATCC 21768	**C**	-	-	-	-	-
B. cereus ATCC 13061	-	**C**	-	-	-	-
B. cereus ATCC 14579	-	-	**C**	**C**	**C**	**C**
B. cereus ATCC 21772	-	-	-	-	**C**	-
B. cereus ATCC 10876	-	-	-	**C**	-	**C**
B. cereus KCTC 3674	-	-	-	-	-	**C**
B. cereus ATCC 10987	-	-	-	-	**T**	-
B. cereus KCTC 1094	-	-	-	**T**	-	-
B. cereus ATCC 12480	-	**C**	-	-	**C**	**C**
B. cereus ATCC 4342	-	-	**C**	**C**	-	-
B. cereus ATCC 53522	**C**	**C**	-	-	-	-
B. cereus ATCC 21366	-	-	-	-	-	-
B. cereus NCCP 14796	-	-	**C**	**C**	-	-
B. thuringiensis ATCC 10792	-	-	-	**T**	**C**	**C**
B. mycoides ATCC 6462	-	-	-	**C**	**C**	**C**
B. subtilis ATCC 23857	-	-	-	-	-	-
B. licheniformis JCM 2505	-	-	-	-	-	-

[a] ATCC, American Type Culture Collection; KCTC, Korean Collection for Type Cultures; NCCP, National Culture Collection for Pathogens; JCM, Japan Collection of Microorganisms.

[b] C, clear plaque; T, turbid plaque; -, no plaque.

II-3-3. Genome analysis of bacteriophages

II-3-3-1. PBC1

I isolated the *B. cereus*-infecting *Siphoviridae* phage PBC1 and announced its genome sequence (Kong et al., 2012). PBC1 contains 41,164 bp of linear double-stranded DNA, including 50 predicted open reading frames (ORFs) **(Fig. II-2)**. Because PBC1 forms clear plaques and does not contain any lysogeny-related genes in its genome, PBC1 is considered to be a virulent phage. Although several virulent variant *B. anthracis Siphoviridae* phages have been reported so far (Fouts et al., 2006; Minakhin et al., 2005; Schuch and Fischetti, 2006), they are derivatives of *B. anthracis* prophage W and their genome contains several lysogeny-related proteins, including an integrase-like protein (Gillis and Mahillon, 2014a). Therefore, to the best of my knowledge, PBC1 is the only naturally isolated virulent *Siphoviridae* phage that infects *B. cereus*.

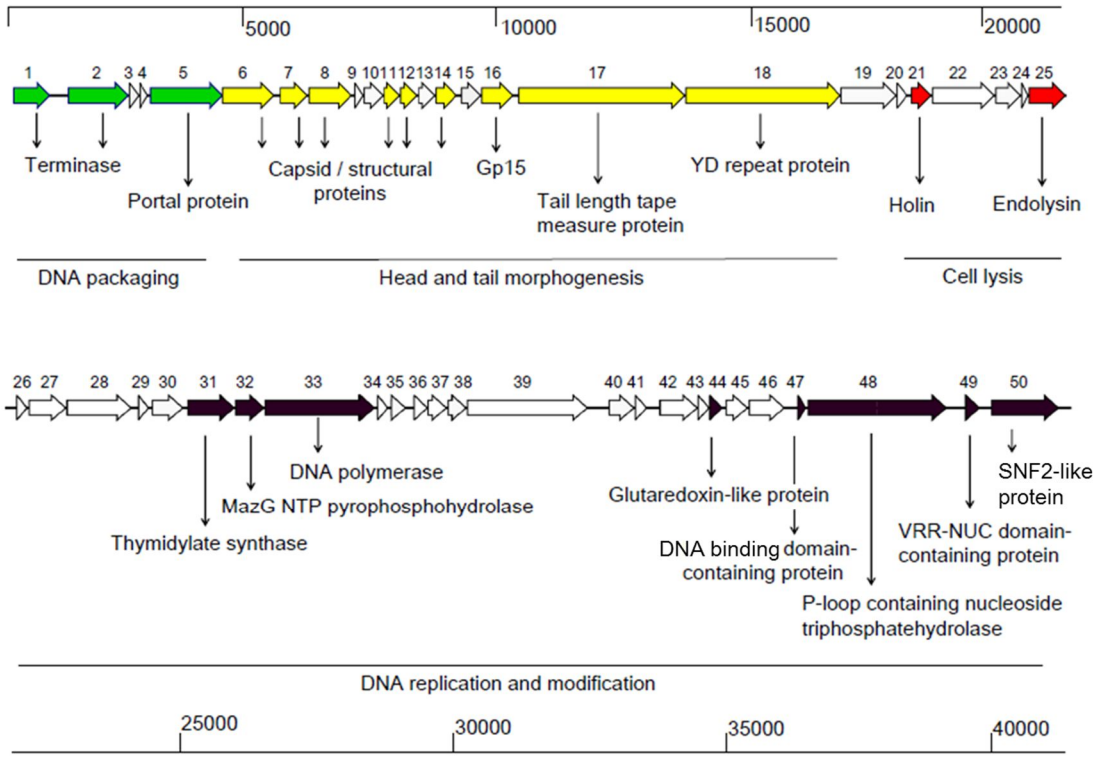

Fig. II-2. Genome map of *B. cereus* phage PBC1.

Genomic analysis revealed that PBC1 contains 41,164 bp of linear double-stranded DNA with a G+C content of 41.7 mol%. PBC1 has terminally redundant and partially permuted genomes, suggesting that PBC1 uses a headful packaging mechanism. I identified 50 predicted ORFs, all of which were transcribed in the same direction, and found no tRNAs. Of the 50 predicted ORFs, 28 were identified as encoding hypothetical proteins. Homology searches identified packaging and structural proteins (a terminase, a portal protein, major/minor capsid proteins, and a tail length measure protein), host lysis proteins (a holin and an endolysin), and DNA replication and modification proteins (a thymidylate synthase, a nucleoside triphosphatase, a DNA polymerase, a resolvase, a glutaredoxin-like protein, a nuclease, and a helicase). No lysogeny-related proteins, such as an integrase or repressors were identified, supporting the notion that PBC1 is a virulent phage. The complete genome sequence of *B. cereus* phage PBC1 is available in GenBank under accession number (JQ619704).

To compare its genome with other phages, phylogenetic analysis based on the amino acid sequence of a terminase large subunit (TerL) and a major capsid protein (MCP) were conducted. Phylogenetic analysis of the TerL showed that the TerL of PBC1 shared a maximum identity (69%) with

that of *B. cereus* phage 250 (GenBank ID: GU229986.1) (**Fig. II-3A**) (Lee and Park, 2010). Although both phages belong to the *Siphoviridae* family and show significant amino acid sequence similarities in the late gene regions, the genome size of PBC1 (41.2 kb) is smaller than that of phage 250 (56.5 kb) **(Fig. II-4)**. Phage 250 is a mitomycin C-induced temperate phage, the genome of which contains two transposase genes; on the other hand, PBC1 is a virulent phage lacking genes associated with lysogeny control, potential virulence, and antibiotic resistance. These results suggest that PBC1 is more appropriate for biocontrol or as a therapeutic agent than phage 250. The TerL in PBC1 showed a 54% amino acid sequence identity with that of *Listeria monocytogenes* phage A006 (GenBank ID: DQ003642) (Dorscht et al., 2009). Considering that TerL is responsible for packaging the phage genome and determining the DNA packaging strategy of the phage (Casjens and Gilcrease, 2009), the terminally redundant and circularly permuted genome of the phage A006 suggest that PBC1 engages in a headful packaging mechanism (Casjens et al., 2005).

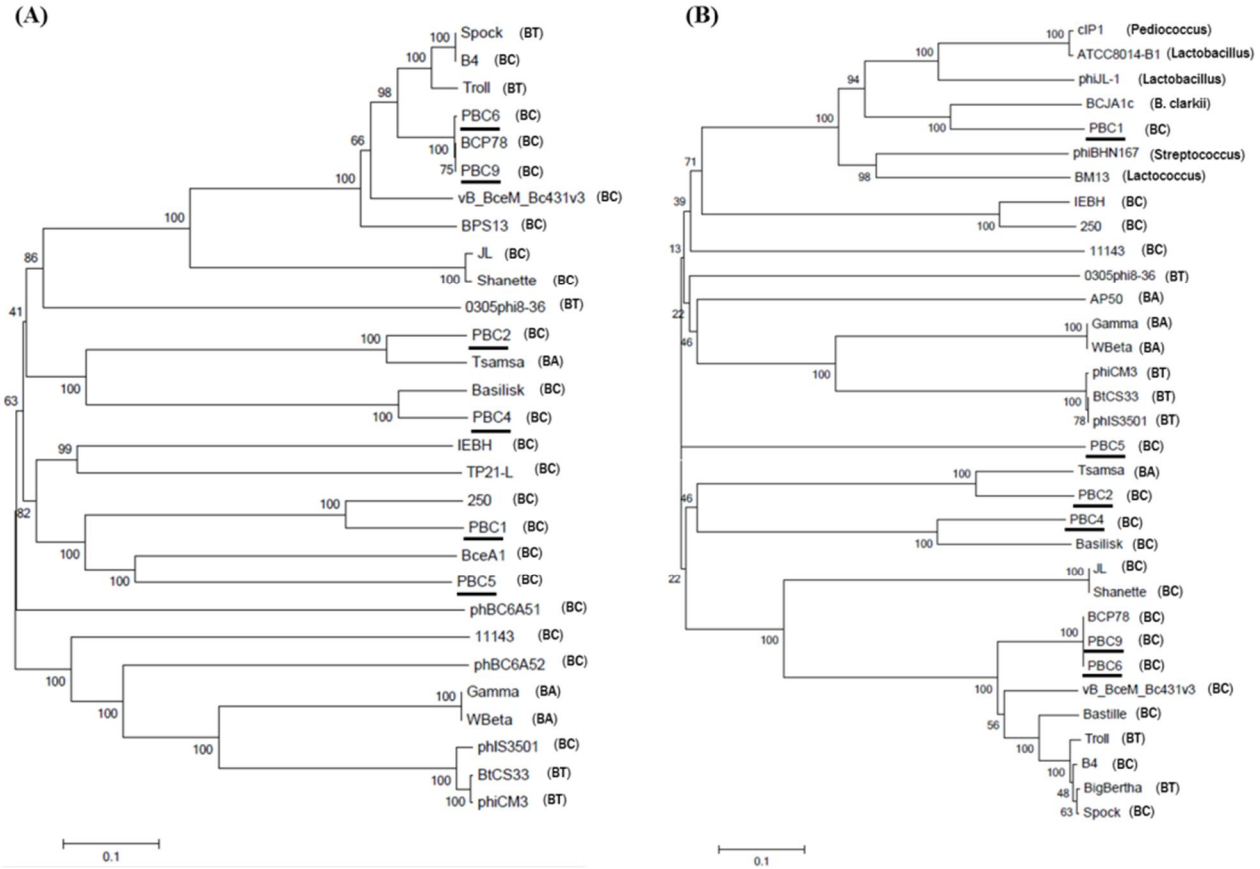
(A)
Spock (BT)
B4 (BC)
Troll (BT)
PBC6 (BC)
BCP78 (BC)
PBC9 (BC)
vB_BceM_Bc431v3 (BC)
BPS13 (BC)
JL (BC)
Shanette (BC)
0305phi8-36 (BT)
PBC2 (BC)
Tsamsa (BA)
Basilisk (BC)
PBC4 (BC)
IEBH (BC)
TP21-L (BC)
250 (BC)
PBC1 (BC)
BceA1 (BC)
PBC5 (BC)
phBC6A51 (BC)
11143 (BC)
phBC6A52 (BC)
Gamma (BA)
WBeta (BA)
phIS3501 (BC)
BtCS33 (BT)
phiCM3 (BT)
0.1
(B)
cIP1 (Pediococcus)
ATCC8014-B1 (Lactobacillus)
phiJL-1 (Lactobacillus)
BCJA1c (B. clarkii)
PBC1 (BC)
phiBHN167 (Streptococcus)
BM13 (Lactococcus)
IEBH (BC)
250 (BC)
11143 (BC)
0305phi8-36 (BT)
AP50 (BA)
Gamma (BA)
WBeta (BA)
phiCM3 (BT)
BtCS33 (BT)
phIS3501 (BT)
PBC5 (BC)
Tsamsa (BA)
PBC2 (BC)
PBC4 (BC)
Basilisk (BC)
JL (BC)
Shanette (BC)
BCP78 (BC)
PBC9 (BC)
PBC6 (BC)
vB_BceM_Bc431v3 (BC)
Bastille (BC)
Troll (BT)
B4 (BC)
BigBertha (BT)
Spock (BC)
0.1

Fig. II-3. Phylogenetic trees of the terminase large subunits and the major capsid proteins. Comparative phylogenetic analysis of the terminase large subunits (A) and the major capsid proteins (B). The host species is presented in abbreviated form after the name of each phage (BC, *B. cereus*; BA, *B. anthracis*; BT, *B. thuringiensis*). Phages used in this study were underlined. The numbers at the nodes represent the bootstrap probabilities.

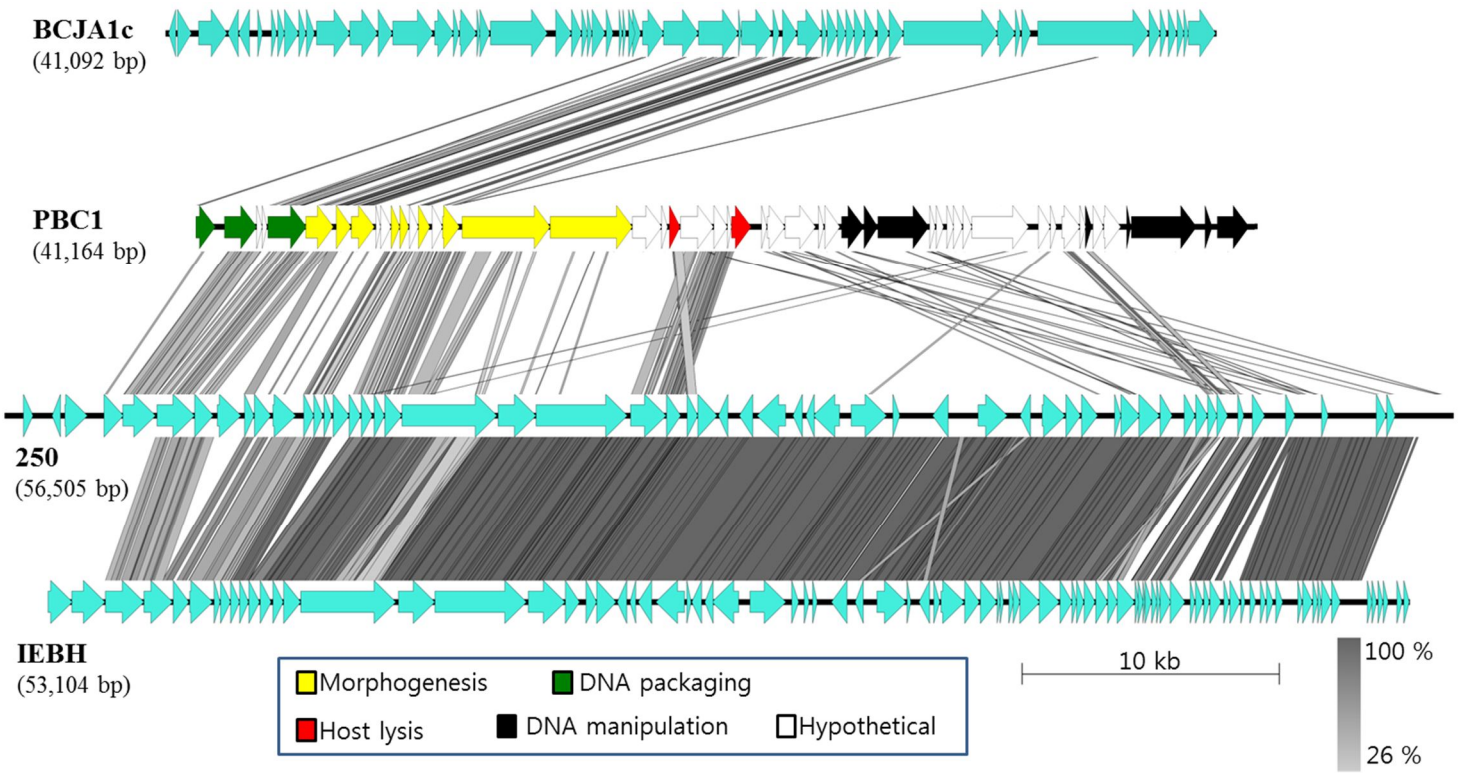
BCJA1c
(41,092 bp)
PBC1
(41,164 bp)
250
(56,505 bp)
IEBH
(53,104 bp)
Morphogenesis
DNA packaging
Host lysis
DNA manipulation
Hypothetical
10 kb
100 %
26 %

Fig. II-4.Alignment of the proteome among the following PBC1-related phages: *B. clarkii* temperate phage BCJA1c, *B. cereus* virulent phage PBC1, *B. cereus* temperate phage vB_BceS-IEBH, and *B. cereus* temperate phage 250. Predicted ORFs are denoted by arrows. Shading indicates the degree of amino acid sequence identity of the gene products with an identity >26%. To facilitate the genome comparison, the genome of IEBH was rearranged commencing with the small terminase gene.

Phylogenetic analysis of the MCP revealed that the MCP of PBC1 (gp8) showed low homology (less than 15%) with other MCPs of the *B. cereus* group phages **(Fig. II-3B)**. Instead, the MCP of PBC1 displayed the highest homology (67% identity) with the MCP of *B. clarkii* temperate phage BCJA1c (GenBank ID: AY616446) (Kropinski et al., 2005). The alkaliphilic *Siphoviridae* phage BCJA1c shares similar morphology, genome length (~ 41 kb), and a mol% G+C content (41.7) with PBC1. As shown in **Fig. II-4**, a portal protein and other structural proteins of PBC1 also showed significant homology with those of the BCJA1c. Interestingly, the MCP of PBC1 exhibited considerable homology with the MCPs from phages of lactic acid bacteria, such as *Lactobacillus* phage ATCC 8014-B1 (50% identity), *Pediococcus* phage cIP1 (50% identity), *Lactobacillus* phage phiJL-1 (48% identity), and *Lactococcus* phage BM13 (44% identity). These results demonstrate that phage PBC1 has distinct characteristics compared to other phages of the *B. cereus* group. Phylogenetic analysis of TerL and MCP of PBC1 prompted me to make whole genome comparisons among PBC1-related phages at the protein level. Note that genome comparison at the DNA level did not identify any genes with significant similarity (data not shown). The structural proteins, including head and tail morphogenesis protein, of

PBC1 showed significant similarity with those of the phage 250 and *B. cereus* temperate phage vB_BceS-IEBH (GenBank ID: NC_011167), which shares more than 98% DNA sequence identity with phage 250 (Smeesters et al., 2011). Interestingly, while the holins of PBC1 and phage 250 share significant homology (55% identity), their endolysins showed only limited amino acid sequence similarity (14% identity).

II-3-3-2. PBC2

Compete genomic analysis revealed that the PBC2 contains 168,689 bp including 251 ORFs and 17 tRNAs **(Fig. II-5)**, which is the second largest sequenced *Bacillus* siphovirus following *B. anthracis* phage vB_BanS_Tsamsa, which has 168,876 bp (Ganz et al., 2014). As shown in **Fig. II-6**, both PBC2 and Tsamsa phages demonstrated similar genomic structure and high nucleotide identity. The genes encoding putative tail structure and packaging module of PBC2 also showed significant similarity to those of *Lactococcus lactis* phage 949, which has a very long noncontractile tail (Samson and Moineau, 2010), implying the possible roles of those genes in phage morphology. PBC2 has three integrase or

recombinase enzymes, indicative of a temperate life style. About 70% of the genome of PBC2 is related to DNA replication, modification and repair, host takeover, and nucleotide metabolism, suggesting that PBC2 largely involved in interaction with host, particularly in replication of phage genome. The large size of tail tape measure protein (2305 aa) corresponds to the exceptionally long tail (500 nm) observed in a TEM image (Belcaid et al., 2011). Interestingly, ORF206, the gene located near tail measure protein, contains a SH3_3 domain (PF08239), which is usually found in phage endolysins as a cell-wall binding domain (Oliveira et al., 2013). This protein may serve as means to access and bind to the receptor on the host cell surface. The endolysin of PBC2 (LysPBC2) shares overall 81% amino acid sequence identity with the endolyisn of Tsamsa and has a conserved amidase_2 domain (PF01510). LysPBC2 also contains two SH3_3 domains (PF08239) at the C-terminus, which presumably functions as a cell wall binding domain. However, the SH3_3 domains in a putative tail protein (ORF206) and an endolysin share only 11% of amino acid sequence identity, suggesting that each SH3_3 domain may recognize different epitopes on the cell wall surface.

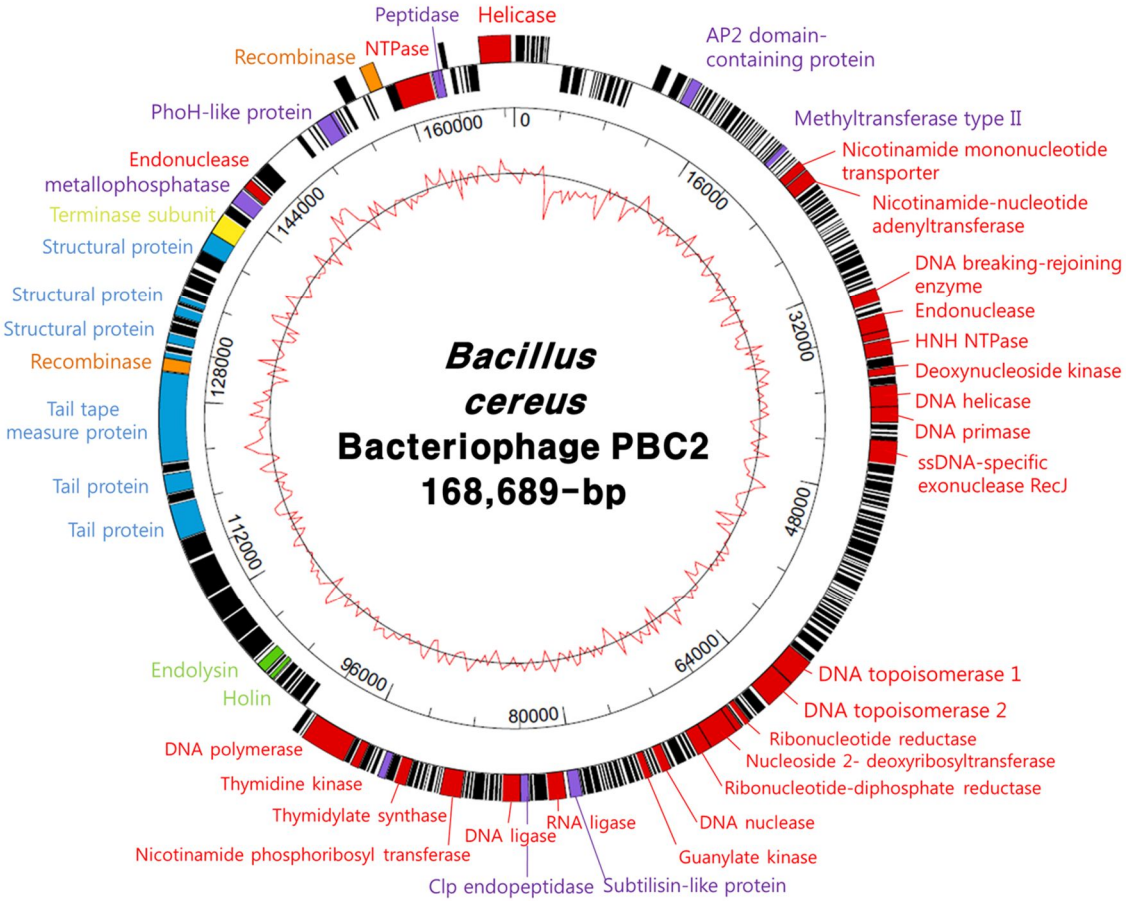
Bacillus cereus
Bacteriophage PBC2
168,689-bp
0
16000
32000
48000
64000
80000
96000
112000
128000
144000
160000
Peptidase
Helicase
Recombinase
NTPase
PhoH-like protein
Endonuclease metallophosphatase
Terminase subunit
Structural protein
Structural protein
Structural protein
Recombinase
Tail tape measure protein
Tail protein
Tail protein
Endolysin
Holin
DNA polymerase
Thymidine kinase
Thymidylate synthase
Nicotinamide phosphoribosyl transferase
DNA ligase
RNA ligase
Clp endopeptidase
Subtilisin-like protein
DNA nuclease
Guanylate kinase
Ribonucleotide-diphosphate reductase
Nucleoside 2- deoxyribosyltransferase
Ribonucleotide reductase
DNA topoisomerase 2
DNA topoisomerase 1
ssDNA-specific exonuclease RecJ
DNA primase
DNA helicase
Deoxynucleoside kinase
HNH NTPase
Endonuclease
DNA breaking-rejoining enzyme
Nicotinamide-nucleotide adenyltransferase
Nicotinamide mononucleotide transporter
Methyltransferase type II
AP2 domain-containing protein

Fig. II-5. **Genome map of *B. cereus* phage PBC2.** Outer circle indicates the gene coding regions by strand. The color of each gene refers to the functional categories such as phage structure (blue), DNA packaging (yellow), host lysis (green), nucleotide metabolism (red), integrase (orange), and additional function (purple). The inner circle with red line indicates the G+C content. Scale unit is base pair.

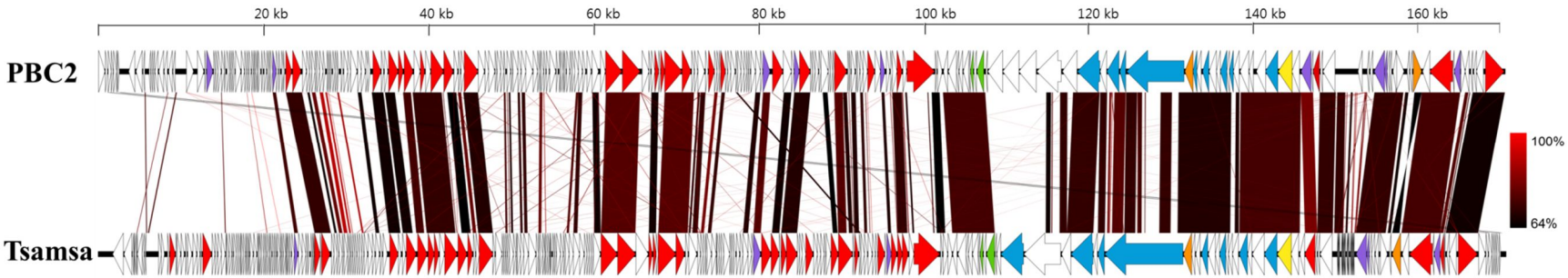

Fig. II-6. Comparative genomic analysis of PBC2 and Tsamsa. DNA-level alignment of the genomes of phage PBC2 and Tsamsa, the largest sequenced *Bacilus* siphovirus (168,876 bp). Predicted ORFs are denoted by arrows and the color of each gene refers to the functional categories such as phage structure (blue), DNA packaging (yellow), host lysis (green), nucleotide metabolism (red), integrase (orange), and additional function (purple). The regions with at least 64% nucleotide identity are indicated by shaded bars.

II-3-3-3. PBC4

The genome of phage PBC4 is a double-stranded DNA consisting of 80,647 bp of nucleotides with G+C contents of 34% **(Fig. II-7)**. Bioinformatical analysis revealed that the PBC4 genome has 137 ORFs and two tRNAs. The predicted ORFs were classified into six different groups according to their function; phage DNA packaging, virion structure, host lysis, DNA manipulation, additional function and hypothetical protein. The existence of a putative integrase gene in the genome suggests that PBC4 is a temperate phage having both lytic and lysogenic life cycles. Although a major capsid protein (MCP) was not identified by sequence analysis, ORF06 could be predicted as MCP because it showed high sequence identity (71 %) with that of *B. cereus* phage Basilisk, whose MCP was experimentally proven (Grose et al., 2014). A putative terminase large subunit (TerL) belonging to terminase_1 superfamily was identified, but a small subunit of terminase encoding gene was not found. Among the predicted phage's structural proteins, the presence of a putative tail fiber protein (ORF21) corresponds to a short tail fiber observed in a TEM image (**Fig. II-1**).

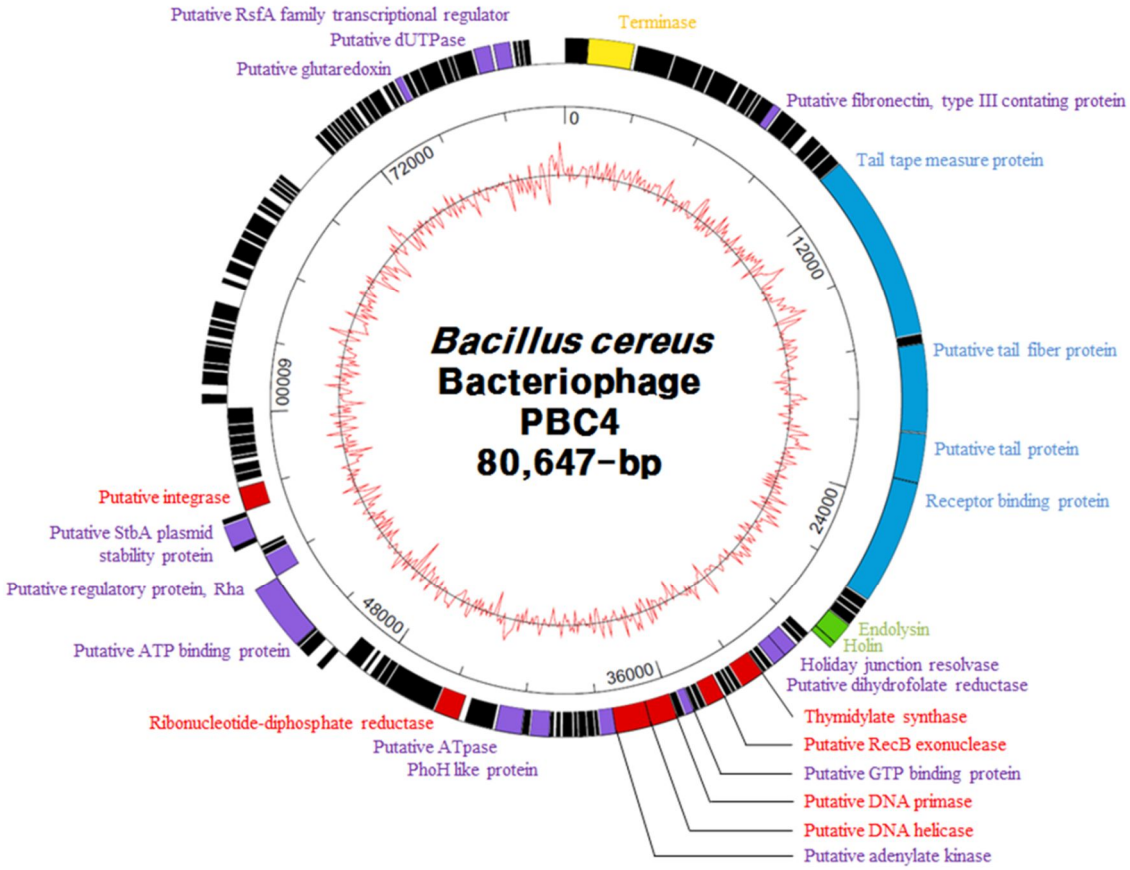
Bacillus cereus
Bacteriophage
PBC4
80,647-bp
0
12000
24000
36000
48000
60000
72000
Terminase
Putative fibronectin, type III contating protein
Tail tape measure protein
Putative tail fiber protein
Putative tail protein
Receptor binding protein
Endolysin
Holin
Holiday junction resolvase
Putative dihydrofolate reductase
Thymidylate synthase
Putative RecB exonuclease
Putative GTP binding protein
Putative DNA primase
Putative DNA helicase
Putative adenylate kinase
Ribonucleotide-diphosphate reductase
Putative ATpase
PhoH like protein
Putative ATP binding protein
Putative regulatory protein, Rha
Putative StbA plasmid stability protein
Putative integrase
Putative glutaredoxin
Putative dUTPase
Putative RsfA family transcriptional regulator

Fig. II-7. **Genome map of *B. cereus* phage PBC4.** Outer circle indicates the gene coding regions by strand. The color of each gene refers to the functional categories such as phage structure (blue), DNA packaging (yellow), host lysis (green), nucleotide metabolism (red), and additional function (purple). The inner circle with red line indicates the G+C content. Scale unit is base pair.

The comparative analysis of genomes between PBC4 and Basilisk revealed that they are closely-related phages as they share a 83.3% average nucleotide identity over the entire genome with the same architectures **(Fig. II-8)**. This is also evident from a phylogenetic tree based on TerL and MCP, which clearly showed PBC4 and Basilisk belong to the same subgroup **(Fig. II-3)**. Interestingly, although the late gene products, such as terminase, structural proteins, lysis-related proteins of PBC4 and Basilisk demonstrated high sequence homology, their putative tail fiber proteins showed relatively low sequence identity. Also, Basilisk has a putative chitinase adjacent to a tail fiber protein, whereas PBC4 does not possess the chitinase. Considering that tail fiber proteins of phages have been known to determine the host range of phages (Le et al., 2013), the host specificity of the two *B. cereus* phages might be different to each other.

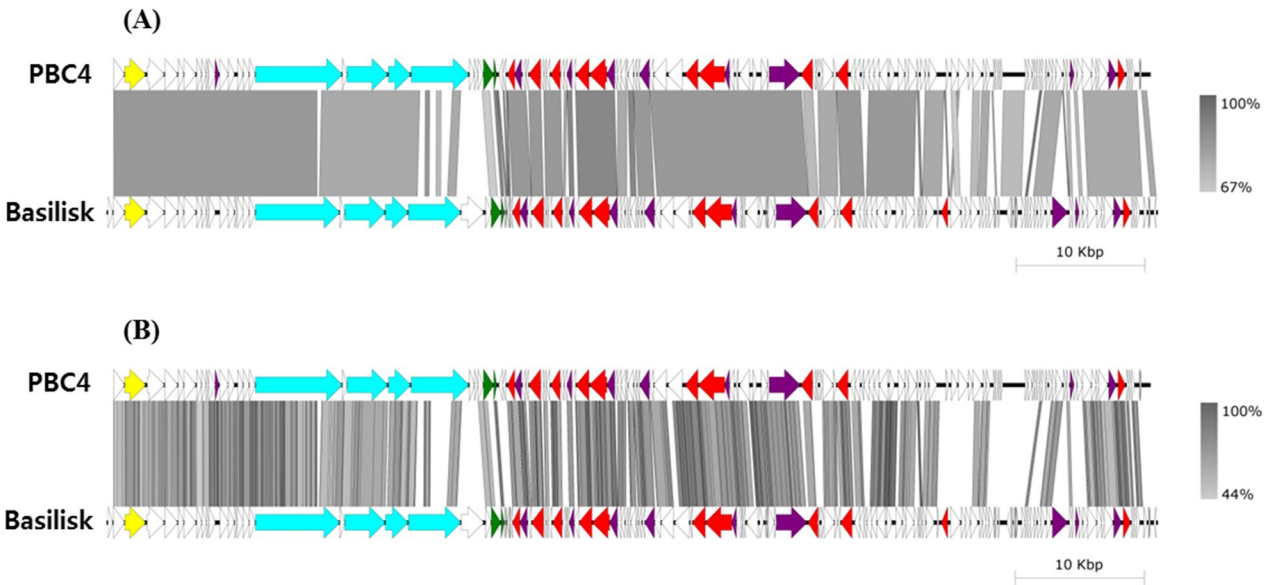

Fig. II-8. Comparative genomic analysis of PBC4 and Basilisk. Comparative genome analysis between phage PBC4 and Basilisk on nucleotide sequence level (A) and amino acid sequence level (B). Each color of ORF indicates its function; yellow, packaging; blue, structural genes; green, host lysis; red, DNA manipulation; purple, additional function; white, hypothetical genes. The genome sequence of phage Basilisk was rearranged for better visualization.

II-3-3-4. PBC5

The genome sequence of PBC5 is 56,332 bp in length **(Fig. II-9)**. The GC content is 40.3%, higher than published genome sequences of *B. cereus* (about 35%). A total of 95 ORFs were predicted, where 66 ORFs were assigned as unknown function. PBC5 has two copies of gamma-glutamyl cyclotrasferases and a glutaredoxin protein, indicating that PBC5 is involved in host glutathione homeostasis (Oakley et al., 2008). Interestingly, PBC5 harbors beta-lactamase inhibitor protein in its genome. Although many phages have been known to possess beta-lactamase genes and contribute to spread of these antibiotic resistance genes (Muniesa et al., 2004), phages encoding beta-lactamase inhibitor genes are very unusual case. Further study will elucidate the exact role of this gene in PBC5. PBC5 appears to be a virulent phage as it does not have lysogeny-related genes such as repressors and site-specific integrases. However, PBC5 harbors a putative dUTPase (ORF069), which has been shown to control transfer of virulence genes (Payne and Elder, 2001; Tormo-Mas et al., 2013), so adequate studies are required prior to use of PBC5 as a biocontrol agent.

Phylogenetic trees reveal that the TerL and MCP of PBC5 showed a low degree of homology to those from other reported *B. cereus* phages **(Fig.**

II-3), suggesting that PBC5 is a novel phage. PBC5 contains a putative endolysin (ORF029) to degrade the host cell wall. The endolysin only has a glycoside hydrolase family 25 domain (PF01183) at the N-terminus, whereas there is no apparent cell wall binding domain at the C-terminus. BLASTP analysis revealed that the endolysin of PBC5 is related to bacterial autolysins, rather than phage endolysins, proposing a novelty of this endolysin. A putative holin, typically accompanied by an endolysin for host lysis, was not identified by sequence comparison. These results suggest that this novel endolysin of PBC5 may offer potential tools for biocontrol of *B. cereus*.

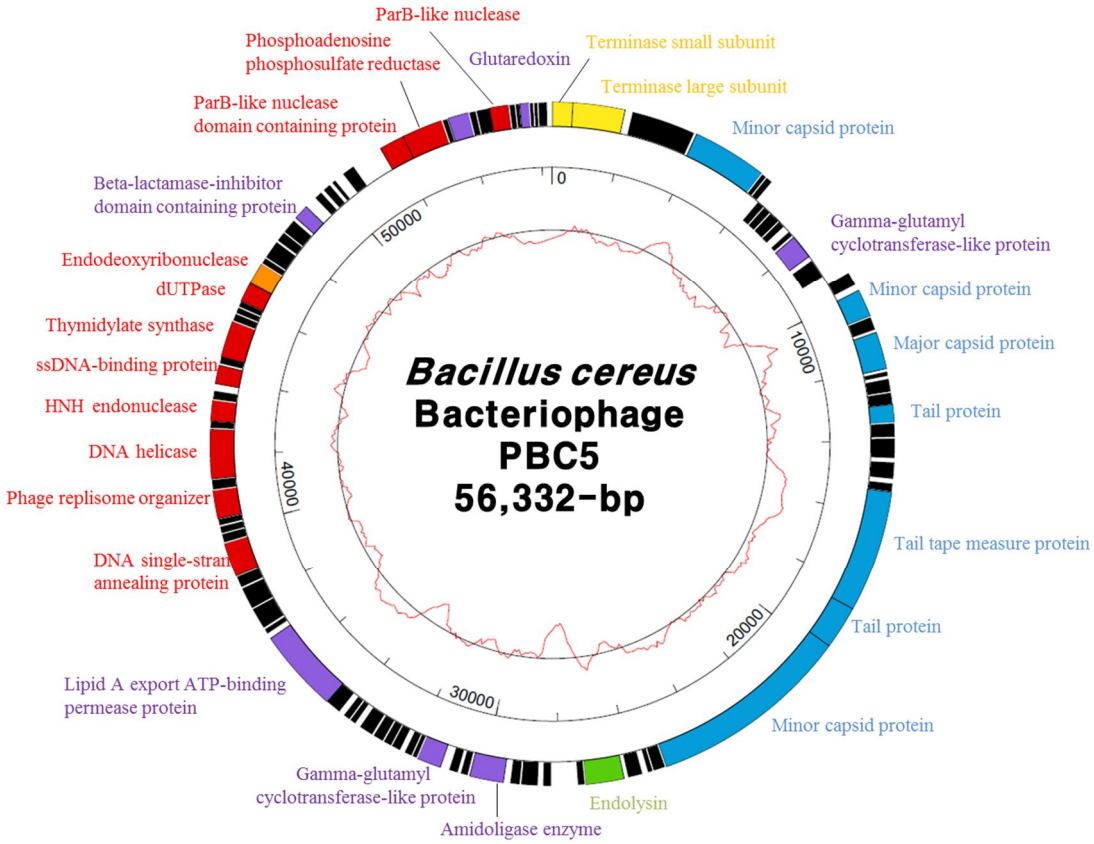
ParB-like nuclease
Phosphoadenosine phosphosulfate reductase
Glutaredoxin
Terminase small subunit
Terminase large subunit
ParB-like nuclease domain containing protein
Minor capsid protein
Beta-lactamase-inhibitor domain containing protein
Gamma-glutamyl cyclotransferase-like protein
Endodeoxyribonuclease
dUTPase
Minor capsid protein
Thymidylate synthase
Major capsid protein
ssDNA-binding protein
Tail protein
HNH endonuclease
DNA helicase
Tail tape measure protein
Phage replisome organizer
DNA single-strand annealing protein
Tail protein
Lipid A export ATP-binding permease protein
Minor capsid protein
Gamma-glutamyl cyclotransferase-like protein
Endolysin
Amidoligase enzyme
0
10000
20000
30000
40000
50000
Bacillus cereus
Bacteriophage
PBC5
56,332-bp

Fig. II-9. **Genome map of *B. cereus* phage PBC5.** Outer circle indicates the gene coding regions by strand. The color of each gene refers to the functional categories such as phage structure (blue), DNA packaging (yellow), host lysis (green), nucleotide metabolism (red), and additional function (purple). The inner circle with red line indicates the G+C content. Scale unit is base pair.

II-3-3-5. PBC6 and PBC9

The complete genome of *B. cereus* phage PBC6 showed a 157,147 bp-length with a GC content of 39.9%, 227 ORFs, and 17 tRNAs **(Fig. II-10)**. This phage genome encodes a packaging and structural proteins, such as a terminase, a major capsid protein, minor structural proteins, tail fiber proteins, baseplate proteins, a tail sheath protein, a portal protein, tail lysins, and an adsorption associated tail protein. ORF203 and ORF205 are putative tail lysins having an endopeptidase (NLPC/P60, PF00877) domain and a glucosaminidase (PF01832) domain, respectively at their C-terminus. These tail lysins may play an important role in the efficient phage genome penetration of thick peptidoglycan layer of *B. cereus* at the initiation of infection (Moak and Molineux, 2004). PBC6 also encodes an endolysin and a holin for host cell lysis at the late stage of phage infection. In addition, PBC6 encodes many DNA manipulation proteins (DNA polymerase, HNH endonuclease, helicase, exonuclease, primase, recombinase) and additional functions (protease, phosphoesterase, thioredoxin, dUTPase, FtsK/SpoIIIE family protein, RNA polymerase sigma factors). Although PBC6 lacks lysogeny-related determinants, it possesses several genes that can contribute to pathogenenic and fitness traits of the host. PBC6 harbors a PhoH-like

protein (ORF018) that may promote bacterial survival under conditions of phosphate starvation (Kim et al., 1993), and a FtsK/SpoIIIE family protein (ORF096) which may be involved in host sporulation and ecological adaption of the host (Schuch and Fischetti, 2006). It is interesting to note that this FtsK/SpoIIIE family protein was highly conserved in *Spounavirinae* subfamily of *Bacillus* phages. Further experiments are needed to investigate the exact role of this protein in *Spounavirinae* phages.

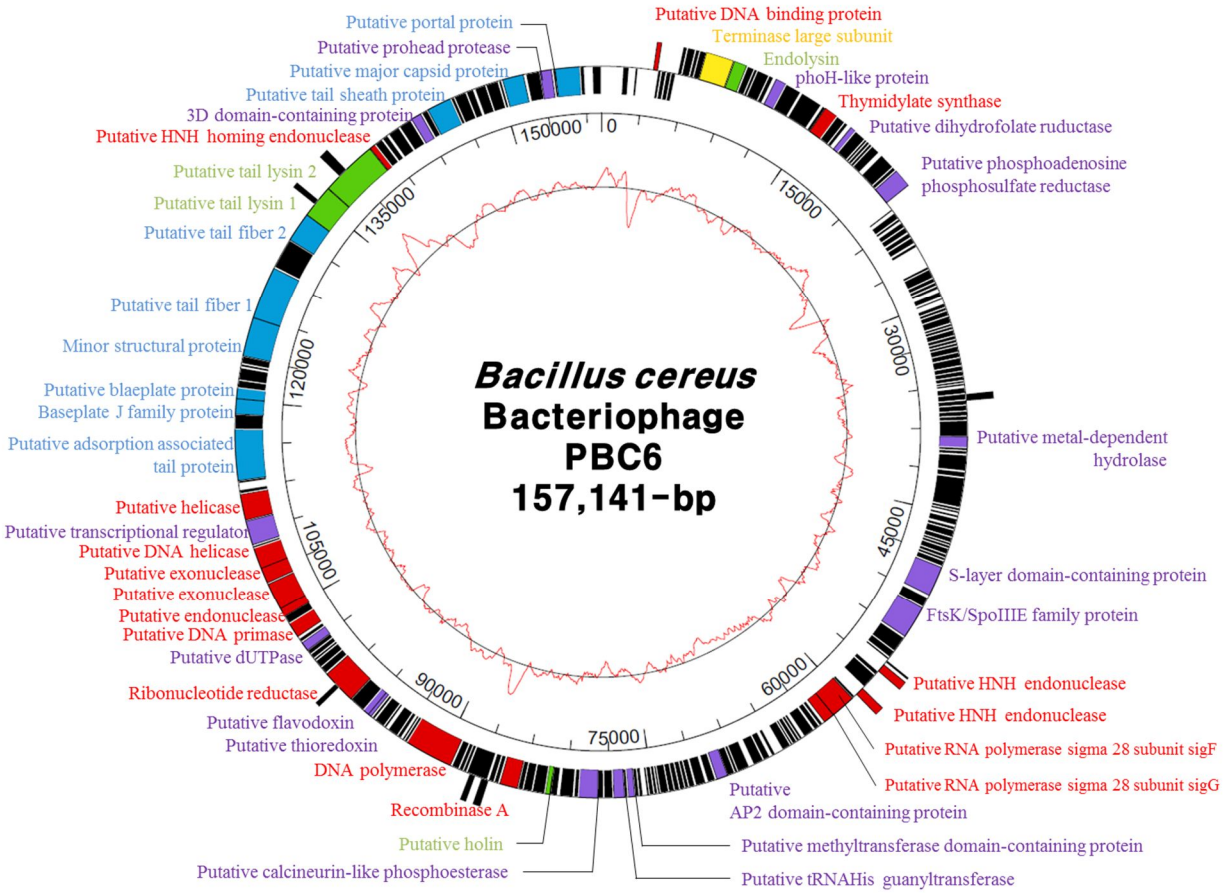
Bacillus cereus
Bacteriophage
PBC6
157,141-bp
0
15000
30000
45000
60000
75000
90000
105000
120000
135000
150000
Putative DNA binding protein
Terminase large subunit
Endolysin
phoH-like protein
Thymidylate synthase
Putative dihydrofolate ruductase
Putative phosphoadenosine phosphosulfate reductase
Putative metal-dependent hydrolase
S-layer domain-containing protein
FtsK/SpoIIIE family protein
Putative HNH endonuclease
Putative HNH endonuclease
Putative RNA polymerase sigma 28 subunit sigF
Putative RNA polymerase sigma 28 subunit sigG
Putative AP2 domain-containing protein
Putative methyltransferase domain-containing protein
Putative tRNAHis guanyltransferase
Putative holin
Putative calcineurin-like phosphoesterase
Recombinase A
DNA polymerase
Putative flavodoxin
Putative thioredoxin
Ribonucleotide reductase
Putative dUTPase
Putative DNA primase
Putative endonuclease
Putative exonuclease
Putative exonuclease
Putative DNA helicase
Putative transcriptional regulator
Putative helicase
Putative adsorption associated tail protein
Baseplate J family protein
Putative blaeplate protein
Minor structural protein
Putative tail fiber 1
Putative tail fiber 2
Putative tail lysin 1
Putative tail lysin 2
Putative HNH homing endonuclease
3D domain-containing protein
Putative tail sheath protein
Putative major capsid protein
Putative prohead protease
Putative portal protein

Fig. II-10. **Genome map of *B. cereus* phage PBC6.** Outer circle indicates the gene coding regions by strand. The color of each gene refers to the functional categories such as phage structure (blue), DNA packaging (yellow), host lysis (green), nucleotide metabolism (red), and additional function (purple). The inner circle with red line indicates the G+C content. Scale unit is base pair.

The genome of *B. cereus* phage PBC9 was also sequenced and annotated. PBC9 contains 156,179 bp of double-stranded DNA, with 229 ORFs and 17 tRNAs. The genome of PBC9 is almost identical (99.99% average nucleotide identity) to the previously reported genome of *B. cereus* phage BCP78 (Lee et al., 2012) **(Fig. II-11**). Comparative genomic analysis also revealed PBC9 and PBC6 as highly similar phages (94.94%), consequently, both phages can be assigned as BCP78-like phages. Their morphological and genetic characteristics suggest that both PBC6 and PBC9 are the members of the newly proposed Bastille group within the *Spounavirinae* subfamily (Barylski et al., 2014; Klumpp et al., 2010). The most strikingly difference between the genome of PBC6 and PBC9 is a region encoding a minor structural protein (ORF199) and a tail fiber protein 1 (ORF200). Considering that the host ranges of PBC6 and PBC9 are different **(Table II-2)**, these two proteins may be essential components for determining host specificity of phage PBC6 and PBC9.

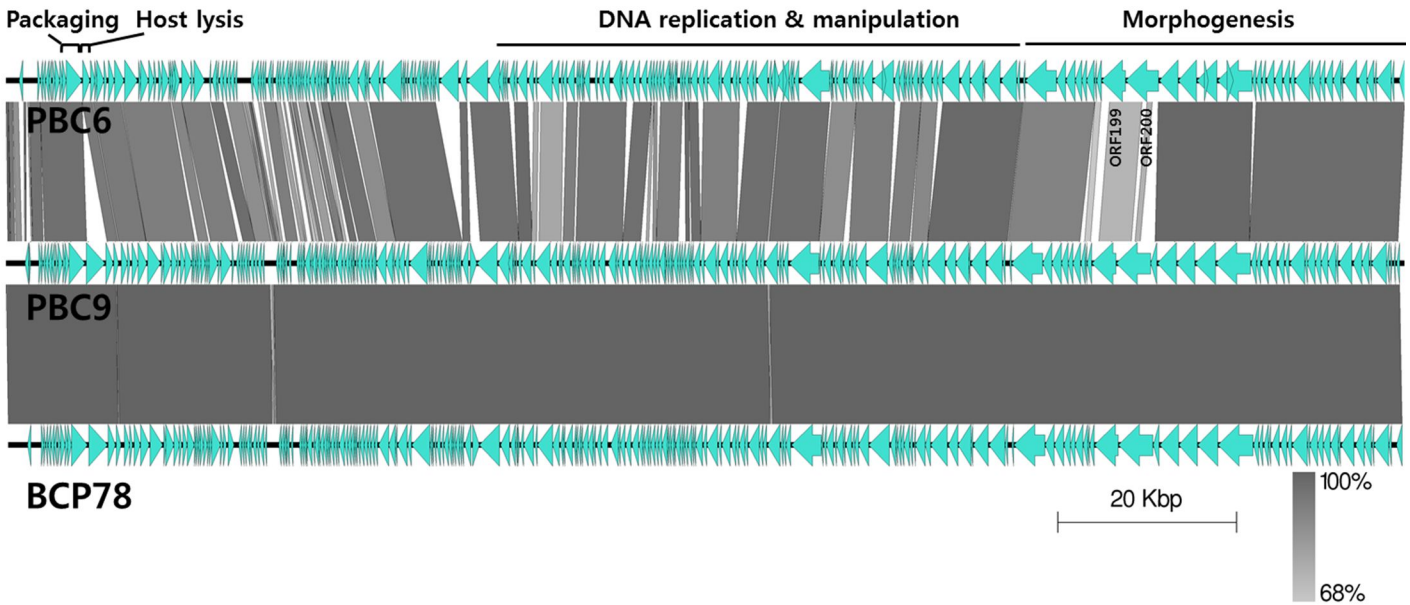

Fig. II-11. Comparative genomic analysis of PBC6, PBC9 and BCP78. DNA-level alignment of the genomes of phage PBC6, PBC9, and BCP78. Predicted ORFs are denoted by arrows and the regions with at least 68% nucleotide identity are indicated by shaded bars.

II-3-3-6. General features of *B. cereus* phage genomes

The complete genome sequences of six double-stranded DNA *B. cereus* phages were determined and studied in silico. Of the *Siphoviridae*, PBC1 has the smallest genome, of 41.2 kb, followed by PBC5 (56.3 kb), PBC4 (80.6 kb), and PBC2 (168.7 kb). The genomes of the highly related *Myovidae* phages PBC6 and PBC9 are 157.1 and 157.2 kb, respectively. The G+C contents of the isolated *B. cereus* phages cover wide range from 34 mol% to 41.7 mol%. Particularly, PBC1 contains a G+C content of 41.7 mol%, which is the highest value among the reported *B. cereus* phages so far. The giant siphovirus PBC2 is closely related to the *B. anthracis* phage Tsamsa, while PBC4 showed high similarity to the *B. cereus* phage Basilisk over the entire genome. PBC1 and PBC5 seemed to be novel *B. cereus* phage as they showed a very low degree of homology to previously reported phages.

Genome analysis revealed that the phage PBC1 is the only virulent phage that lacks virulence and antibiotic resistance determinants among the isolated *B. cereus* phages. PBC1 has very narrow host specificity, and consequently, PBC1 alone would not be an efficient biocontrol agent against diverse strains of *B. cereus*. However, as mentioned above, PBC1 can infect a *B. cereus* strain (ATCC 21768) that is not killed by other phages, so I

suspected that PBC1 could be a potential candidate for an effective phage cocktail lytic for *B. cereus*. Therefore, I further characterized PBC1.

II-3-4. One-step growth curve of the phage PBC1

The one-step growth kinetics of PBC1 indicated that PBC1 has an eclipse period time of 10 min, a latent period time of 20 min and a burst size of 45 PFU/infected cell when infecting its host bacteria *B. cereus* ATCC 21768 (**Fig. II-12**).

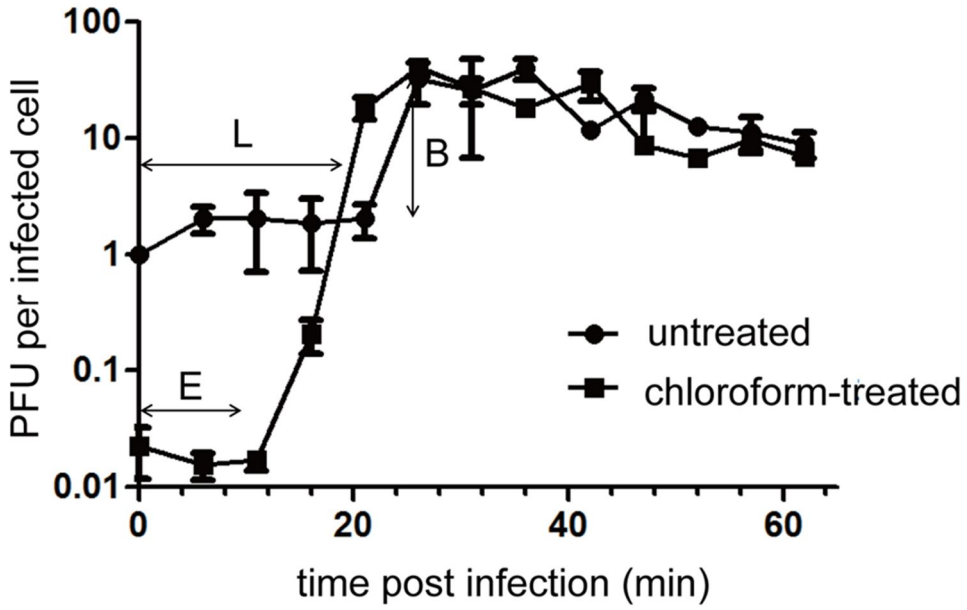

Fig. II-12. One-step growth curve of PBC1. E, eclipse period; L, latent period; B, burst size. Means with standard deviations (SD) of three independent assays are given.

II-3-5. Inhibition of *B. cereus* growth by the phage PBC1 in liquid culture and boiled rice

To evaluate the ability of PBC1 to lyse host bacteria in broth, I performed a host growth inhibition assay in the presence of PBC1. PBC1 inhibited bacterial growth, and the inhibition patterns were dependent on the added phage concentrations (**Fig. II-13A**). After an infection of *B. cereus* ATCC 21768 with 10^{10} PFU/ml of PBC1 (MOI of 10), the host bacteria were lysed rapidly, and clear lysate-containing cell debris was formed only after 30 min. With 10^{8} PFU/ml of PBC1 (MOI of 0.1), host growth inhibition was observed 1.5 h after phage infection, and the broth culture became clear approximately 2 h after infection. However, the growth inhibition only lasted approximately 5 h and regrowth occurred regardless of MOI even though growth inhibition started faster with high MOI **(Fig. II-13A)**. Several isolates from the re-growth culture showed PBC1 insensitivity, indicating that PBC1-resistant mutants were generated. These results showed that phage infection with an MOI of 10 efficiently lysed host bacteria, whereas phage-resistant mutants appeared more rapidly than during infection with an MOI of 0.1. It has been stated that increasing phage inoculum density could lead to increased emergence of mutant bacteria by limiting the opportunity for

reproduction of mutant phage variants (Kysela and Turner, 2007). These results led to the conclusion that the appropriate MOI should be considered for the successful use of PBC1 for biocontrol purposes. To confirm the lytic activity of PBC1 in foods, *B. cereus* and PBC1 were added to boiled rice and bacterial growth was monitored. Since several studies showed the efficacy of high concentration of phage for food control purposes (Bigwood et al., 2009; Guenther et al., 2009), I used a sufficiently high concentration (10^8 PFU/ml) of PBC1 in the assay. As shown in **Fig. II-13B**, no viable cells were detected from phage-treated samples, indicating that phage PBC1 was very effective in preventing the growth of *B. cereus* ATCC 21768 in boiled rice. In addition, prolonged incubation time did not neutralize the lytic activity of phage, suggesting that the virulent phage PBC1 could be a useful component for the development of a phage cocktail against *B. cereus*.

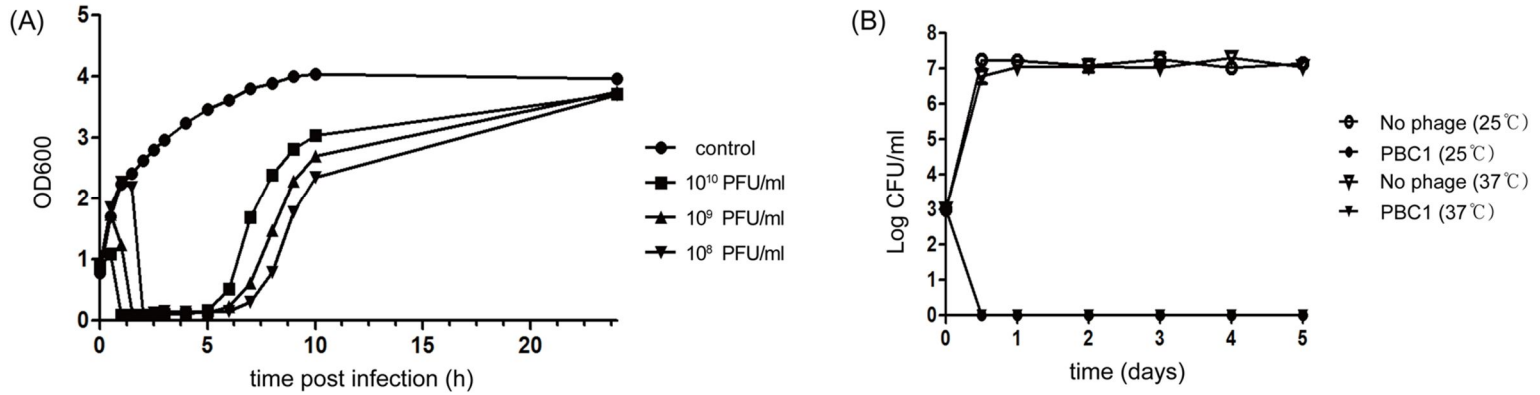

Fig. II-13. Bacterial challenge test of PBC1 with *B. cereus* ATCC 21768. (A) PBC1 inhibited the growth of *B. cereus* in liquid medium. The growth inhibition pattern was dependent on the amount of phages added. Non-PBC1-infected cells (circle) are shown as a control. (B) Boiled rice samples were spiked with bacteria (1 x 10^3 CFU/ml), and PBC1 (1 x 10^8 PFU/ml) was applied to the samples. Treated samples were stored at different temperatures of incubation and the concentration of viable cells was determined at time points indicated.

II-3-6. The PBC1 phage binds to a carbohydrate moiety of *B. cereus* ATCC 21768.

With 10 mM of calcium and magnesium chloride, the majority (~90%) of PBC1 particles were found to be attached to the bacteria after 15 min of incubation **(Fig. II-14A)**. To explain the narrow host specificity of PBC1, five different *B. cereus* strains were used for the PBC1 adsorption assay **(Fig. II-14B)**. Among the five *B. cereus* strains, only the *B. cereus* ATCC 21768 strain significantly adsorbed the PBC1 phage ($P<0.05$). Treatments of bacteria with periodate or proteinase K before phage adsorption assay revealed that PBC1 may use carbohydrate structure as a phage receptor. As seen in **Fig. II-14C**, treatment with periodate, which cleaves saccharide rings with vicinal diols (Sorensen et al., 2011), reduced phage binding, whereas treatment with proteinase K did not affect the binding of PBC1 to the cell surface. Although further studies are needed to identify the exact PBC1 receptor of the host, these results suggest that the host strain, *B. cereus* ATCC 21768, has a distinct carbohydrate structure on its cell surface that is used by PBC1 as a phage receptor.

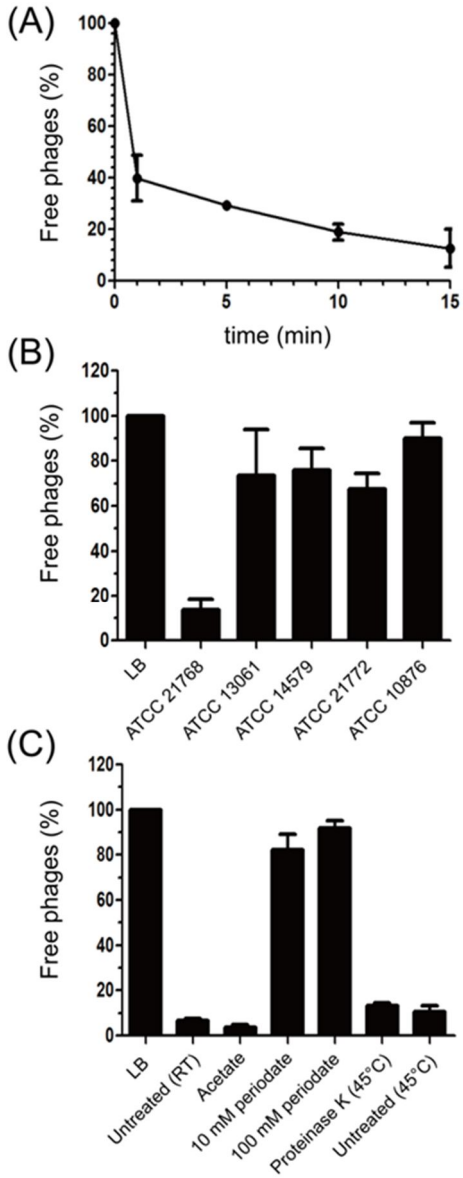
(A)
Free phages (%)
100
80
60
40
20
0
0
5
10
15
time (min)
(B)
Free phages (%)
120
100
80
60
40
20
0
LB
ATCC 21768
ATCC 13061
ATCC 14579
ATCC 21772
ATCC 10876
(C)
Free phages (%)
120
100
80
60
40
20
0
LB
Untreated (RT)
Acetate
10 mM periodate
100 mM periodate
Proteinase K (45°C)
Untreated (45°C)

Fig. II-14. PBC1 adsorption assay. (A) The majority (~90%) of PBC1 particles were adsorbed into *B. cereus* ATCC 21768 within 15 min. (B) PBC1 adsorption into different *B. cereus* strains showed that PBC1 specifically bound to the host strain, *B. cereus* ATCC 21768. LB media without bacterial cells was used as a control (LB), and the treatments are indicated below the columns. (C) PBC1 binding was inhibited by periodate treatment of the host cell, whereas proteinase K treatment did not affect phage adsorption. The means with SDs of three independent assays are given.

II-4. References

Ackermann, H.W., (2003) Bacteriophage observations and evolution. Res. Microbiol. 154, 245-251.

Ackermann, H.W., (2007) 5500 Phages examined in the electron microscope. Arch. Virol. 152, 227-243.

Altschul, S.F., Gish, W., Miller, W., Myers, E.W., Lipman, D.J., (1990) Basic local alignment search tool. J. Mol. Biol. 215, 403-410.

Bandara, N., Jo, J., Ryu, S., Kim, K.P., (2012) Bacteriophages BCP1-1 and BCP8-2 require divalent cations for efficient control of Bacillus cereus in fermented foods. Food microbiology 31, 9-16.

Baptista, C., Santos, M.A., Sao-Jose, C., (2008) Phage SPP1 reversible adsorption to Bacillus subtilis cell wall teichoic acids accelerates virus recognition of membrane receptor YueB. J. Bacteriol. 190, 4989-4996.

Barylski, J., Nowicki, G., Gozdzicka-Jozefiak, A., (2014) The discovery of phiAGATE, a novel phage infecting Bacillus pumilus, leads to new insights into the phylogeny of the subfamily Spounavirinae. PLoS One 9, e86632.

Belcaid, M., Bergeron, A., Poisson, G., (2011) The evolution of the tape measure protein: units, duplications and losses. BMC Bioinformatics 12 Suppl 9, S10.

Besemer, J., Lomsadze, A., Borodovsky, M., (2001) GeneMarkS: a self-training method for prediction of gene starts in microbial genomes. Implications for finding sequence motifs in regulatory regions. Nucleic Acids Res. 29, 2607-2618.

Bigwood, T., Hudson, J.A., Billington, C., (2009) Influence of host and bacteriophage concentrations on the inactivation of food-borne pathogenic bacteria by two phages. FEMS Microbiol. Lett. 291, 59-64.

Brussow, H., Hendrix, R.W., (2002) Phage genomics: small is beautiful. Cell 108, 13-16.

Casjens, S.R., Gilcrease, E.B., (2009) Determining DNA packaging strategy by analysis of the termini of the chromosomes in tailed-bacteriophage virions. Methods Mol. Biol. 502, 91-111.

Casjens, S.R., Gilcrease, E.B., Winn-Stapley, D.A., Schicklmaier, P., Schmieger, H., Pedulla, M.L., Ford, M.E., Houtz, J.M., Hatfull, G.F., Hendrix, R.W., (2005) The generalized transducing Salmonella bacteriophage ES18: complete genome sequence and DNA packaging strategy. J. Bacteriol. 187, 1091-1104.

Comeau, A.M., Hatfull, G.F., Krisch, H.M., Lindell, D., Mann, N.H., Prangishvili, D., (2008) Exploring the prokaryotic virosphere. Res. Microbiol. 159, 306-313.

Delcher, A.L., Bratke, K.A., Powers, E.C., Salzberg, S.L., (2007) Identifying bacterial genes and endosymbiont DNA with Glimmer. Bioinformatics 23, 673-679.

Dorscht, J., Klumpp, J., Bielmann, R., Schmelcher, M., Born, Y., Zimmer, M., Calendar, R., Loessner, M.J., (2009) Comparative Genome Analysis of Listeria Bacteriophages Reveals Extensive Mosaicism, Programmed Translational Frameshifting, and a Novel Prophage Insertion Site. J. Bacteriol. 191, 7206-7215.

El-Arabi, T.F., Griffiths, M.W., She, Y.M., Villegas, A., Lingohr, E.J., Kropinski, A.M., (2013) Genome sequence and analysis of a broad-host range lytic bacteriophage that infects the Bacillus cereus group. Virol J. 10, 48.

Fouts, D.E., Rasko, D.A., Cer, R.Z., Jiang, L.X., Fedorova, N.B., Shvartsbeyn, A., Vamathevan, J.J., Tallon, L., Althoff, R., Arbogast, T.S., Fadrosh, D.W., Read, T.D., Gill, S.R., (2006) Sequencing Bacillus anthracis typing phages Gamma and Cherry reveals a common ancestry. J. Bacteriol. 188, 3402-3408.

Ganz, H.H., Law, C., Schmuki, M., Eichenseher, F., Calendar, R., Loessner, M.J., Getz, W.M., Korlach, J., Beyer, W., Klumpp, J., (2014) Novel giant siphovirus from Bacillus anthracis features unusual genome characteristics. PLoS One 9, e85972.

Gillis, A., Mahillon, J., (2014a) Phages preying on Bacillus anthracis, Bacillus cereus, and Bacillus thuringiensis: past, present and future. Viruses 6, 2623-2672.

Gillis, A., Mahillon, J., (2014b) Prevalence, genetic diversity, and host range of tectiviruses among members of the Bacillus cereus group. Appl. Environ. Microbiol. 80, 4138-4152.

Grande, M.J., Lucas, R., Abriouel, H., Valdivia, E., Omar, N.B., Maqueda, M., Martinez-Bueno, M., Martinez-Canamero, M., Galvez, A., (2006) Inhibition of toxicogenic Bacillus cereus in rice-based foods by enterocin AS-48. Int. J. Food Microbiol. 106, 185-194.

Grose, J.H., Belnap, D.M., Jensen, J.D., Mathis, A.D., Prince, J.T., Merrill, B.D., Burnett, S.H., Breakwell, D.P., (2014) The genomes, proteomes, and structures of three novel phages that infect the Bacillus cereus group and carry putative virulence factors. J. Virol. 88, 11846-11860.

Guenther, S., Huwyler, D., Richard, S., Loessner, M.J., (2009) Virulent bacteriophage for efficient biocontrol of Listeria monocytogenes in ready-to-eat foods. Appl. Environ. Microbiol. 75, 93-100.

Guinebretiere, M.H., Auger, S., Galleron, N., Contzen, M., De Sarrau, B., De Buyser, M.L., Lamberet, G., Fagerlund, A., Granum, P.E., Lereclus, D., De Vos, P., Nguyen-The, C., Sorokin, A., (2013) Bacillus cytotoxicus sp. nov. is a novel thermotolerant species of the Bacillus cereus Group occasionally associated with food poisoning. International journal of systematic and evolutionary microbiology 63, 31-40.

Hendrix, R.W., Lawrence, J.G., Hatfull, G.F., Casjens, S., (2000) The origins and ongoing evolution of viruses. Trends Microbiol. 8, 504-508.

Jensen, G.B., Hansen, B.M., Eilenberg, J., Mahillon, J., (2003) The hidden lifestyles of Bacillus cereus and relatives. Environ. Microbiol. 5, 631-640.

Kiljunen, S., Datta, N., Dentovskaya, S.V., Anisimov, A.P., Knirel, Y.A., Bengoechea, J.A., Holst, O., Skurnik, M., (2011) Identification of the lipopolysaccharide core of Yersinia pestis and Yersinia pseudotuberculosis as the receptor for bacteriophage phiA1122. J. Bacteriol. 193, 4963-4972.

Kim, S.K., Makino, K., Amemura, M., Shinagawa, H., Nakata, A., (1993) Molecular analysis of the phoH gene, belonging to the phosphate regulon in Escherichia coli. J. Bacteriol. 175, 1316-1324.

Klumpp, J., Lavigne, R., Loessner, M., Ackermann, H., (2010) The SPO1-related bacteriophages. Arch. Virol. 155, 1547 - 1561.

Klumpp, J., Schmuki, M., Sozhamannan, S., Beyer, W., Fouts, D.E., Bernbach, V., Calendar, R., Loessner, M.J., (2014) The odd one out: Bacillus ACT bacteriophage CP-51 exhibits unusual properties compared to related Spounavirinae W.Ph. and Bastille. Virology 462-463, 299-308.

Kong, M., Kim, M., Ryu, S., (2012) Complete genome sequence of Bacillus cereus bacteriophage PBC1. J. Virol. 86, 6379 - 6380.

Kropinski, A.M., Hayward, M., Agnew, M.D., Jarrell, K.F., (2005) The genome of BCJA1c: a bacteriophage active against the alkaliphilic bacterium, Bacillus clarkii. Extremophiles 9, 99-109.

Kumar, S., Nei, M., Dudley, J., Tamura, K., (2008) MEGA: a biologist-centric software for evolutionary analysis of DNA and protein sequences. Briefings in bioinformatics 9, 299-306.

Kysela, D.T., Turner, P.E., (2007) Optimal bacteriophage mutation rates for phage therapy. J. Theor. Biol. 249, 411-421.

Larkin, M.A., Blackshields, G., Brown, N.P., Chenna, R., McGettigan, P.A., McWilliam, H., Valentin, F., Wallace, I.M., Wilm, A., Lopez, R., Thompson, J.D., Gibson, T.J., Higgins, D.G., (2007) Clustal W and Clustal X version 2.0. Bioinformatics 23, 2947-2948.

Lassmann, T., Sonnhammer, E.L., (2005) Kalign--an accurate and fast multiple sequence alignment algorithm. BMC Bioinformatics 6, 298.

Le, S., He, X.S., Tan, Y.L., Huang, G.T., Zhang, L., Lux, R., Shi, W.Y., Hu, F.Q., (2013) Mapping the Tail Fiber as the Receptor Binding Protein Responsible for Differential Host Specificity of Pseudomonas aeruginosa Bacteriophages PaP1 and JG004. PLoS One 8.

Lee, J., Shin, H., Son, B., Ryu, S., (2012) Complete genome sequence of

Bacillus cereus bacteriophage BCP78. J. Virol. 86, 637 - 638.

Lee, J.H., Shin, H., Son, B., Heu, S., Ryu, S., (2013) Characterization and complete genome sequence of a virulent bacteriophage B4 infecting food-borne pathogenic Bacillus cereus. Arch. Virol. 158, 2101-2108.

Lee, W.J., Billington, C., Hudson, J.A., Heinemann, J.A., (2011) Isolation and characterization of phages infecting Bacillus cereus. Lett. Appl. Microbiol. 52, 456-464.

Lee, Y.D., Park, J.H., (2010) Genomic Sequence of Temperate Phage 250 Isolated from Emetic B. cereus and Cloning of Putative Endolysin. Food Science and Biotechnology 19, 1643-1648.

Lowe, T.M., Eddy, S.R., (1997) tRNAscan-SE: a program for improved detection of transfer RNA genes in genomic sequence. Nucleic Acids Res. 25, 955-964.

Marchler-Bauer, A., Anderson, J.B., Derbyshire, M.K., DeWeese-Scott, C., Gonzales, N.R., Gwadz, M., Hao, L., He, S., Hurwitz, D.I., Jackson, J.D., Ke, Z., Krylov, D., Lanczycki, C.J., Liebert, C.A., Liu, C., Lu, F., Lu, S., Marchler, G.H., Mullokandov, M., Song, J.S., Thanki, N., Yamashita, R.A., Yin, J.J., Zhang, D., Bryant, S.H., (2007) CDD: a conserved domain database for interactive domain family analysis. Nucleic Acids Res. 35, D237-240.

Minakhin, L., Semenova, E., Liu, J., Vasilov, A., Severinova, E., Gabisonia, T., Inman, R., Mushegian, A., Severinov, K., (2005) Genome sequence and gene expression of Bacillus anthracis bacteriophage Fah. J. Mol. Biol. 354, 1-15.

Moak, M., Molineux, I.J., (2004) Peptidoglycan hydrolytic activities associated with bacteriophage virions. Mol. Microbiol. 51, 1169-1183.

Muniesa, M., Garcia, A., Miro, E., Mirelis, B., Prats, G., Jofre, J., Navarro, F., (2004) Bacteriophages and diffusion of beta-lactamase genes. Emerg. Infect. Dis. 10, 1134-1137.

Oakley, A.J., Yamada, T., Liu, D., Coggan, M., Clark, A.G., Board, P.G., (2008) The identification and structural characterization of C7orf24 as

gamma-glutamyl cyclotransferase. An essential enzyme in the gamma-glutamyl cycle. J. Biol. Chem. 283, 22031-22042.

Oliveira, H., Melo, L.D., Santos, S.B., Nobrega, F.L., Ferreira, E.C., Cerca, N., Azeredo, J., Kluskens, L.D., (2013) Molecular aspects and comparative genomics of bacteriophage endolysins. J. Virol. 87, 4558-4570.

Payne, S.L., Elder, J.H., (2001) The role of retroviral dUTPases in replication and virulence. Current protein & peptide science 2, 381-388.

Rohwer, F., (2003) Global phage diversity. Cell 113, 141-141.

Samson, J.E., Moineau, S., (2010) Characterization of Lactococcus lactis phage 949 and comparison with other lactococcal phages. Appl. Environ. Microbiol. 76, 6843-6852.

Schuch, R., Fischetti, V.A., (2006) Detailed genomic analysis of the W beta and gamma phages infecting Bacillus anthracis: Implications for evolution of environmental fitness and antibiotic resistance. J. Bacteriol. 188, 3037-3051.

Shin, H., Bandara, N., Shin, E., Ryu, S., Kim, K.P., (2011) Prevalence of Bacillus cereus bacteriophages in fermented foods and characterization of phage JBP901. Res. Microbiol. 162, 791-797.

Shin, H., Lee, J.H., Park, J., Heu, S., Ryu, S., (2014) Characterization and genome analysis of the Bacillus cereus-infecting bacteriophages BPS10C and BPS13. Arch. Virol. 159, 2171-2175.

Smeesters, P.R., Dreze, P.A., Bousbata, S., Parikka, K.J., Timmery, S., Hu, X., Perez-Morga, D., Deghorain, M., Toussaint, A., Mahillon, J., Van Melderen, L., (2011) Characterization of a novel temperate phage originating from a cereulide-producing Bacillus cereus strain. Res. Microbiol. 162, 446-459.

Sorensen, M.C., van Alphen, L.B., Harboe, A., Li, J., Christensen, B.B., Szymanski, C.M., Brondsted, L., (2011) Bacteriophage F336 recognizes the capsular phosphoramidate modification of Campylobacter jejuni NCTC11168. J. Bacteriol. 193, 6742-6749.

Tormo-Mas, M.A., Donderis, J., Garcia-Caballer, M., Alt, A., Mir-Sanchis, I.,

Marina, A., Penades, J.R., (2013) Phage dUTPases control transfer of virulence genes by a proto-oncogenic G protein-like mechanism. Mol. Cell 49, 947-958.

Zdobnov, E.M., Apweiler, R., (2001) InterProScan--an integration platform for the signature-recognition methods in InterPro. Bioinformatics 17, 847-848.

Chapter III.

Characterization of endolysins and their various domains

III-1. Introduction

Bacteriophage endolysins are expressed at the end of the phage reproductive cycle, hydrolyzing the cell wall peptidoglycan to release virion progeny. Since endolysins are bactericidal enzymes with highly evolved specificity toward target bacteria, their potentials as antibacterial agents have been intensively studied (Fenton et al., 2010; Fischetti, 2008). Typical endolysins from phages infecting Gram-positive bacteria have a modular structure, consisting of one or more enzymatic active domains (EADs) and a C-terminal cell wall binding domain (CBD) (Loessner, 2005). While the EAD has conserved active site residues, and cleaves specific bonds within the peptidoglycan, the CBD recognizes highly specific ligand in the cell wall, and target the endolysin to its substrate (Oliveira et al., 2013). In addition to the EAD and the CBD, Gram-positive phage endolysins often have a flexible linker that connects the two globular domains, but little is known about the function of this linker region (Schmelcher et al., 2010).

The role of the CBD in the enzymatic efficiency is somewhat controversial. Some CBDs have been found to be essential for the lytic activity of endolysin as the EAD alone has diminished or entirely abolished activity against the host bacteria (Loessner et al., 2002; Porter et al., 2007;

Sanz et al., 1992; Sass and Bierbaum, 2007; Zimmer et al., 2002). In these cases, CBD helps the EAD access the substrate, increases enzyme-substrate proximity, and consequently, only random encounters between the EAD and the sessile bond of the peptidoglycan result in limited lysis (Korndorfer et al., 2008; Porter et al., 2007). On the other hand, a number of endolysins have showed the opposite effect, where deleting the CBD does not affect the lytic activity (Low et al., 2005) or even increases the muralytic activity (Cheng and Fischetti, 2007; Low et al., 2005; Mayer et al., 2011). It has also been hypothesized that the CBD interacts with the EAD in the absence of the cognate substrate, and this interaction has inhibitory effect on the enzymatic activity of endolysin (Low et al., 2005; Pohane et al., 2014). Taken together, the role of the CBD is variable, and therefore, each case should be studied individually.

Although several *B. cereus* phage endolysins have been reported to date (Loessner et al., 1997; Park et al., 2012; Son et al., 2012), it has not been until recently that exploiting modular nature of endolysins has become a biotechnological focus. Furthermore, in the case of CBDs, very few of these have been validated clearly to be true CBDs. Here, I characterize several endolysins from newly isolated *B. cereus* phages and identify their

functional domains, including EADs, CBDs, and a spore binding domain. In addition, a facile and efficient method for identifying a novel CBD from a sequenced bacterial genome is presented. The molecular and biochemical studies of the endolysins may have broad implications for the design of effective therapeutics and novel diagnostic tools.

III-2. Materials and Methods

III-2-1. Bacterial strains and growth conditions

All of the *Bacillus* strains and Gram-negative bacteria were grown in Luria-Bertani (LB) broth at 37℃. *Listeria*, *Staphylococcus*, and *Enterococcus* strains were grown in brain-heart infusion broth at 37℃. *Clostridium* strains were grown in reinforced clostridial medium at 37℃ under anaerobic condition. To create agar medium, the broth medium was supplemented with 1.5% agar. All of the media used in this study were purchased from Difco and used according to the manufacturer's instructions.

III-2-2. *In silico* analysis

Putative functional domains of endolysins were identified through bioinformatics analyses. Amino acid sequence alignments of the proteins were conducted using ClustalX2 (Larkin et al., 2007). A conserved domain search was conducted using BLASTP (Altschul et al., 1990), InterProScan (Zdobnov and Apweiler, 2001), and NCBI Conserved Domain Database (Marchler-Bauer et al., 2007). Secondary and tertiary structures of

endolysins were predicted using Phyre2 and the ESyPred3D server (Kelley and Sternberg, 2009; Lambert et al., 2002). Visual inspection of protein structural models was performed using PyMol software (DeLano, 2005). Gene fragments encoding functional domains were amplified by polymerases chain reaction (PCR) for subsequent steps. A phylogenetic tree of CBDs from reported *Bacillus* phage endolysins was generated with the MEGA5 program using the neighbor-joining method with P-distance values (Tamura et al., 2011).

The BLAST search program (http://www.ncbi.nlm.nih.gov/BLAST) were used to survey lytic enzymes in the genome of *C. perfringens* ATCC 13124. I exploited the amino acid sequences from catalytic domains of Psm (endolysin of *C. perfringens* episomal phage phiSM101, NCBI accession ID: YP_699978.1) (Nariya et al., 2011; Tamai et al., 2014) and Ply3626 (endolysin of *C. perfringens* phage phi3626, NCBI accession ID: NP_612849.1) (Zimmer et al., 2002) as query sequences because those two endolysins are well-characterized N-acetylmuramidase and N-acetylmuramoyl-L-alanine amidase, respectively. The NCBI non-redundant protein sequences (nr) were utilized as the reference database, with default parameters. The positions of the selected lytic enzymes within the genome

were identified using CLS genomics workbench (version 3. 61). A conserved domain search within the selected lytic enzymes was conducted using InterProScan (Zdobnov and Apweiler, 2001) and NCBI Conserved Domain Database (Marchler-Bauer et al., 2007). Amino acid sequences of the putative lytic enzymes were aligned with each other or the reported endolysins using ClustalX2 (Larkin et al., 2007). Three dimensional structural analysis of proteins were conducted using the PyMol program (DeLano, 2002) and the Phyre server (Kelley and Sternberg, 2009).

III-2-3. Construction of recombinant proteins

For endolysins, the endolysin genes from the phage genome were PCR amplified with the corresponding primers (**Table III-1**). In the case of LysPBC1_EAD, I inserted a stop codon after Asn 174. The PCR product was cloned into pET15b (Novagen), which has an N-terminal hexahistidine (His)-tag sequence. For enhanced green fluorescent protein (EGFP)-fused CBD proteins, *egfp* and *mcherry* gene was amplified by PCR using pEGFP, pmCherry-C1 (Clontech, Palo Alto, USA) as a template. The native stop codon was omitted for translational fusions. The amplified DNA product was

double-digested using NdeI and BamHI, and ligated into a pET28a vector (Novagen, Madison, USA). Gene fragment encoding the CBD was digested with corresponding restriction enzymes (Takara Clontech, Kyoto, Japan), and subcloned into the EGFP- or mCherry-containing pET28a. The sequences were verified for all constructs. The correctly cloned plasmid was transformed into *E. coli* BL21 (DE3) (Invitrogen, Carlsbad, USA). All recombinant plasmids used in this chapter were summarized in **Table III-2.**

For CPF369_CBD, a gene fragment encoding 140 amino acids from the C-terminal of YP_694826 was predicted as a putative CBD and the coding sequence was PCR (polymerase chain reaction) amplified from a colony of *C. perfringens* ATCC 13124 with the following primers: gcgggatcc GTAAAAAATAATTTTAAATTGTATAATGCAACCACTAAG (fwd) and gcgaagctt CTAAATCTTTTTAACAAAGTCAGCCTTAACAAAA (rev). To confirm and visualize the cell binding activity of the CPF369_CBD, I fused EGFP at the N-terminal of CPF369_CBD. EGFP encoding gene was PCR amplified from pEGFP (Clontech), and its native stop codon was omitted for translational fusions. The amplified DNA products were cloned into NdeI/BamHI sites of a modified 10His-pET28a vector (Novagen) which intentionally inserting additional four histidine residues to make an N-

terminal decahistidine tag. The CBD fragment was inserted into BamHI/HindIII sites of EGFP-containing 10His-pET28a, creating in-frame fusion of N-terminal deca-His-tagged EGFP-CBD. The constructed plasmid was transformed into E. coli BL21 (DE3) for protein expression. The clone was grown in LB broth and induced with 0.5 mM isopropyl-β-D-thiogalactoside (IPTG) once an optical density at 600 nm of 0.8 was reached. The induced culture was shaken for 21 h at 18℃. The cells were pelleted, resuspended in a buffer A (200 mM NaCl and 50 mM Tris-Cl (pH 8.0)), and disrupted on ice by Sonifier 250 (Branson) at a duty cycle of 20% and output control of 5. The suspension was centrifuged (21,000 x g, 1 h, 4oC) and the supernatant was filtered (0.2- μm-pore-size syringe filter (Sartorious). The soluble protein was purified by immobilized metal affinity chromatography (IMAC) by using Poly-Prep® Chromatography columns (Bio-Rad) packed with Ni-NTA superflow resin (Qiagen). Buffer B (200 mM Tris-Cl (pH 8.0), 200 mM NaCl, 250 mM imidazole) was used for protein elution. Eluates were dialyzed against buffer A and stored at -20℃ after addition of 50% (v/v) glycerol.

For SA13_CBD, e CBD fragment specific for *Staphylococcus* species was amplified from the genome of *S. aureus* bacteriophage SA13

(NCBI GenBank ID: NC_021863) (Unpublished data) and inserted into pET28a-EGFP. The production and purification of EGFP-SA13_CBD fusion protein were performed as described above.

Table III-1. Oligonucleotides used in Chapter III

Oligonucleotide	Sequence (5'-3')[a]
fNde_LysPBC1	gcg cat ATGGATAAATTTACAGTACATGCAGGGC
rBamH_LysPBC1	gcg ggatcc TTAATACTCAATCACTTCTTCTTGATACCACCA
rBamH_LysPBC1_EAD	gcg ggatcc tta ATTTACTGCTTTGCCTGTAACGGCTT
fBamH_LysPBC1_CBD	gcg ggatcc GGCAAAGCAGTAAATGTTGATCCGC
rHind_LysPBC1_CBD	gcg aagctt TTAATACTCAATCACTTCTTCTTGATACCACCA
fNde_LysPBC2	gcg cat ATGGCTATTTCAGTAAGACAAAAATTGGTG
rBamH_LysPBC2	gcg ggatcc TTAGTCTCTTACAAAACGAACGAATGAAGAGT
fBamH_LysPBC2_CBD	gcg ggatcc GGAGGAAGCACAGGTGGCGGTAC
rHind_LysPBC2_CBD	gcg aagctt TTAGTCTCTTACAAAACGAACGAATGAAGAGT
fEcoR_LysPBC2_SBD1	gcg gaattc GCTTTAGCTATCAAGTTCGTTGCACAAC
rXho_LysPBC2_SBD1	gcg ctcgag tta AGTACCGCCACCTGTGCTTCCTC
fNde_LysPBC4	gcggcgcatATGGCTAAAGTATCTAGTCACG
rEcoR_LysPBC4	gcgGAATTCTTAAACTTCGTATAACTCAACGAA
fBamH_ LysPBC4_CBD1	gcgggatccGGACAAGAAACAAGTGGAGGTTCTAACAAT
fBamH_ LysPBC4_CBD2	gcgggatccGTTATGAAAACTGGTGGTCTTGGTTGTCC

rHind_ LysPBC4_CBD	gcgaagcttTTAAACTTCGTATAACTCAACGAACCAACCTT
fBamH_LysB4_CBD1	gcg ggatcc GGAGGCTCTGGTAGCACAGGCG
rHind_LysB4_CBD	gcg aagctt TTATTTGAACGTACCCCAGTAGTTCTGACG
fBamH_LysPBC5_CBD	gcg ggatcc GGGCGTACTCTTCAGTGGTTCTTAGGA
rXho_LysPBC5_CBD	gcg ctcgag CTACTTAGCCGTGATTGTAACGTGTTCTTC
fBamH_LysPBC6_CBD	gcg ggatcc GGAGGTGGATACGATTCTAGTTGGTTCA
rHind_LysPBC6_CBD	gcg aagctt TTACTGGAAAGTTCCCCAGTAAGAGATACGT
fBamH_LysPBC10_CBD	gcg ggatcc GGAAGTAAAGGGATGGACTTCTTCACG
rXho_LysPBC10_CBD	gcg ctcgag TTATGCGTAGAACACAACCTCTTCCGC
fBamH_SA13_CBD	gcg ggatcc TCAAGCGCTTCAAGTAATACAGTTAAACCA
rHind_SA13_CBD	gcg aagctt CTAACTGATTTCTCCCCATAAGTCACCTAATAT
fBamH_CPF369_CBD	gcg ggatcc GTAAAAAATAATTTTAAATTGTATAATGCAACCACTAAG
rHind_CPF369_CBD	gcg aagctt CTAAATCTTTTTAACAAAGTCAGCCTTAACAAAA
fNde_EGFP	gcg cat ATGGTGAGCAAGGGCGAGGAG
rBamH_EGFP_nostop	gcg ggatcc CTTGTACAGCTCGTCCATGCCGA
rHind_EGFP	gcg aagctt TTACTTGTACAGCTCGTCCATGCCG
fNde_mCherry	gcg cat ATGGTGAGCAAGGGCGAGGAGG
rBamH_mCherry_no stop	gcg ggatcc CTTGTACAGCTCGTCCATGCCGC

fBgl_pET28a	gcg agatct CGATCCCGCGAAATTAATACG
r10HisSG_pET28a	agcggc gtggtggtggtg GTGATGATGATGATGATGGCTGCTG
f10HisSG_pET28a	caccaccaccac agcggc AGCAGCGGCCTGGTGCCG
rXho_pET28a	gcg ctcgag TGCGGCCGCAAGC
10His confirm_fwd	CACCACCACCACAGCGGCAG

[a] Restriction sites for cloning are underlined. Capital letters delineate regions homologous to the respective template DNA.

Table III-2. Plasmids used in Chapter III

Plasmid	Relevant characteristics	Source
pET15b	Amp^R expressing vector with a T7 promoter	Novagen
pET28a	Kan^R expressing vector with a T7 promoter	Novagen
pEGFP	Amp^R *egfp* cassette vector	Clontech
pmCherry-C1	Kan^R *mcherry* cassette vector	Clontech
pET28a-EGFP	EGFP gene cloned into NdeI-BamHI site of pET28a	This work
pET28a-mCherry	mCherry gene cloned into NdeI-BamHI site of pET28a	This work
pET15b-LysPBC1	LysPBC1 gene cloned into NdeI-BamHI site of pET15b	Kong and Ryu, 2015
pET15b-LysPBC1_EAD	The EAD fragment (Met1-Asn174) of LysPBC1 cloned into NdeI-BamHI site of pET15b	Kong and Ryu, 2015
pET15b-LysPBC2	LysPBC2 gene cloned into NdeI-BamHI site of pET15b	This work
pET28a-LysPBC4	LysPBC4 gene cloned into NdeI-EcoRI site of pET28a-EGFP	This work
pET28a-EGFP-PBC1_CBD	The CBD fragment (Gly170-Tyr254) of LysPBC1 cloned into BamHI-HindIII site of pET28a-EGFP	This work
pET28a-EGFP-PBC2_CBD	The CBD fragment (Gly163-Asp311) of LysPBC2 cloned into BamHI-HindIII site of pET28a-EGFP	This work
pET28a-EGFP-PBC4_CBD1	The CBD fragment (Gly170-Val257) of LysPBC4 cloned into BamHI-HindIII site of pET28a-EGFP	This work
pET28a-EGFP-PBC4_CBD2	The CBD fragment (Val189-Val257) of LysPBC4 cloned into BamHI-HindIII site of pET28a-EGFP	This work
pET28a-EGFP-B4_CBD	The CBD fragment (Val156-Lys262) of LysB4 cloned into BamHI-HindIII site of pET28a-EGFP	This work

pET28a-EGFP-PBC5_CBD	The CBD fragment (Gly192-Lys339) of LysPBC5 cloned into BamHI-XhoI site of pET28a-EGFP	This work
pET28a-EGFP-PBC6_CBD	The CBD fragment (Gly168-Gln280) of LysPBC6 cloned into BamHI-HindIII site of pET28a-EGFP	This work
pET28a-EGFP-PBC10_CBD	The CBD fragment (Gly196-Ala293) of LysPBC10 cloned into BamHI-XhoI site of pET28a-EGFP	This work
pET28a-EGFP-PBC2_SBD1	The SBD fragment (Ala108-Thr170) of LysPBC2 cloned into EcoRI-XhoI site of pET28a-EGFP	This work
pET28a-EGFP-PBC2_SBD2	The SBD fragment (Arg127-Gly147) of LysPBC2 cloned into EcoRI-XhoI site of pET28a-EGFP	This work
pET28a-mCherry-PBC1_CBD	The CBD fragment (Gly170-Tyr254) of LysPBC1 cloned into BamHI-HindIII site of pET28a-mCherry	This work
pET28a-mCherry-PBC4_CBD	The CBD fragment (Gly170-Val257) of LysPBC4 cloned into BamHI-HindIII site of pET28a-mCherry	This work
pET28a-mCherry-B4_CBD	The CBD fragment (Val156-Lys262) of LysB4 cloned into BamHI-HindIII site of pET28a-mCherry	This work
pET28a-EGFP-SA13_CBD	The CBD fragment (Ser373-Ser481) of *S. aureus* phage SA13 endolysin cloned into BamHI-HindIII site of pET28a-EGFP	This work
10His-pET28a-EGFP-CPF369_CBD	The CBD fragment (Val203-Ile342) of a gene (Gene ID: CPF_0369) from *C. perfringens* ATCC 13124 cloned into BamHI-HindIII site of 10His-pET28a-EGFP	This work

III-2-4. Protein expression and purification

Freshly transformed cells were grown in LB at 37°C to an OD_{600} of 0.6-1.0 and isopropyl-β-D-thiogalactoside (IPTG) (0.5 mM) was added. After incubation for 20 h at 18°C, the cells were harvested by centrifugation, and frozen at -20°C. After thawing, cells were resuspended in a lysis buffer containing 200 mM NaCl and 50 mM Tris-Cl (pH 8.0), and lysed by sonication at a duty cycle of 25% and output control of 5 (Sonifier 250, Branson, Danbury, USA). After centrifugation (21,000 x g, 1 h, 4°C) and sterilization by 0.20 μm filter (Sartorious, Goettingen, Germany), the soluble protein was purified by immobilized metal affinity chromatography (Poly-Prep® Chromatography column Cat. #731-1550, Bio-Rad, Hercules, USA) using Ni-NTA agarose (Qiagen, Valencia, USA). For affinity chromatography, the protein solution (5 ml) was incubated with 0.5 ml of the Ni-NTA resin for 1 h and followed by column purification by gravity flow. After washing the resin twice with the lysis buffer containing imidazole (10-20 mM), the protein was eluted in elution buffer (200 mM NaCl, 50 mM Tris-Cl, and 240 mM imidazole; pH 8.0) and divided into four 500 μl aliquots. The purity of the proteins was confirmed by sodium dodecyl sulfate-polyacrylamide gel electrophoresis (SDS-PAGE) with protein size

marker (GenDEPOT, Barker, USA). The purified protein was stored at -20^{o}C after buffer exchange to the storage buffer (50 mM Tris-Cl, 200 mM NaCl, and 50% glycerol; pH 8.0) using PD Miditrap G-25 (GE Healthcare, Waukesha, USA).

III-2-5. Turbidity reduction assay

The lytic activity of the endolysin was assessed by turbidity reduction assay as described previously (Son et al., 2012). Bacterial cells were grown to exponential phase and resuspended with the reaction buffer (20 mM Tris-Cl, pH 8.0) to adjust the OD_{600} to about 1.0. Then, the purified endolysin was added to a final concentration of 0.4 μM, and OD_{600} values were monitored over time. For the lytic activity of EADs, an equimolar concentration (0.4 μM) was used to take into account the difference in protein molecular weight. For Gram-negative bacteria, the exponentially growing bacterial cells were pretreated with a buffer containing 20 mM Tris-Cl (pH 8.0) and 0.1 M EDTA for 5 min at RT. Then, the cells were washed three times with reaction buffer to remove residual EDTA, and the endolysin was added.

III-2-6. Cell binding assay with fluorescence microscopy

The binding property of GFP-CBD fusion protein was examined as previously described (Loessner et al., 2002). Briefly, 1 ml of exponentially grown bacterial cells was centrifuged (16,000 g, 1 min) and resuspended in 1 ml of PBS. Next, 100 μl of cells was incubated together with 0.4 μM GFP-CBD fusion protein at room temperature for 5 min. For Gram-negative strains, EDTA-pretreated cells were incubated with 4 μM of GFP-CBD fusion proteins for 10 min. The cells were washed twice with PBS buffer and observed by epifluorescence microscopy (DE/Axio Imager A1 microscope, Carl Zeiss, Oberkochen, Germany) with a GFP filter (470/40 nm excitation, 495 nm dichroic, 525/50 nm emission).

III-2-7. Influence of NaCl and pH on CBD binding capacity

The effect of NaCl on the binding of the CBDs to *B. cereus* cells was investigated in 20 mM Tris-Cl (pH 8.0) buffer supplemented with 0, 0.05, 0.1, 0.2, 0.5, 1.0 and 2.0 M NaCl. *B. cereus* cells (ATCC 21768 for PBC1_CBD, ATCC 13061 for B4_CBD) were mixed with the corresponding mCherry-CBD proteins, incubated (5 min at room temperature), and

centrifuged (16,000 x g, 1 min). After the supernatant was discarded, cells were resuspended in 200 µl of PBS, and the cell-associated fluorescence was measured by using an SpectraMax i3 multimode microplate reader (Molecular Devices, Sunnyvale, CA) with excitation at 585 nm and emission at 610 nm. The cell density at 600 nm was measured, and the normalization was calculated as whole-cell fluorescence per OD_{600}. Relative binding capacity of the CBDs was given in percentage by comparing to the optimal binding condition (the highest measured value). The influence of pH on the CBD binding was assessed using cells resuspended in an universal pH buffer (10 mM KH_2PO_4, 10 mM Na-citrate and 10 mM H_3BO_4) (Oliveira et al., 2014) adjusted to different pH values between 4 to 10. The cell binding assay was carried out as described above. All experiments were performed in triplicate.

III-2-8. Preparation of spores

B. cereus spores were prepared Difco Sporulation Medium (DSM) as described earlier (Nicholson and Setlow 1990). In brief, cells were spread on DSM agar, with incubation at 37℃ for 3 to 5 days. The resulting

bacterial lawns were scraped from the plates and resuspended in ice-cold deionized water, and harvested by centrifugation at 16,000 x g for 5 min at 4℃. The spore pellets were washed approximately ten times in ice-cold water by repeated centrifugation. Microscopic examination was conducted to check the spores were >95% pure. Spores were stored at -20℃ until further use. To remove the exosporium, physical and detergent methods were used (Thompson et al., 2011; Wang et al., 2009). For detergent method, PBS buffer-washed spores were subjected to boiling in SDS-8M urea sample buffer (62.5 mM Tris-Cl, pH 6.8, 10% glycerol, 2% SDS, 8 M urea, 2% β-mercaptoethanol, and 0.005% bromophenol blue) for 10 min. Spores were then harvested by centrifugation (21,000 x g, 1.5 min) and the spore pellets were washed two times in PBS buffer. For physical method, spores were sonicated (Vibra Cell, Sonics & Materials, USA) with amplitude of 20% and 120 pulse cycles on ice (5-s on/9-s off). Then, spores were pelleted by centrifugation (9,000 x g, 5 min) and washed two times with PBS buffer.

III-2-9. Spore binding assays with SBD

Spores were reacted with 1 uM of the EGFP-tagged SBD (spore

binding domain) proteins at RT for 5 min. After washing three times with PBS by centrifugation (16, 000 x g, 1 min), the labeled spores were analyzed by either a fluorescence microscopy (DE/Axio Imager A1 microscope, Carl Zeiss, Oberkochen, Germany) or SpectraMax i3 multimode microplate reader (Molecular Devices, Sunnyvale, CA) with excitation at 585 nm and emission at 610 nm.

III-2-10. Transmission electron microscopy

Spore sections were prepared and viewed as described previously (Thompson et al., 2011) with some modifications. Spores were fixed for 1 h at 37℃ in a 1 ml of 2% glutaldehyde and 0.1 M sodium cacodylate buffer (pH 7.4) containing 0.1% ruthenium red (Electron Microscopy Sciences, Fort Washington, PA). Spore pellets were then washed in 0.1 M sodium cacodylated buffer (pH 7.4) and postfixed for 3 h at room temperature in a 1% osmium tetroxide (Electron Microscopy Sciences), 0.1 M sodium cacodylate solution containing 0.1% ruthenium red. Spores were then washed twice in distilled water and further stained with 0.5% uranyl acetate for 30 min at 4℃. The spores were dehydrated in a graded ethanol series including 30%, 50%,

70%, 90%, and 100% ethanol (three times), which was followed by two times of 15-min rinses in propylene oxide. The spores were infiltrated for 2 h in a 1:1 mixture of Spurr's low-viscosity resin (Electron Microscopy Sciences) and propylene oxide and then overnight in 100% Spurr's resin. The spores were infiltrated for 2 h in fresh Spurr's resin and embeded again in fresh resin. This suspension was incubated at 70℃ for 24 h to embed the spores in polymerized resin. Sections were cut at 100 nm thickness (Ultramicrotome, MT-X, RMC, Tucson, AZ, USA) and placed on copper grids and stained with 2% uranyl acetate for 7 min. The sections were then treated with Reynolds' lead citrate (Reynolds, 1981) for 7 min and examined with TEM (JEM1010, JEOL, Japan) at 80 kV.

III-3. Results and Discussion

III-3-1. Modular structure of endolysins

III-3-1-1. LysPBC1

Pfam and Conserved Domain Database analysis showed that LysPBC1 is a putative N-acetylmuramoyl-L-alanine amidase, consisting of an N-terminal type 3 amidase domain (PF01520) and a C-terminal Amidase02_C domain (PF12123) **(Fig. III-1A)**. Amino acid sequence alignment revealed that LysPBC1 presents a 73% overall identity with an endolysin of *B. cereus* phage 12826 (Loessner et al., 1997) **(Fig. III-1B)**. In addition, the LysPBC1 was aligned with non-Bacillus lysins, such as *Listeria* monocytogens phage endolysin PlyPSA (Korndorfer et al., 2006) and *Clostridium* difficile phage endolysin CD27L (Mayer et al., 2008), due to the conserved catalytic amidase_3 domains. LysPBC1 has three Zn2+-coordinating residues (Glu23, His79, Glu140) in the catalytic domain, and these residues are conserved in all four endolysins. Considering that the C-terminal amidase02_C domain of LysPBC1 did not show any homology to the PlyPSA and CD27L and several endolysins have an amidase02_C domain (PF12123) as a cell wall binding domain (Mo et al., 2012; Yuan et al.,

2012), the C-terminal domain is presumed to function in binding the *B. cereus* cell wall.

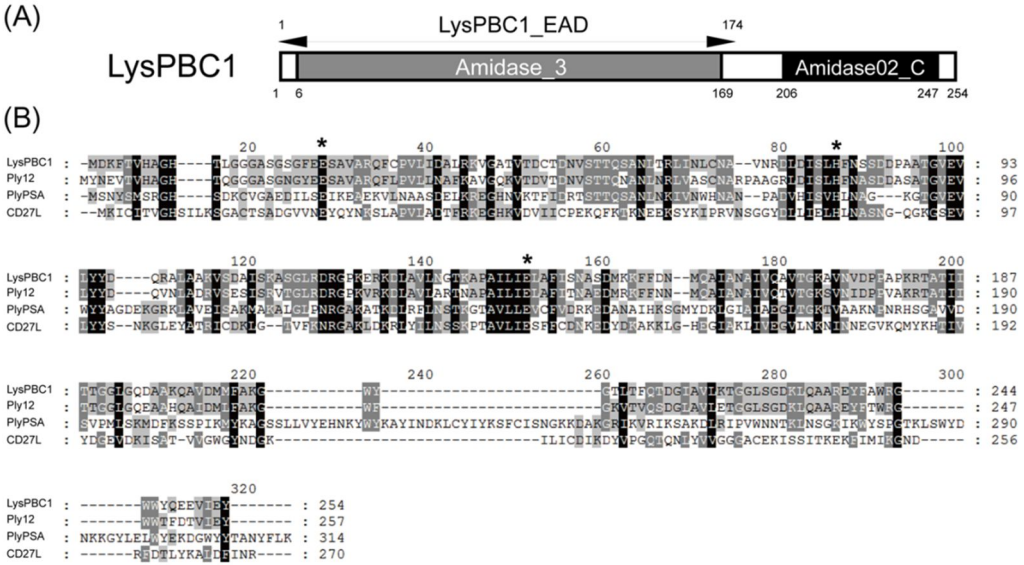

Fig. III-1. Modular structure of *B. cereus* phage endolysin LysPBC1. (A) Schematic representation of LysPBC1. (B) Sequence alignment of LysPBC1-related endolysins. Ply12, *B. cereus* phage 12826 endolysin; PlyPSA, *L. monocytogenes* phage PSA endolysin; CD27L, *C. difficile* phage ϕCD27 endolysin. Conserved and identical residues are shaded in gray (dark gray, >70% conserved; light gray, >40%) and black, respectively. Asterisks represent the conserved Zn2+-coordinating catalytic residues in N-acetylmuramoyl-L-alanine amidase.

III-3-1-2. LysPBC2

The endolysin of PBC2 (LysPBC2) harbors three domains, one N-terminal amidase_2 domain (PF01510) and two C-terminal SH3_3 domains (PF08239) **(Fig. III-2A)**. LysPBC2 shares overall sequence identity of 81% with the endolysin of *B. anthracis* phage Tsamsa (Ganz et al., 2014a). In addition, LysPBC2 demonstrates close relatedness to *B. anthracis* phage Gamma endolysin, PlyG (34% identity) (Kikkawa et al., 2008), and LysBPS13 (31% identity), an endolysin of *B. cereus* phage BPS13 (Park et al., 2012) **(Fig. III-2B)**. LysPBC2 has three conserved Zn^{2+} binding residues (His31, His131, and Cys139) in the amidase_2 enzymatic active domain. The C-terminal SH3_3 domains may function as cell wall binding domains (CBDs) since many SH3 domains, observed in phage endolyisns and bacterial autolysins, have been uncovered to recognize specific epitopes of peptidoglycan of the host cell (Chapot-Chartier, 2014). Although LysPBC2 has the conserved amidase_2 domain at the N-terminus, the two C-terminal SH3_3 domains of LysPBC2 seems to be novel as they showed a very low degree of homology to CBDs from other reported endolysins. Rather, BLASTP results showed that these two SH3_3 domains are commonly found in sporulation proteins of *B. cereus*.

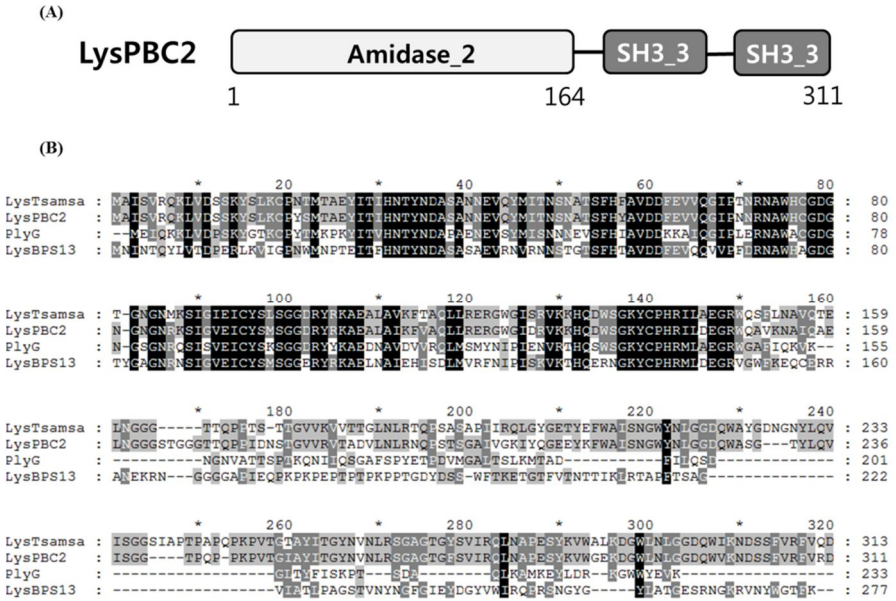

Fig. III-2. Schematic diagram of the domain organization of LysPBC2. (A) Modular structure of LysPBC2. (B) Sequence alignment of LysPBC2-related endolysins. LysTsamsa, *B. anthracis* phage Tsamsa endolysin; PlyG, *B. anthracis* phage Gamma endolysin; LysBPS13, *B. cereus* phage BPS13 endolysin. Conserved and identical residues are shaded in gray and black, respectively.

III-3-1-3. LysPBC4

The endolysin of phage PBC4, LysPBC4, has two distinct domains; an amidase_3 domain (PF01520) at the N-terminal region, and an amidase02_C domain (PF12123) at the C-terminal region **(Fig. III-3A)**. These two distinct domains appeared to be connected by flexible linker region since the region between 170th to 185th amino acid is rich in glycine, alanine having short side chains, and also serine, threonine, asparagine having polar side chains, all of which are predicted to form random coils and are usually found from many linker proteins (Schmelcher et al., 2010; Schmelcher et al., 2011). Because of the conserved amidase_3 domain, LysPBC4 showed overall 63% amino acid sequence identity with an endolysin of Basilisk (Grose et al., 2014), 51% with endolysin of BCP78 and 49% with PlyM19 (Schmitz et al., 2010) **(Fig. III-3B)**. LysPBC4 also showed close relatedness (30% identity) to LysPBC1 as they have similar domain structure (amidase_3 and amidase02_C). However, the amidase_02C domains of both endolysins showed only marginal sequence identity (23%). This result implies that some key residues or motifs in both amidase02_C domains are conserved (that's why they named as amidase02_C domains), whereas their overall structure or binding targets may be different to each

other.

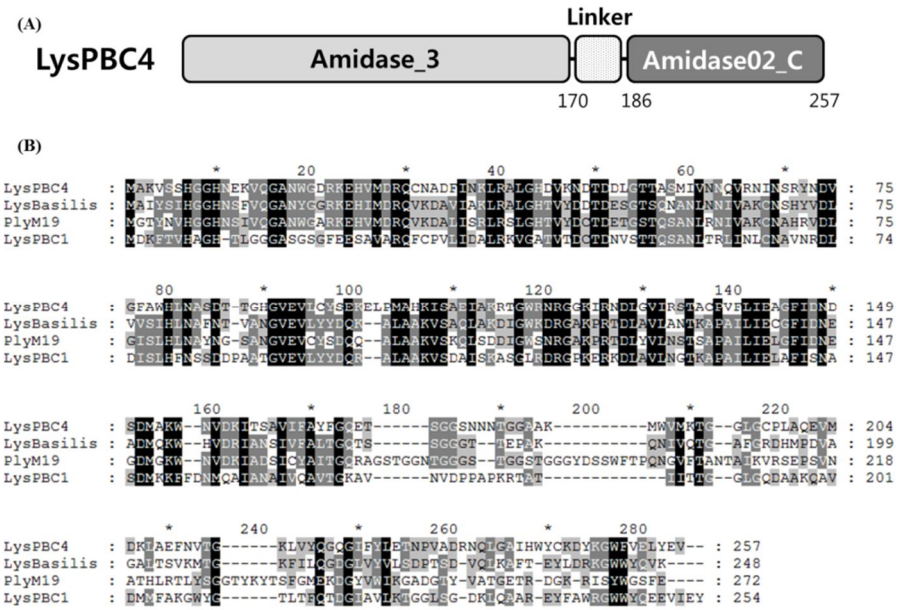

Fig. III-3. Schematic representation of LysPBC4. (A) Schematic representation of LysPBC1. (B) Sequence alignment of LysPBC4-related endolysins. LysBasilis, *B. cereus* phage Basilisk endolysin; PlyM19, an endolysin found from viral metagenome; LysPBC1, *B. cereus* phage PBC1 endolysin. Conserved and identical residues are shaded in gray (dark gray, >70% conserved; light gray, >40% conserved) and black, respectively.

III-3-1-4. Other endolysins

The endolysin of PBC6 (LysPBC6) contains an amidase_3 (PF01520) domain at the N-terminus for catalytic domain, and a SH3_5 domain (PF08460), probably functions as a cell wall binding domain (CBD). The LysPBC6 showed overall 98% amino acid sequence identity with the endolysin of BCP78 phage (Lee et al., 2012). Due to the conserved amidase_3 doamin, LysPBC6 showed close relatedness to LysPBC4 (37% identity), LysPBC1 (34% identity), while their CBDs showed insignificant homologies to each other. LysPBC6 also has a conserved CBD (SH3_5 domain), which shares more that 50% of sequence identity with the CBDs of LysB4 (Son et al., 2012) and LysBPS13 (Park et al., 2012).

LysPBC5 and LysPBC10 are endolysins from *B. cereus* phage PBC5 and PBC10 (Na et al., unpublished), respectively, and both of which showed similar domain structure. They have a conserved N-terminal glycoside hydrolase family 25 domain (GH25, PF01183), which shares >40% identity to enzymatic active domains of a *B. anthracis* endolysin PlyB (Porter et al., 2007). LysPBC5 and LysPBC10, however, showed limited overall homology (23% identity) with each other due to the different C-terminal regions. Although most endolyisn from Gram-positive-infecting phages have modular

structure, consisting of N-terminal catalytic domain(s) and C-terminal CBD(s), these two endolysins lack any apparent C-terminal domains. I speculate that LysPBC5 and LysPBC10 have novel CBDs, which cannot be identified by current database-based domain prediction methods. Further work should be needed to verify these novel CBDs.

III-3-1-5. Summary of endolysins

All endolysins studied in this chapter were summarized in **Table III-3**. *B. cereus* phage endolysins are between 250 and 350 amino acids in length, and their predicted isoelectric points (pI) lie within 5.9 to 9.3 range. Most endolysins have distinct modular structure, consisting of an N-terminal enzymatic active domain (EAD) and a C-terminal CBD, whereas LysPBC5 and LysPBC10 are devoid of recognizable CBDs. Endolysins with amidase_2 type and CHAP domain tend to be basic with high pI values (>8.7). For the CBDs, SH3_5 domains are commonly found in endolysins regardless of their enzymatic catalytic family. In general, while the EADs of *B. cereus* phage endolysins are conserved across the bacterial autolysins and phage endolysins, the CBDs, except the SH3_5 domains, are variable, which

may explain the great specificity of the endolysins, allowing them to bind specifically to a unique component of the host cell wall.

Table III-3. General features of *B. cereus* phage endolysins

Endolysin	Size (aa)	pI	Domain(s) identified	Remarks	Source
LysPBC1	254	5.94	AMI-3, AMI02_C	73% amino acid identity to Ply12 (Loessner et al., 1997)	Kong and Ryu, 2015
LysPBC2	311	8.73	AMI-2, 2x SH3-3	81% amino acid identity to Tsamsa endolysin (Ganz et al., 2014)	This work
LysPBC4	257	6.45	AMI-3, AMI02_C	36% amino acid identity to PlyM19 (Schmitz et al., 2010)	This work
LysPBC5	339	5.92	GH25	No apparent CBD	This work
LysPBC6	272	6.65	AMI-3, SH3-5	92% amino acid identity to PlyM19	This work
LysPBC10	313	7.25	GH25	No apparent CBD	This work
LysB4	262	9.21	CHAP, SH3-5	Broad lytic spectrum, 42% amino acid identity to Ply500 (Korndörfer et al, 2008)	Son et al., 2012

III-3-2. Endolysins show broader lytic activity than phages

III-3-2-1. Lytic activity of LysPBC1

Although PBC1 has a virulent lifestyle and rapidly lyses the host *B. cereus* strain, its extremely narrow host range may limit its efficiency as a biocontrol agent unless it is used in a phage cocktail. It has been reported that the endolysin, phage-encoded peptidoglycan hydrolase, generally shows a broader lytic spectrum than the phage (Borysowski et al., 2006; Ganz et al., 2014a; Son et al., 2010; Yuan et al., 2012; Zhang et al., 2013). Moreover, the development of resistance against endolysins has not been reported (Callewaert et al., 2011; Hermoso et al., 2007; Oliveira et al., 2012; Rodriguez-Rubio et al., 2013). Therefore, I chose the endolysin of PBC1 (LysPBC1) as an alternative or complementary antimicrobial against *B. cereus* and tested it's lytic activity.

The LysPBC1 was highly expressed in soluble form in *E. coli*, and the protein was purified by Ni-NTA affinity chromatography, resulting in a homogenous preparation **(Fig. III-4A)**. The purified LysPBC1 was able to lyse all strains of *B. cereus* group bacteria, including *B. cereus, B. thuringiensis, B. mycoides,* and *B. weihenstephanensis*, when it was added

exogenously **(Table III-4)**. This broad lytic activity was in sharp contrast to the very narrow host specificity of phage PBC1. In addition, the LysPBC1 showed modest lytic activities towards the *Bacillus* genus, such as *B. subtilis, B. megaterium,* and *B. licheniformis*. It is interesting that the exogenously added LysPBC1 alone cannot lyse Gram-negative bacteria, whereas the EDTA-treated Gram-negative cells were susceptible to the lytic action of LysPBC1. These results might be attributed to *Bacillus* and the Gram-negative bacteria tested having the same peptidoglycan type (A1γ) (Mo et al., 2012). I observed that the LysPBC1 did not lyse *Listeria* and *Clostridium* species, both of which have the same peptidoglycan type A1γ (Schleife.Kh and Kandler, 1972). These results suggest that the genus- or species-specific moieties of the cell wall are required for the enzymatic action of LysPBC1.

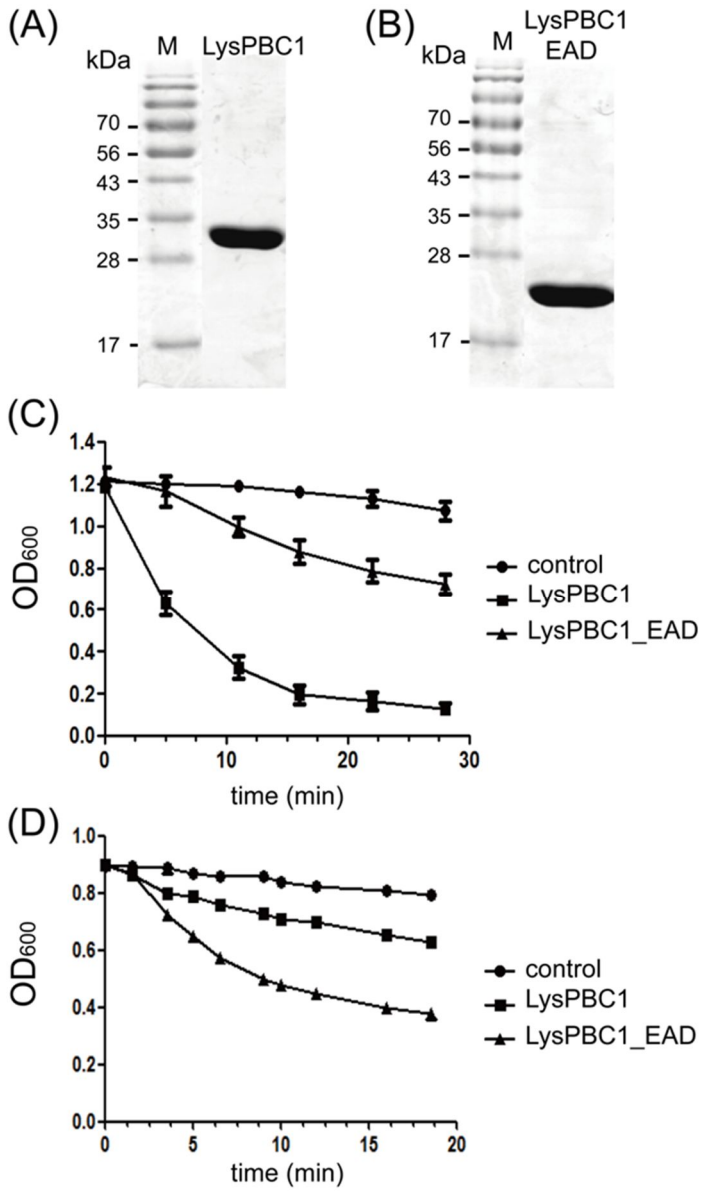
(A)
kDa
M
LysPBC1
70
56
43
35
28
17
(B)
kDa
M
LysPBC1
EAD
70
56
43
35
28
17
(C)
OD600
time (min)
control
LysPBC1
LysPBC1_EAD
(D)
OD600
time (min)
control
LysPBC1
LysPBC1_EAD

Fig. III-4. The lytic activities of LysPBC1 and LysPBC1_EAD. Ni-NTA-purified LysPBC1 (A) and LysPBC1_EAD (B) were loaded on SDS-PAGE gel (M: protein size marker). Equimolar concentrations (0.4 μM) of LysPBC1 and LysPBC1_EAD were added to the suspension of *B. cereus* (C) and *B. subtilis* (D), and the decrease in turbidity was monitored. Values are the means with SDs from triplicate assays.

Table III-4. Lytic range of LysPBC1 and LysPBC1_EAD and comparison with the host range of PBC1

Species	Strain number[a]	Plaque	Relative lytic activity (%)[b]	
		PBC1	LysPBC1	LysPBC1_EAD
***B. cereus* group strains**				
Bacillus cereus	ATCC 27348	-	+++	+
Bacillus cereus	ATCC 21768	+	+++	+
Bacillus cereus	ATCC 13061	-	+++	+
Bacillus cereus	ATCC 14579	-	++	+
Bacillus cereus	ATCC 21772	-	+++	++
Bacillus cereus	ATCC 10876	-	++	+
Bacillus cereus	KCTC 3674	-	++	+
Bacillus cereus	ATCC 10987	-	+++	+
Bacillus cereus	KCTC 1094	-	++	-
Bacillus cereus	NCCP 10623	-	++	+
Bacillus cereus	NCCP 10624	-	+++	+
Bacillus cereus	NCCP 10634	-	+	+
Bacillus cereus	NCCP 10715	-	++	-
Bacillus cereus	NCCP 10841	-	++	+
Bacillus cereus	NCCP 10856	-	+	-
Bacillus cereus	NCCP 11306	-	++	+
Bacillus cereus	NCCP 11308	-	+++	++
Bacillus cereus	NCCP 11309	-	++	+
Bacillus cereus	NCCP 11311	-	++	+
Bacillus cereus	NCCP 12448	-	+++	+
Bacillus cereus	NCCP 14043	-	++	++
Bacillus cereus	NCCP 14796	-	++	+
Bacillus thuringiensis	ATCC 10792	-	++	+

Bacillus mycoides	ATCC 6462	-	++	+
Bacillus weihenstephanensis	KCTC 3975	-	+	-
Other Gram-positive strains				
Bacilus megaterium	JCM 2506	-	+	+
Bacillus subtilis	ATCC 6051	-	+	++
Bacillus subtilis	ATCC 6633	-	+	++
Bacillus subtilis	ATCC 23857	-	+	++
Bacillus pumilus	JCM 2508	-	-	+
Bacillus licheniformis	JCM 2505	-	+	++
Bacillus sphaericus	JCM 2502	-	+	+
Bacillus circulans	JCM 2504	-	+	+
Listeria monocytogenes	Scott A	-	-	-
Listeria innocua	ATCC 33090	-	-	-
Clostridium perfringens	ATCC 3624	-	-	-
Clostridium indolis	ATCC 25771	-	-	-
Staphylococcus aureus	ATCC 29213	-	-	-
Enterococcus faecalis	ATCC 29212	-	-	-
Gram-negative strains[c]				
Escherichia coli	MG1655	-	++	++
Shigella flexineri	2a strain 2457T	-	++	+++
Cronobacter sakazakii	ATCC 29544	-	++	++

[a] Source abbreviations: ATCC, American Type Culture Collection; KCTC, Korean Collection for Type Cultures; NCCP, National Culture Collection for Pathogens; JCM, Japan Collection of Microorganisms.

[b] Relative lytic activity of endolysin was obtained by measuring the percent drop in OD at 600 nm in 8 min. -, no lysis; +, limited lysis; ++, medium lysis; +++, rapid lysis.

[c] Gram-negative bacteria (G(-)) were pretreated with EDTA.

III-3-2-2. Lytic activities of LysPBC2 and LysPBC4

LysPBC2 features a broad lytic spectrum and is able to lyse all *B. cereus* strains tested **(Table III-5)**. This is in sharp contrast to the phage host range since PBC2 can infect *B. cereus* ATCC 13061 strain only. Surprisingly, LysPBC2 can more efficiently lyse *B. subtilis* than *B. cereus* group strains **(Fig. III-5A, B)**. This pattern was also observed with *B. megaterium*, *B. circulans, B. licheniformis,* and *B. pumilus.* These results are contradictory to a previous study where the endolysin of Tsamsa (81% overall identity with LysPBC2) did not lyse *B. subtilis* and *B. megaterium* (Ganz et al., 2014a). One possible explanation for these differences is that their putative CBD regions have relatively weak sequence similarity (72%) compared to those from EAD regions (89%). Further study would be required to demonstrate how these closely related endolysins have different lytic spectrum.

LysPBC4, on the other hand, showed specific lytic activity against *B. cereus* group strains, whereas other *Bacillus* species were insensitive to the LysPBC4 (**Table III-5, Fig. III-5C,** and **D)**. Considering that some *Bacillus* species, such as *B. subtilis*, have been granted as GRAS, and widely used for the starter strain for fermented foods (Cladera-Olivera et al., 2004), the *B. cereus*-specific lytic activity could render the LysPBC4 a promising tool for

controlling pathogenic bacteria.

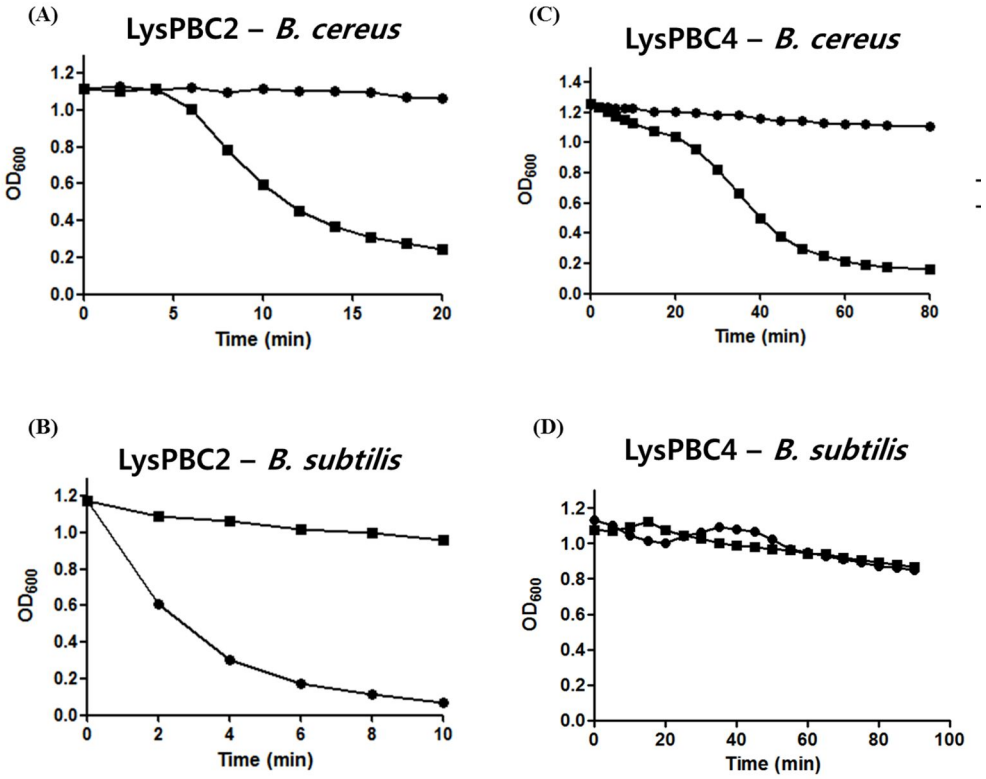

Fig. III-5. The lytic activities of LysPBC2 and LysPBC4. LysPBC2 (5 ug) was added to the 1 ml suspension of *B. cereus* (A) and *B. subtilis* (B), and the decrease in turbidity was monitored. Likewise, LysPBC4 (15 ug) was added to the 1 ml suspension of *B. cereus* (C) and *B. subtilis* (D), and the decrease in turbidity was monitored.

Table III-5. Lytic and binding spectrum of LysPBC2 and LysPBC4

Species	Source	PBC2 host range	LysPBC2 lytic range	LysPBC2 binding range	PBC4 host range	LysPBC4 lytic range	LysPBC4 binding range
Bacillus cereus	ATCC 27348	-	+	+	-	+	+
Bacillus cereus	ATCC 21768	-	+	-	-	+	-
Bacillus cereus	ATCC 13061	+	+	+	-	+	-
Bacillus cereus	ATCC 14579	-	+	+	+	+	+
Bacillus cereus	ATCC 21772	-	+	+	-	+	-
Bacillus cereus	ATCC 10876	-	+	+	-	+	+
Bacillus cereus	KCTC 3674	-	+	+	-	+	-
Bacillus cereus	ATCC 10987	-	+	+	-	+	-
Bacillus	KCTC	-	+	+	-	+	+

cereus	1094						
Bacillus thuringiensis	ATCC 10792	-	+	+	-	+	+
Bacillus mycoides	ATCC 6462	-	+	-	-	+	+
Bacillus subtilis	ATCC 23857	-	+	-	-	-	-
Bacillus subtilis	ATCC 6501	-	+	-	-	-	-
Bacillus megaterium	JCM 2506	-	+	-	-	-	-
Bacillus circulans	JCM 2504	-	+	-	-	-	-
Bacillus licheniformis	JCM 2505	-	+	-	-	-	-
Bacillus pumilus	JCM 2508	-	+	-	-	-	-

* The black box indicates the *B. cereus* group strains.

III-3-3. The lytic activity of LysPBC1_EAD

A number of studies have shown that the catalytic domains of endolysins can also be utilized as efficient antimicrobial agents (Daniel et al., 2010; Sass and Bierbaum, 2007; Schmelcher et al., 2012; Yang et al., 2014). These truncated endolysins often show increased protein solubility and lytic activity compared to the parental endolysins (Low et al., 2005; Mayer et al., 2011; Oliveira et al., 2013). Therefore, I designed the N-terminal amidase_3 enzymatic active domain of LysPBC1 (hereafter designated as LysPBC1_EAD) by adding a stop codon after 174 Asn and expressed the truncated protein in *E. coli*. Both full-length endolysin LysPBC1 and the truncated endolysin LysPBC1_EAD were overexpressed in *E. coli* and purified to homogeneity **(Fig. III-4A and B)**. The turbidity reduction assays with the same molar concentrations of the both proteins revealed that LysPBC1 showed stronger lytic activity against *B. cereus* cells compared with LysPBC1_EAD (**Fig. III-4C, Table III-4)**. However, LysPBC1_EAD showed higher lytic activity than LysPBC1 against non-native targets such as *B. subtilis* (**Fig. III-4D**). A similar pattern was observed for *B. pumilus* and *B. licheniformis*, both of which belong to the *B. subtilis* group (Matarante et al., 2004). These results indicate that the C-terminal cell wall binding domain of

LysPBC1 is essential for full activity of the endolysin only for its natural target.

The purified LysPBC1_EAD showed broad lytic activities towards *Bacillus* species as well as Gram-negative bacteria treated with EDTA **(Table III-4)**. As with full-length LysPBC1, LysPBC1_EAD did not lyse *Listeria* and *Clostridium* species despite the fact that the EAD of LysPBC1 exhibited significant sequence homology with that of PlyPSA (34% identity) and CD27L (29% identity). These results indicate that the catalytic domain alone maintains the host specificity and the removal of the cell wall binding domain rarely affects the lytic spectrum of LysPBC1. Other studies have also reported retained host specificity of the catalytic domain of endolysins (Mayer et al., 2011; Mayer et al., 2012), suggesting that species-specific structures surrounding catalytic sites determine the lytic activity of the endolysin. Alternatively, it could be that the non-conserved region of the LysPBC1_EAD is necessary for proper function of the protein onto its natural substrate.

It has been proposed that the cell wall binding domain of endolysin has an inhibitory role when it is not bound to the target (Low et al., 2011; Low et al., 2005). However, this is not the case for LysPBC1 because the cell

wall binding domain of LysPBC1 did not bind several *B. cereus* group strains (Kong et al., unpublished data) despite the fact that they were more sensitive to the full-length endolysin. These results suggest that, in addition to cell wall binding, the C-terminal domain of LysPBC1 may confer an additional role for full lytic activity of the endolysin against the *B. cereus* group strains. In the case of *B. subtilis* group strains, on the other hand, I propose that the differences in cell wall component between the *B. cereus group* and *B. subtilis* group are responsible for the variance in lytic activity. *B. subtilis* group bacteria display wall teichoic acid (WTA), containing a negatively charged phosphate group, through the peptidoglycan layer, whereas the *B. cereus* group bacteria lack the WTA (Anderson et al., 2005; Weidenmaier and Peschel, 2008). Instead, the *B. cereus* group contains an uncharged branched polysaccharide as a major cell wall component (Leoff et al., 2008). Consequently, the cell wall of *B. subtilis* is more likely to have a negative charge, and this net charge difference may influence the lytic activity of the endolysin. The theoretical isoelectric point of LysPBC1_EAD (7.15) is higher than that of LysPBC1 (6.79), supporting this explanation. It is also possible that the small size of LysPBC1_EAD (approximately 20.5 kDa) can penetrate the peptidoglycan layer of *B. subtilis* group more efficiently than

the full-length LysPBC1 (approximately 29.4 kDa), resulting in more rapid lysis of the cell.

III-3-4. Cell binding capacity of EGFP-fused CBDs

III-3-4-1. PBC1_CBD

The N-terminal catalytic domain of LysPBC1 is significantly conserved with PlyPSA while the putative CBD sequences of LysPBC1 and PlyPSA are totally different, suggesting that the putative CBD may determine host specificity. Phylogenetic analysis of the putative CBDs of the *B. cereus* group phages indicates that CBD of LysPBC1 is unrelated with other CBDs except for the putative CBD of phage 12826 (Loessner et al., 1997) **(Fig. III-6B)**. The amino acid sequence identity between the CBD of LysPBC1 and the putative CBD of phage 12826 is 76%. Because the putative CBD of phage 12826 is not experimentally proven to date, I selected the CBD of LysPBC1 as a novel recognition element for *B. cereus*. **Fig. III-6C** shows a 3D model of LysPBC1 based on the structure of PlyPSA, an endolysin of *Listeria* phage PSA. This protein structure prediction enabled me to define the putative CBD region in the endolysin sequence.

To examine the binding activity of CBD of LysPBC1, I genetically fused EGFP to the N-terminus of the CBD **(Fig. III-6D)**. The GFP-CBD fusion proteins were overexpressed in *E. coli* in the soluble form and easily purified by Ni-NTA affinity chromatography due to the N-terminal hexahistidine tag of the fusion proteins **(Fig. III-6E)**. The purified EGFP-CBDs were added to intact *B. cereus* strain ATCC 21768 cells and the optical and fluorescent images were observed **(Fig. III-6F)**. The images clearly show that EGFP-CBDs were uniformly attached to *B. cereus* cell surfaces. For comparison, only EGFP was added to *B. cereus*. **Fig. III-6G** shows the optical and fluorescent images of *B. cereus* after the addition of EGFP, indicating negligible binding of EGFP to *B. cereus*. I further examined the binding specificity of the GFP-CBDs by mixing them with various bacterial species. None of the other bacterial species except *B. cereus* were labeled with EGFP-CBDs, confirming that the binding of EGFP-CBDs was highly specific to *B. cereus* **(Table III-6)**. This result demonstrates that the CBDs of LysPBC1 can be highly specific biological probes for *B. cereus* detection.

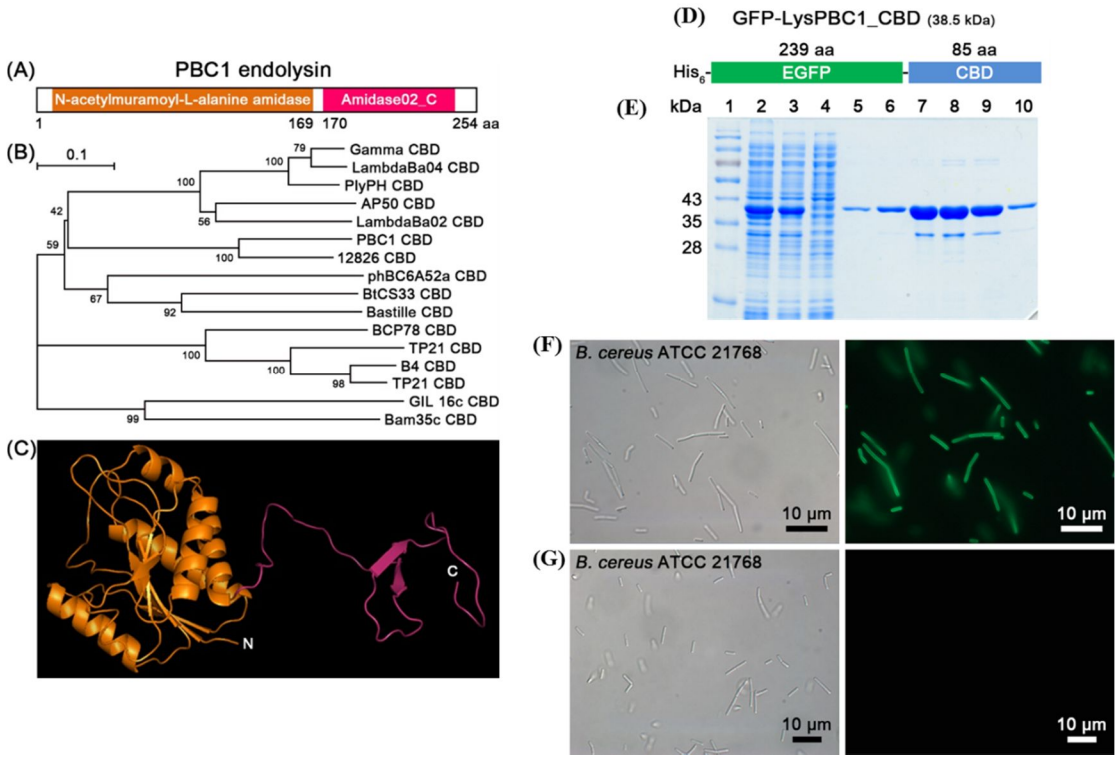
(A)
PBC1 endolysin
N-acetylmuramoyl-L-alanine amidase
Amidase02_C
1
169 170
254 aa
(B)
0.1
Gamma CBD
LambdaBa04 CBD
PlyPH CBD
AP50 CBD
LambdaBa02 CBD
PBC1 CBD
12826 CBD
phBC6A52a CBD
BtCS33 CBD
Bastille CBD
BCP78 CBD
TP21 CBD
B4 CBD
TP21 CBD
GIL 16c CBD
Bam35c CBD
(C)
N
C
(D)
GFP-LysPBC1_CBD (38.5 kDa)
239 aa
85 aa
His6-
EGFP
CBD
(E)
kDa
1 2 3 4 5 6 7 8 9 10
43
35
28
(F)
B. cereus ATCC 21768
10 μm
10 μm
(G)
B. cereus ATCC 21768
10 μm
10 μm

Fig. III-6. Confirmation of cell binding activity of EGFP-PBC1_CBD fusion protein. (A) Schematic representation of PBC1 endolysin (LysPBC1). The N-terminal (orange) and C-terminal (magenta) domains are presented. (B) A phylogenetic tree indicating the relationships between CBDs examined in the present study. For calculation of the tree, the respective amino acid sequences, including the putative linker regions, were used. (C) Predicted 3D structure of LysPBC1 based on the crystal structure of *Listeria* phage endolysin PlyPSA (PDB 1D: 1XOV). (D) Schematic representation of GFP-LysPBC1_CBD. (E) SDS-PAGE analysis of GFP-CBD (Lane 1, size marker; lane 2, cell extract; lane 3, supernatant, lane 4, Ni-NTA flow-through; lane 5, washing (10 mM imidazole); lane 6, washing (20 mM imidazole); lane 7 to 10, elution (240 mM imidazole)). (F) Optical and fluorescent images of *B. cereus* after the addition of GFP-LysPBC1_CBD and (G) GFP. The fluorescent images show that *B. cereus* cell surfaces were evenly decorated with GFP-LysPBC1_CBD while GFP alone was not.

Table III-6. Binding spectrum of CBDs from *B. cereus* phage endolysins

Species	Strain number	PBC1 CBD	PBC2 CBD	PBC4 CBD	PBC5 CBD	PBC6 CBD	PBC10 CBD	B4 CBD
Bacillus cereus	ATCC 27348	-	+	+	-	+	-	+
Bacillus cereus	ATCC 21768	+	-	-	+	-	+	+
Bacillus cereus	ATCC 13061	+	+	-	+	-	+	+
Bacillus cereus	ATCC 14579	-	+	+	+	-	-	+
Bacillus cereus	ATCC 21772	-	+	-	+	+	+	+
Bacillus cereus	ATCC 10876	-	+	+	+	+	-	+
Bacillus cereus	KCTC 3674	-	+	-	-	-	-	+
Bacillus cereus	ATCC 10987	+	+	-	+	+	-	+
Bacillus cereus	KCTC 1094	-	+	+	-	-	-	+
Bacillus thuringiensis	ATCC 10792	-	+	+	+	-	-	+
Bacillus mycoides	ATCC 6462	-	-	+	-	-	-	+
Bacillus subtilis	ATCC 23857	-	-	-	-	-	-	-
Bacillus subtilis	ATCC 6501	-	-	-	-	-	-	-

Bacillus megaterium	JCM 2506	-	-	-	-	-	-	-
Bacillus circulans	JCM 2504	-	-	-	-	-	-	-
Bacillus licheniformis	JCM 2505	-	-	-	-	-	-	-
Bacillus pumilus	JCM 2508	-	-	-	-	-	-	-
Staphylococcus aureus	ATCC 29213	-	-	-	-	-	-	-
Clostridium perfringens	FD-1	-	-	-	-	-	-	-
Listeria monocytogenes	ScottA	-	-	-	-	-	-	-
Escherichia coli	MG1655	-[a]/-[b]	-/+	-/-	-/-	-/ +	-/-	-/+
Cronobacter sakazakii	ATCC 29544	-/-	-/+	-/-	-/-	-/-	-/-	-/+

* The black box indicates the *B. cereus* group strains.

a. Before 0.1 M EDTA treatment

b. After 0.1 M EDTA treatment

III-3-4-2. PBC2_CBD

The C-terminal region of LysPBC2 has two SH3_3 domains, which are also present in several endolysins (Ganz et al., 2014b; Tamai et al., 2014). Crystal structure of the Psm endolyin from *C. perfringens* phage phiSM101 revealed that tandem repeated SH3_3 domains of Psm are expected to recognize peptide side-chains of *C. perfringens* peptidoglycans, suggesting that LysPBC2 has the SH3_3 domains as a CBD. The limited similarity (13% identify) of the SH3_3 domains between LysPBC2 and Psm implies different CBD binding epitopes or cell wall structures of both organisms. The EGFP-tagged CBD gene of LysPBC2 was cloned and expressed in *E. coli* in soluble form. The EGFP-PBC2_CBD fusion protein demonstrated broad binding spectrum towards *B. cereus* group strains **(Fig. III-7A and Table III-6)**. No binding was detected in other *Bacillus* species, as well as other genera of bacteria (**Fig. III-7B)**. Interestingly, PBC2_CBD could bind to *E. coli* and *Cronobacter sakazakii*, only when they were treated with 0.1 M of EDTA for outer membrane permeabilization (**Fig. III-7C)**. These results coincided with the lytic activity of LysPBC2 against the Gram-negative bacteria treated with EDTA. The most likely explanation of these results is that PBC2_CBD recognize and bind to common epitopes, presented by both *B. cereus* group

strains and the Gram-negative bacteria. Since the peptidoglycan type of *Bacillus* and the Gram-negative is same (A1γ) (Mo et al., 2012), the conserved primary structure of the peptidoglycan may be the binding target of PBC2_CBD. Meanwhile, some *B. cereus* strains and other *Bacillus* species were not bound by PBC2_CBD, implicating that strain- or species-specific moieties of cell wall structure are also critical for the binding capacity of PBC2_CBD.

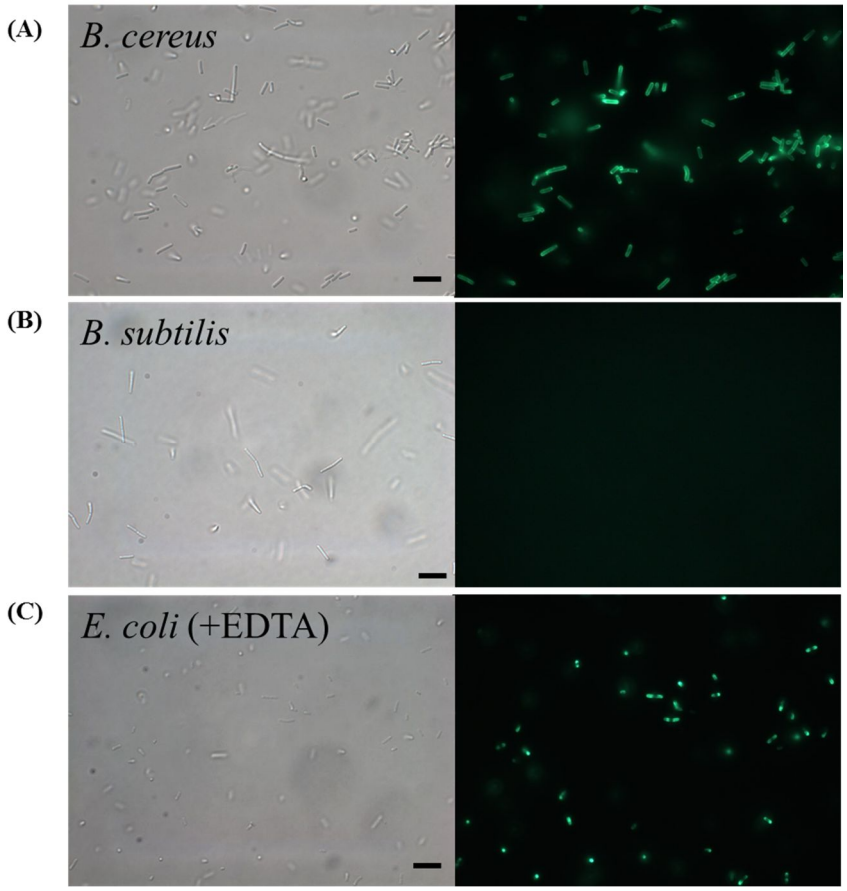

Fig. III-7. Binding of EGFP-PBC2_CBD fusion protein with different bacteria. Binding of GFP-LysPBC2_CBD fusion protein with *B. cereus* (A), *B. subtilis* (B), and EDTA-treated *E. coli* cells (C). Left panel, light microscopy images; Right panel, epifluorescent microscopy images. Scale bars, 10 um.

III-3-4-3. PBC4_CBD

LysPBC4 is composed of two distinct domains (an N-termianal amidase_3 domain and a C-terminal amidase_02C domain) connected by a putative linker region (**Fig. III-8A**). To confirm the binding activities of the C-terminal amidase_02 domain, two different length variants (one is with a putative linker and the other is without a putative linker) were tested (**Fig. III-8B**). Both constructs were tagged with EGFP at their N-terminus, and named as EGFP_PBC4_CBD1 and EGFP_PBC4_CBD2, respectively. As shown in **Fig. III-8C**, the EGFP_PBC4_CBD1, which includes a putative linker sequence, displayed a strong cell wall binding property, whereas the EGFP_PBC4_CBD2, which devoid of the putative linker, showed no binding activity. These results indicate the importance of a putative linker region for cell wall binding capacity of EGFP-tagged PBC4_CBD. The putative linker region of LysPBC4 is rich in flexible residues like glycine and serine, and polar residues, such as asparagine and thereonine. It could be that the putative linker region is critical for proper folding of PBC4_CBD. It is also possible that the linker itself plays an important role in binding cell wall of the *B. cereus*. Further study would be necessary to elucidate the exact role of the linker region of LysPBC4. Binding spectrum of EGFP_PBC4_CBD

showed that PBC4_CBD could bind to 4 of 9 strains of *B. cereus* and two other *B. cereus* group species tested **(Table III-6)**. Other bacteria, such as *B. subtilis* and other bacterial species could not be bound by PBC4_CBD. These results suggest that *B. cereus* group-specific cell wall moieties are the most likely binding target of PBC4_CBD. Interestingly, binding specificity of PBC4_CBD and were complementary to the binding range of PBC1_CBD; *B. cereus* group strains labeled by PBC4_CBD did not react with PBC1_CBD and vice versa. These binding patterns were also reported in *Listeria* phage CBDs, where the CBDs showed distinctive binding patterns to cell walls of different serovar groups (Schmelcher et al., 2010). I speculate that the ligand of PBC4_CBD is probably present in certain *B. cereus* strains, and that could be different from the ligand of PBC1_CBD.

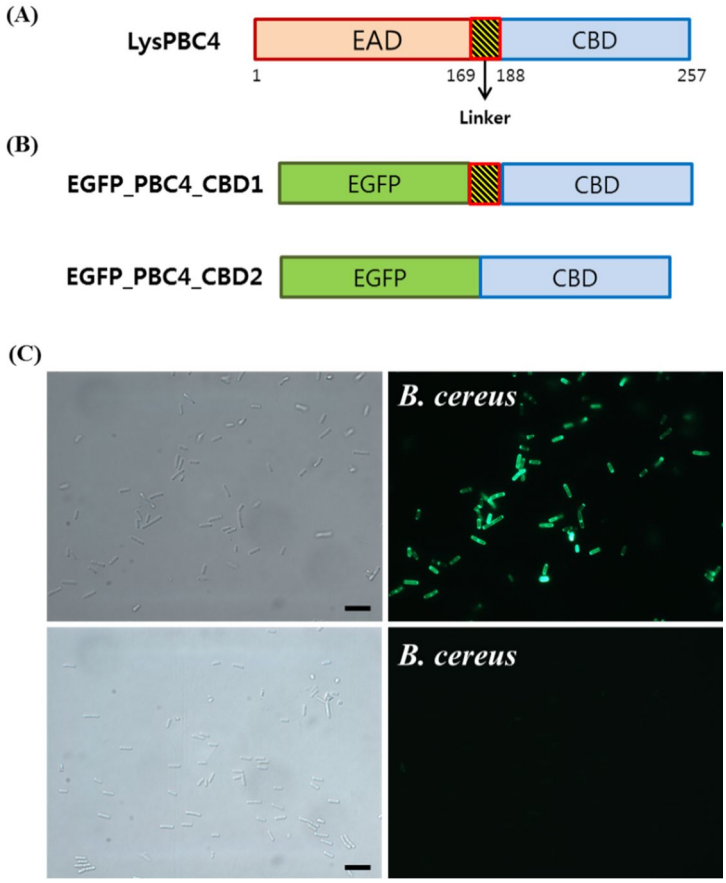

Fig. III-8. Role of the putative linker region for cell binding activity of EGFP-PBC4_CBD fusion protein. Schematic representation of LysPBC4 (A) and two different constructs of EGFP-PBC4_CBD with or without the putative linker region (B). (C) Cell binding assays with EGFP-PBC4_CBD1 (top), and EGFP-PBC4_CBD2 (bottom) indicate that PBC4_CBD has cell binding activity only when it possesses the putative linker region. Scale bars, 10 um.

III-3-4-4. Other CBDs

LysB4 was isolated from *B. cereus* phage B4 and showed strong lytic activity against a broad range of bacteria including *Bacillus*, *Listeria* and EDTA-treated Gram-negative bacteria (Son et al., 2012). It has an N-terminal L-alanoyl-D-glutamate endopeptidase domain (PF02557) and a C-terminal SH3_5 domain (PF08460). Since the SH3_5 domain is commonly found in phage endolysins and known to be functions as a likely CBD, I tested the cell wall binding capacity of LysB4_CBD (B4_CBD). B4_CBD displayed *B. cereus* group-specific, but broad binding spectrum as all *B. cereus* group strains tested were decorated by the B4_CBD **(Fig. III-9A and Table III-6)**. This binding spectrum did not match the lytic range of the endolysin because LysB4 could lyse *B. subtilis* and *Listeria* cells too. These results indicate that the EAD itself, as well as the CBD, determines the lytic specificity of the endolysin LysB4. The broad, but *B. cereus* group specific binding property of B4_CBD could be a useful tool for detection of diverse *B. cereus* group strains.

Both LysPBC5 and LysPBC10 are endolysins harboring a glycoside hydrolase 25 family domain at the N-terminus, but no apparent CBD at the C-terminus. I cloned and produced their putative novel CBDs (PBC5_CBD,

PBC10_CBD) recombinantly in *E. coli* with N-terminal tagging with EGFP. They were well expressed as soluble form, and exhibited cell binding activity in a *B. cereus* strain specific manner **(Fig. III-9C, D, and Table III-6)**. These results confirmed that both PBC5_CBD and PBC10_CBD are unidentified, novel domains, which function to bind cell wall of *B. cereus*.

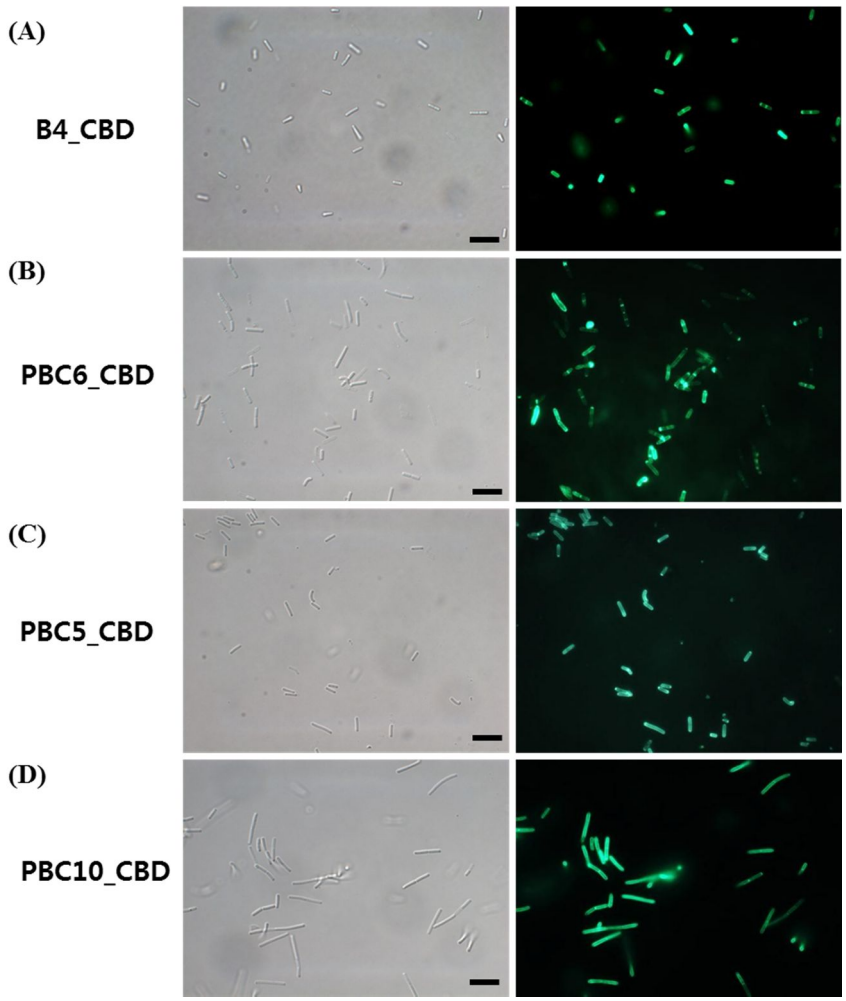

Fig. III-9. Cell binding activities of various EGFP-CBDs. *B. cereus* cells fluorescently labeled by EGFP-tagged B4_CBD (A), PBC6_CBD (B), PBC5_CBD (C), and PBC10_CBD. Left panel, light microscopy images; Right panel, epifluorescent microscopy images. Scale bars, 10 um.

III-3-4-5. Influence of NaCl and pH on the binding activity of CBDs

I chose two CBDs (PBC1_CBD, B4_CBD) for further characterization due to the high binding density of PBC1_CBD and the broad binding range of B4_CBD observed by fluorescence microscopy. Because GFP fluorescence is very sensitive to lower pH (pH >5) (Haupts et al., 1998; Kneen et al., 1998), whereas mCherry is more tolerant to pH change than GFP (Doherty et al., 2010), I produced recombinant mCherry-tagged CBD fusion proteins to examine the effect of NaCl and pH on their binding activity. The optimum NaCl concentration on binding of the PBC1_CBD to *B. cereus* cells was shown to be 200-500 mM **(Fig. III-10A)**, whereas the optimum binding of B4_CBD occurred at 0 mM NaCl **(Fig. III-10B)**, which correlated the optimal lytic activity of LysB4 (Son et al., 2012). Both CBDs showed relatively stable interaction with its ligand even at 2M salt. However, binding of both CBDs were significantly affected by pH of the buffer. The optimum pH for PBC1_CBD is 5, and in the range of pH 5-6 for B4_CBD **(Fig. III-10C, D)**. Increasing pH values resulted in decreased binding of both CBDs, and at pH 10, only about 10% of fluorescence relative to maximum value was remained. The preference of acidic condition for binding of both CBDs did not correspond to the optimal peptidoglycan

hydrolase activity of LysPBC1 (optimum at pH 8) and LysB4 (optimum at pH 8.5) (Son et al., 2012). These results indicate a complex and multifaceted interaction between the endolysins and their cognate targets.

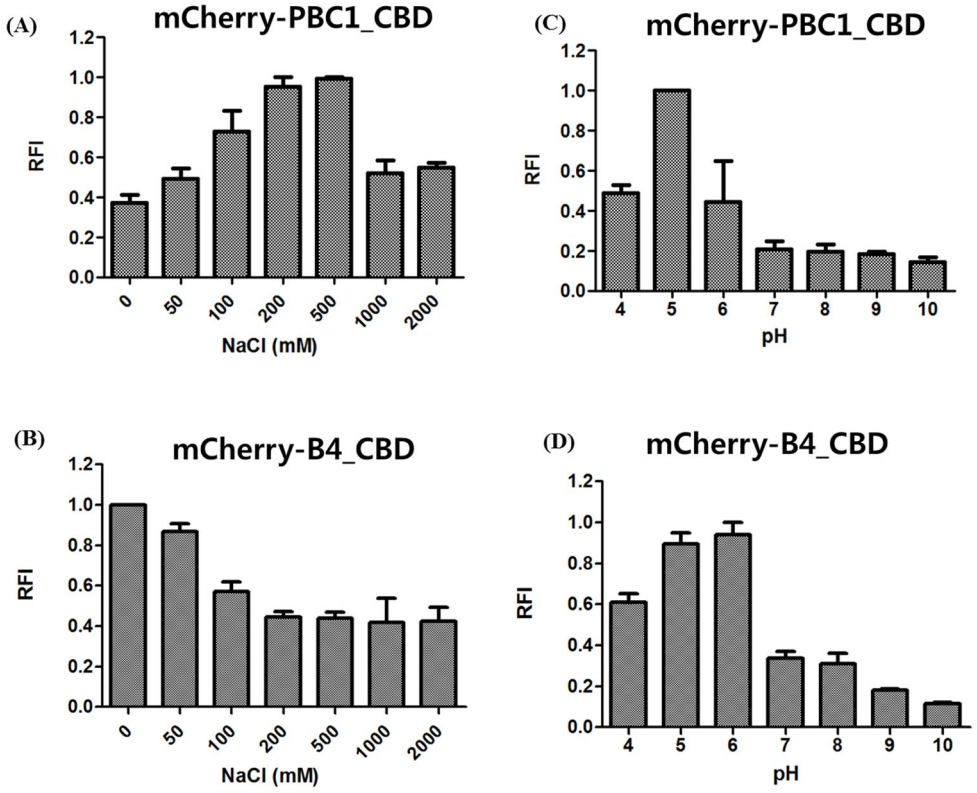

Fig. III-10. The effect of NaCl and pH on the binding activity of mCherry-labeled CBDs.

(A, B) Relative cell binding activities of mCherry-tagged PBC1_CBD (A) and mCherry-tagged B4_CBD (B) to cells of *B. cereus* strains ATCC 21768, and ATCC 13061, respectively, under different NaCl concentrations. (C, D) Binding of mCherry-tagged PBC1_CBD (C) and mCherry-tagged B4_CBD (D) at different pH conditions. All assays were carried out in triplicate.

III-3-5. Spore binding capacity of SBD of LysPBC2

LysPBC2 showed overall sequence similarity to the *B. anthracis* phage endolysin PlyG (34% amino acid identity) (Kikkawa et al., 2008) **(Fig. III-2B)**. Previously, Yang et al., reported that PlyG has separate binding domains to recognize spores and vegetative cells (Yang et al., 2012). A 60-amino-acid domain, located mainly within the catalytic domain of PlyG (residues 106 to 165), specifically binds to *B. anthracis* spores but not vegetative cells. Since the EAD of LysPBC2 has significant amino acid sequence identity (57%) to the catalytic domain of PlyG, I presumed that LysPBC2 also has a spore binding domain (SBD). To confirm the hypothesis, two truncated fragments (residues 108 to 170 for SBD1, residues 127 to 147 for SBD2) of LysPBC2 were fused with EGFP and expressed in *E. coli*. Both recombinant proteins were well expressed and the purified proteins were used for the spore binding assays. Fluorescence microscopic analysis revealed that the EGFP-SBD1 fusion protein displayed an obvious ability to bind to *B. cereus* spores, but only limited labeling was observed with the EGFP-SBD2 fusion protein. Thus, the SBD1 was identified as SBD of LysPBC2 (hereafter, I refer to this construct as PBC2_SBD). PBC2_SBD contains 63 amino acids, and has a high degree of sequence identity (46%)

with the SBD of PlyG.

The multi-functional modular structure of LysPBC2 was shown in **Fig. III-11A**. The PBC2_ SBD could discriminate between spores and vegetative form of *B. cereus* as it did not bind to vegetative cells **(Fig. III-11B)**. On the other hand, PBC2_CBD could label vegetative cells, but not the spores of *B. cereus*. The binding specificity of PBC2_SBD was examined by incubation with other *Bacillus* spores (*B. subtilis*, *B. megaterium*) as well as spores from other *B. cereus* strains. As shown in **Table III-7**, PBC2_SBD specifically binds to *B. cereus* spores, whereas spores of *B. subtilis* and *B. megaterium* did not react with PBC2_SBD. This binding spectrum differs from that in a previous report (Yang et al., 2012), showing that the SBD of PlyG specifically recognized *B. anthracis* spores and did not bind to *B. cereus* spores. Given that *B. cereus* spores are closely related to the spores of *B. anthracis* (Mukhopadhyay et al., 2009), the different binding range implied that both SBDs may have different binding targets despite their high sequence homologies (46% identity). The complementary binding properties of SBD and CBD prompted me to combine both domains for labeling both spores and vegetative form of *B. cereus*. The resulting EGFP-tagged SCBD fusion protein showed binding capacity to both spores and vegetative cells,

though cells were more strongly decorated by the protein in the mixed samples (**Fig. III-11C)**. Altogether, the results presented here validated the existence of separate domains within LysPBC2 for specific recognition of *B. cereus* spores and cells. The specific binding activity of PBC2_SBD can be harnessed for the specific detection of the *B. cereus* spores, the common contaminants in foods (Carlin, 2011).

Table III-7. Spore binding selectivity of the LysPBC2_SBD

Species	Strain number	LysPBC2_SBD
Bacillus cereus	ATCC 13061	+
Bacillus cereus	ATCC 21768	+
Bacillus cereus	ATCC 14579	+
Bacillus cereus	ATCC 10876	+
Bacillus subtilis	ATCC 23857	-
Bacillus megaterium	JCM 2506	-

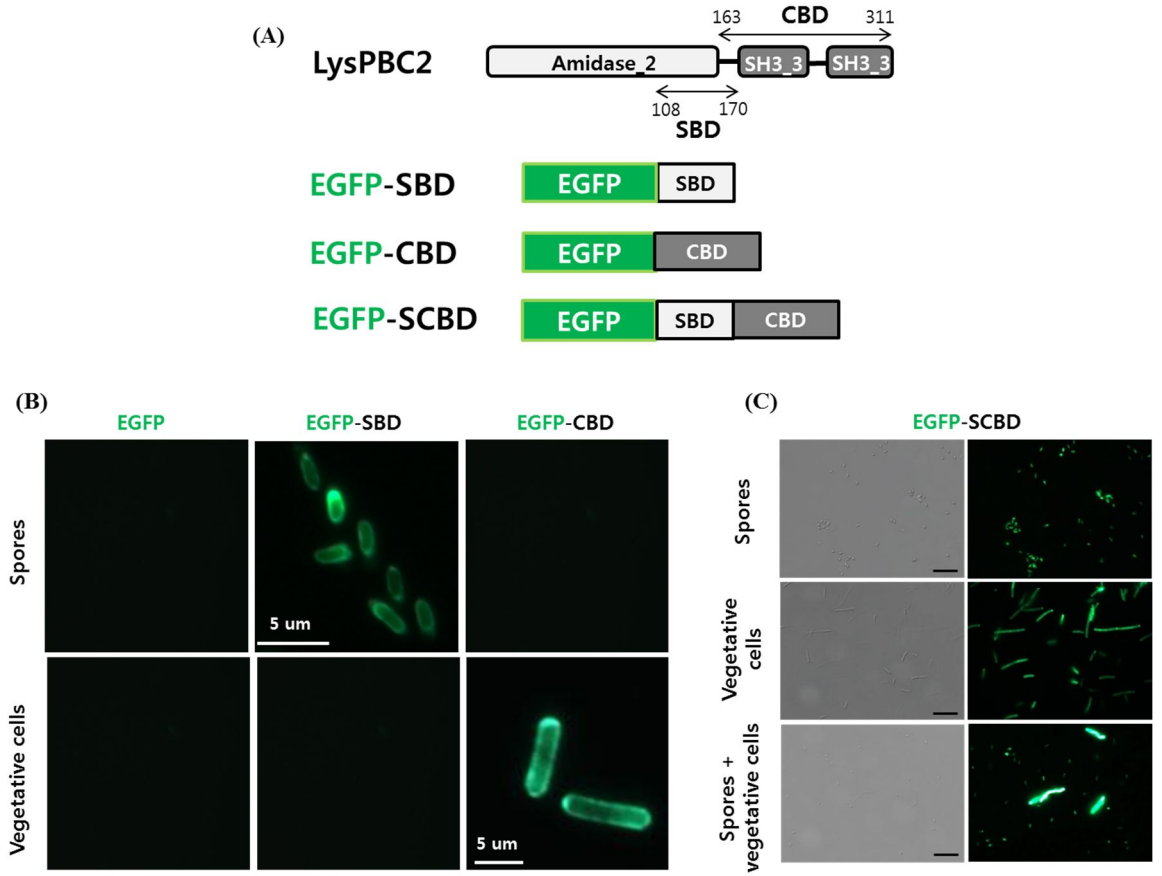
(A)
LysPBC2
163
CBD
311
Amidase_2
SH3_3
SH3_3
108
170
SBD
EGFP-SBD
EGFP
SBD
EGFP-CBD
EGFP
CBD
EGFP-SCBD
EGFP
SBD
CBD
(B)
EGFP
EGFP-SBD
EGFP-CBD
Spores
Vegetative cells
5 um
5 um
(C)
EGFP-SCBD
Spores
Vegetative cells
Spores + vegetative cells

Fig. III-11. Spore binding activity of EGFP-PBC2_SBD fusion protein. (A) Schematic diagram of the multi-functional modular structure of LysPBC2 and EGFP-fused constructs used in this study. (B) Binding capacities of the EGPF-only, EGFP-SBD, and EGFP-CBD for *B. cereus* spores and vegetative cells. (C) EGFP-tagged SCBD fusion protein showed binding activity to both *B. cereus* spores and vegetative cells. Scale bars = 5 um.

An earlier study reported that the exosporium of the spores may be the most probable binding target of the PlyG_SBD (Yang et al., 2012). In *B. cereus*, the outer portions of spores consist of a cortex, a spore coat layer, and an exosporium. The cortex is an innermost thick peptidoglycan layer, and is responsible for maintaining the highly dehydrated state of the core (Imamura et al., 2011). A thin proteinaceous spore coat encases the core and the cortex, and is essential for protecting spores from various environmental stresses (Nicholson et al., 2000). Separated from the coat by an interspace, the exosporium is the outermost spore layer and is composed of an inner basal layer and an outer hair-like nap (Fazzini et al., 2010). To test whether the exosporium is a likely binding target of PBC2_SBD, I used two different methods (sonication, detergent) to disrupt the exosporium layer (Thompson et al., 2011; Wang et al., 2009). Electron microscopy of sectioned spores showed that there was no noticeable detects in the exosporium or spore coat layers of the untreated spores **(Fig. III-12A)**. Closer analysis of the ruthenium red-stained hair-like nap on the exosporium revealed that sonicated spores had almost intact nap layer while the spores extracted with both SDS and urea exhibited greater disruption of the hair-like nap layer. Further experiments showed that the EGFP-fused PBC2_SBD could bind to

sonicated spores as well as the spores treated with SDS and urea **(Fig. III-12B)**. Especially, the SDS-urea treated spores displayed much higher fluorescence intensity than that of intact spores and sonicated spores. Quantitative fluorescence analysis confirmed this result that more than seven times higher signal was observed with SDS-urea treated spores compared to intact spores **(Fig. III-12C)**. The addition of sonication treatment slightly enhanced the binding of PBC2_SBD. My observations were opposed to the previous results of PlyG_SBD, which showed significantly reduced fluorescence intensity towards sonicated spores (Yang et al., 2012). The contradictory results between PBC2_SBD and PlyG_SBD may be due in part to different nature of the binding targets or strain differences (spores from *B. cereus* ATCC 13061 versus *B. anthracis* A16) or even how the spores were prepared prior to sonication (Thompson et al., 2011).

Both TEM and fluorescence microscopic data suggest that the exosporium nap layer may not be the binding target of the PBC2_SBD. Although the biological role of this PBC2_SBD remains to be determined, it is intriguing that the phage PBC2 encodes a separate spore binding domain within its endolysin, LysPBC2. Considering that the interchange of functional domains of endolysins occurs naturally between phages and

bacterial hosts (Hendrix, 2002), it could that PBC2 acquired the spore binding motif of host sporulation proteins through horizontal gene transfer during evolution. BLASTP analysis using the cell wall binding domain (CBD) of LysPBC2 as query revealed the significant homology of the CBD with many spore-lytic enzymes of *B. cereus,* supporting this speculation. From the standpoint of the bacterial host, the localization of LysPBC2 on the spores could be beneficial if the amidase domain would be involved in degrading the cortex peptidoglycan during spore germination. Indeed, a number of germination-specific N-acetylmuramoyl-L-alanine amidase have been identified in *B. cereus* spores (Moriyama et al., 1999), and several of these major cortex-lytic enzymes are thought to be localized on the spore coat (Bagyan and Setlow, 2002; Chirakkal et al., 2002). In addition, trapping the phage endolysin on spores could prevent possible 'lysis from without' caused by released endolysins during the late phase of infection, which keeps survival of neighboring cells and eventually the ecological balance between phages and their hosts.

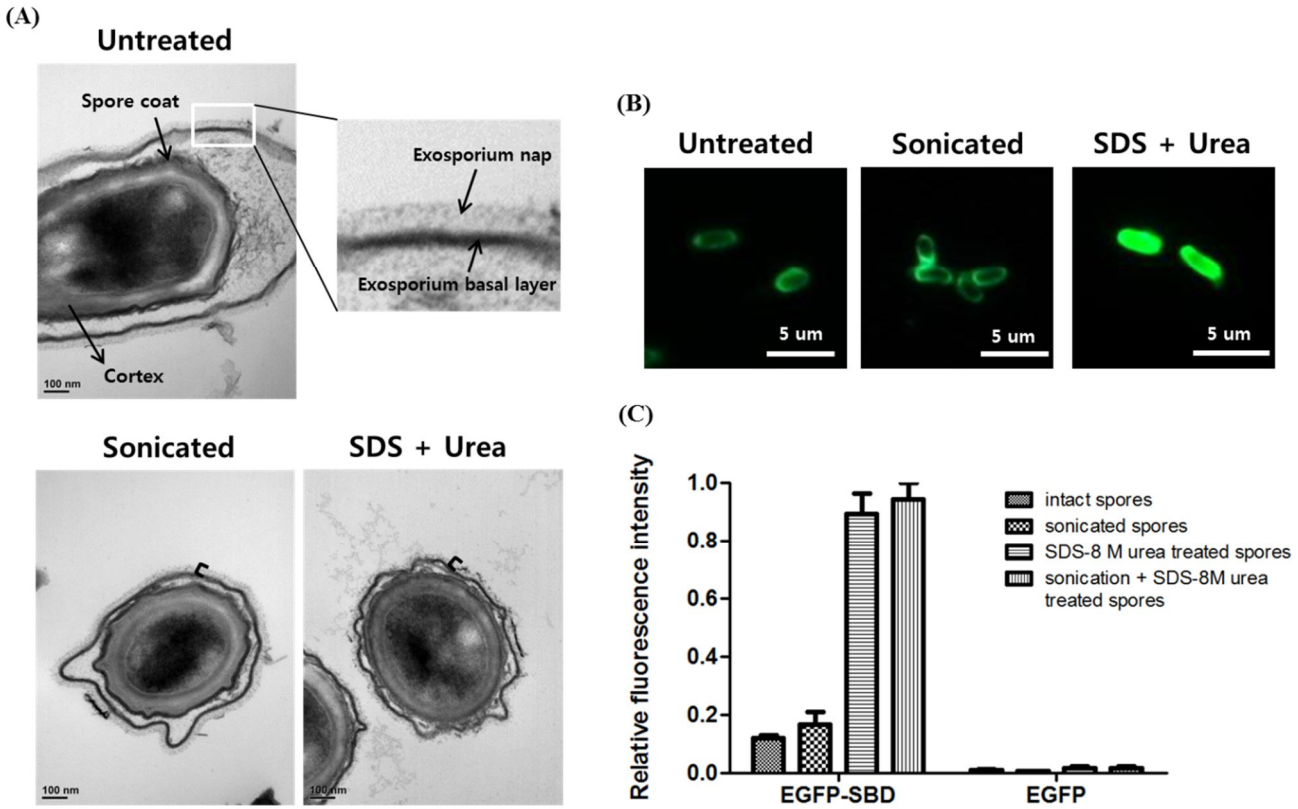
(A)
Untreated
Spore coat
Exosporium nap
Exosporium basal layer
Cortex
100 nm
Sonicated
SDS + Urea
100 nm
100 nm
(B)
Untreated
Sonicated
SDS + Urea
5 um
5 um
5 um
(C)
Relative fluorescence intensity
1.0
0.8
0.6
0.4
0.2
0.0
intact spores
sonicated spores
SDS-8 M urea treated spores
sonication + SDS-8M urea treated spores
EGFP-SBD
EGFP

Fig. III-12. Exosporium nap may not be the binding target of the SBD. (A) Top, TEM of untreated spores. Inset shows exosporium basal layer and hair-like nap. Bottom, TEM of spores sonicated or treated with SDS and urea buffer. The brackets denote the hair-like nap layer on the exosporium. All panels stained with ruthenium red to visualize the heavily glycosylated exosporium nap. (B) Binding profiles of the EGFP-SBD with *B. cereus* intact spores, sonicated spores and SDS-urea treated spores. (C) Relative fluorescence intensities of differently treated spores after incubation with EGFP- SBD and EGFP-only proteins.

III-3-6. CBD from bacterial genome

Although there has been an increasing interest in the use of CBDs to detect bacterial pathogens as alternatives to currently used antibodies, identifying a novel CBD from a phage endolysin is time-consuming and labor-intensive due to the following reasons. First, a novel phage should be isolated and its genome should be extracted and sequenced. Second, the full genome annotation requires skilled person and considerable time. Therefore, a novel method to find a CBD is needed for the wide use of CBDs as bioprobes. Here, I present a facile and efficient method for identifying a novel CBD from a sequenced bacterial genome. This method relies on the idea that most bacteria harbor phage genes within their genome as prophages or short phage remnants (Brussow et al., 2004). For example, the genome of *Escherichia coli* O157:H7 strain Sakai contains 16% of prophage elements (Hayashi et al., 2001), and in *Streptococcus pyogenes*, phage-related sequences account for more than 10% of the total genome (Beres et al., 2002). These phage genes are often involved in lateral gene transfer and they have a major impact on bacterial genome evolution (Canchaya et al., 2003). Based on this idea, I hypothesized that I could exploit these sequences as potential reservoir for extracting CBDs of various target pathogens. In this

thesis, I chose *C. perfringens* as a model organism because anaerobic nature of this bacterium makes it tricky to grow, which in turn leads to difficulties in *C. perfringens* phage isolation.

III-3-6-1. Analysis of lytic enzymes in *C. perfringens* ATCC 13124

C. perfringens ATCC 13124 originally isolated from a gas gangrene patient (Myers et al., 2006) was used as a source for finding a putative CBD within a bacterial genome as its complete genome sequence is available at NCBI database (reference sequence: NC_008261.1). I used amino acid sequences of catalytic domains of the selected endolysins for BLAST search because the catalytic domains are conserved relatively higher than the full-length endolysins, which generally contain host-specific cell wall binding domain(s). The BLAST results showed four Psm homologs and one Ply3626 homolog in the genome of *C. perfringens* ATCC 13124 **(Table III-8)**. Among these five putative lytic enzymes, YP_695420 is identical to the well-characterized muramidase, PlyCM (Schmitz et al., 2011), and encoded within prophage region of the genome containing phage terminase, holin, and capsid protein encoding genes. YP_696011 is almost same as Psm (96% identity) and resides in another prophage region. The absence of phage associated genes nearby both YP_695964 and YP_696189 encoding genes

suggests that these two lytic enzymes may be bacterial cell wall autolysins. Especially, YP_696189 (putative amidase) showed a 64% amino acid sequence identity with the phage endolysin Ply3626, indicating close relationship between phage endolysins and bacterial autolysins (Loessner et al., 1997). YP_694826 seemed to reside in small prophage remnant region due to the lack of nearby phage-related genes except a holin (YP_694827).

Table III-8. Homologs of Psm and Ply3626 in *C. perfringens* ATCC 13124

Protein	AA Identity (Psm)	Holin	Phage genes nearby	Identified domains
YP_696011	96%	No	Yes	GH25, 2 x SH3_3
YP_695420	93%	Yes (YP_695418)	Yes	GH25, 2 x SH3_3
YP_694826	71%	Yes (YP_694827)	No	GH25, 2 x SH3_3
YP_695964	22%	No	No	GH25
YP_696189	64% (Ply3626)	No	No	Amidase_3

III-3-6-2. Identification of CBD from CPF369

Among the five lytic enzymes, I analyzed YP_694826 (Gene symbol: CPF_0369, I hereafter refer to YP_694826 protein as CPF369) further for two reasons. First, the CPF369 protein contains an N-terminal catalytic N-acetylmuramidase (glucoside hydrolase 25 family) domain and two C-terminal tandem repeated SH3_3 domains **(Fig. III-13A)**, which are presumed to function in bacterial cell wall binding (Xu et al., 2009). Second, I could predict the protein structure of CPF369 more accurately **(Fig. III-13B)** because the crystal structure of Psm endolysin, which shares significant amino acid identity (71%) with the CPF369 **(Fig. III-13C)**, is available at the Protein Data Bank (PDB ID: 4KRT) (Tamai et al., 2014). Although both YP_696011 and YP_695420 (PlyCM) also fulfill these criteria, I preferred to give priority to dissimilarity of CPF369 to previously characterized endolysins. As shown in **Fig. III-13B**, I could identify putative linker region between N-terminal enzymatic active domain (EAD) and C-terminal CBD consisting of two SH3_3 domains. These results made it easier for me to predict CBD of CPF369 (CPF369_CBD) starting from Val 203 to stop codon.

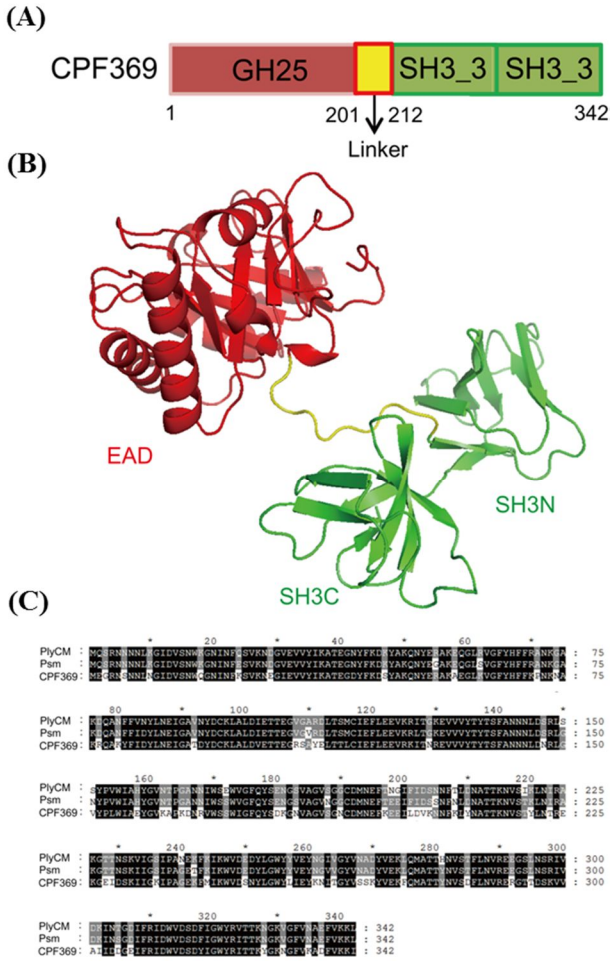

Fig. III-13. Schematic description of CPF369. (A) Schematic description of CPF369. (B) Deduced three-dimensional model of CPF369. An enzymatic active domain (GH25, red) and tandem-repeated SH3_3 domains (green) are connected by flexible linker (yellow). (C) Amino acid sequence alignment among CPF369-related endolysins. PlyCM, endolyins of *C. perfringens* phage phiSM101; Psm, endolysin of *C. perfringens* phage phi3626.

III-3-6-3. *C. perfringens*-specific binding activity of CPF369_CBD

The EGFP-CPF369_CBD fusion protein was expressed in *E. coli* and easily purified to homogeneity by single Ni-NTA affinity chromatography because of the N-terminal decahistidine tag **Fig. III-14A**. EGFP-CPF369_CBD could bind all *C. perfringens* strains tested, whereas other genus or species bacteria could not be labeled by the fusion protein **Fig. III-14B** and **Table III-9**). EGFP alone did not label the *C. perfringens* cells **(Fig. III-14C)**. These results confirmed that CPF369_CBD specifically binds to *C. perfringens* cells. The effects of NaCl and pH on the binding activity of EGFP-CPF369_CBD fusion protein were investigated **(Fig. III-14D**, **E)**. The optimum NaCl concentration was 50 mM, but the CPF369_CBD retained a certain degree (43%) of its binding activity even at 2 M of NaCl. The optimum pH condition for binding activity of CPF369_CBD was between pH 7 and 8. The binding activity decreased rapidly at pH 10, resulting in only 17% of binding compared to the value at pH 7.

In sum, I successfully identified a CBD from a genome (NCBI gene ID: 4201291) of *C. perfringens* ATCC 13124 and confirmed its specific binding to *C. perfringens*. This method only requires simple homology analysis; neither phage isolation nor phage genome sequencing is needed. I

think that it could be a general approach for CBD identification from sequenced bacterial genomes. With the rapid increase of bacterial genome announcements, my method will be useful for discovering novel bioprobes for detection of pathogenic bacteria.

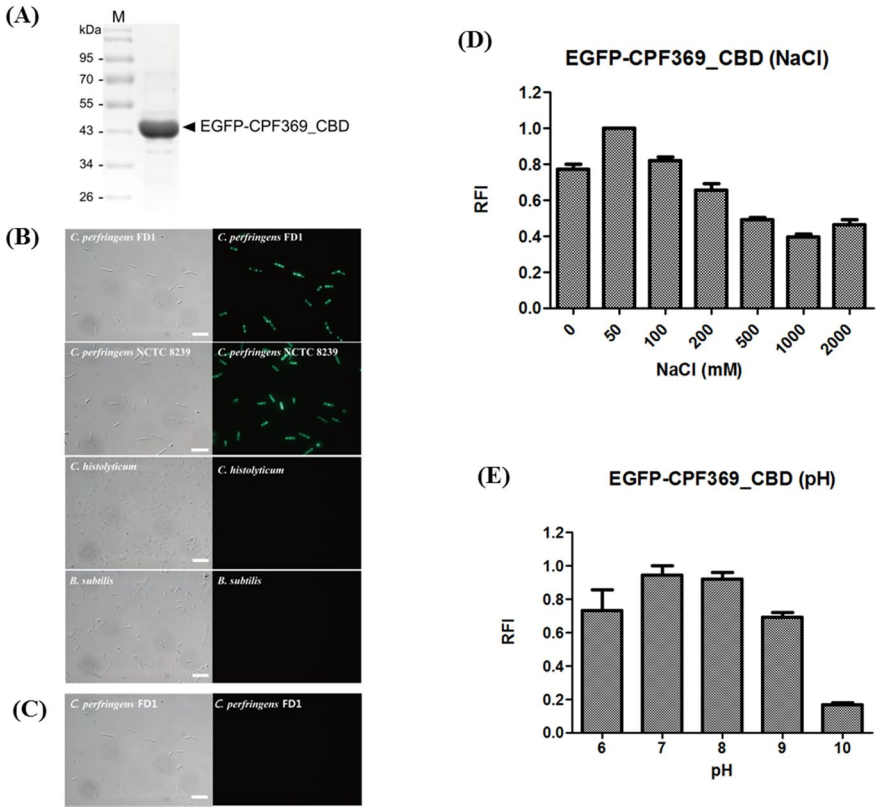

Fig. III-14. *C. perfringens*-specific binding activity of EGFP-CPF369_CBD and the effect of NaCl and pH on the binding activity of EGFP-CPF369_CBD. (A) Purified EGFP-CPF369_CBD fusion protein. M, prosi prestained protein marker (GenDepot). (B) *C. perfringens*-specific binding activity of CPF369_CBD. (C) EGFP alone did not bind to *C. perfringens* cells. Scale bars, 10 um. (D-E) Binding of EGFP-tagged CPF369_CBD on *C. perfringens* cells under different NaCl (D) and pH (E) conditions. All assays were carried out in triplicate.

Table III-9. Binding spectrum of CPF369_CBD

Species	Strain number	CPF369_CBD
Clostridium perfringens	ATCC 13124	+
Clostridium perfringens	NCTC 8798	+
Clostridium perfringens	NCTC 8239	+
Clostridium perfringens	ATCC 3624	+
Clostridium perfringens	FD1	+
Clostridium indolis	ATCC 25771	-
Clostridium histolytycum	ATCC 19401	-
Bacillus cereus	ATCC 14579	-
Bacillus subtilis	ATCC 23857	-
Listeria monocytogenes	EGDe	-
Staphylococcus aureus	ATCC 29213	-

ATCC, American Type Culture Collection; NCTC, National Collection of Type Cultures.

III-3-7. Cell binding capacity of a CBD from a *Staphylococcus* phage SA13

To provide a CBD toolbox for simultaneous detection of multiple pathogens, I aimed to find a CBD from a phage infecting *Staphylococcus aureus*. The ORF61 of *S. aureus* phage SA13 (NC_021863) is a putative endolysin consisting of three distinct domains: an N-terminal CHAP domain (PF05257), a central amidase_2 domain (PF01510), and a C-terminal SH3_5 domain (PF08460) **(Fig. III-15A)**. Since the SH3_5 domain was presumed to be CBD, I cloned and produced the EGFP tagged SA13_CBD protein in *E. coli*. The fusion protein was overexpressed in the soluble form, and purified by Ni-NTA chromatography **(Fig. III-15B)**. Florescence microscopy analysis revealed that SA13_CBD showed broad binding spectrum against *S. aureus* cells as all of tested *S. aureus* strains, including methisillin-resistant *S. aureus* (MRSA) strains, were decorated by SA13_CBD **(Fig. III-15C, Table III-10)**. Not only *S. aureus* strains, but also other *Staphylococcal* strains (except *S. cohinii*) were labeled by the SA13_CBD. SA13_CBD did not bind to other genera of bacteria. Taken together, SA13_CBD has broad binding properties towards *Staphylococcus* cells, supposing that conserved epitopes of cell wall of *Staphylococcal* cells may be the binding target of SA13_CBD.

In addition, the broad, but *Staphylococcal*-specific binding of SA13_CBD could be used as a primary capture probe for the detection of *Staphylococcus* cells.

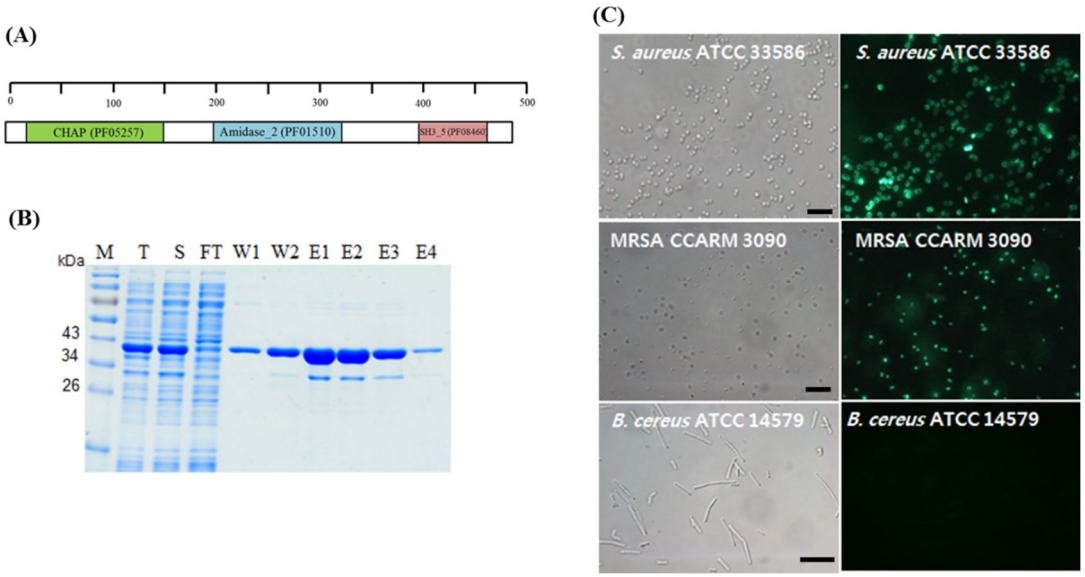

Fig. III-15. *Staphylococcal*-specific binding activity of SA13_CBD. (A) Schematic description of *S. aureus* phage SA13 endolysin. (B) SDS-PAGE analysis of EGFP-SA13_CBD (M, size marker; T, cell extract; S, supernatant, FT, Ni-NTA flow-through; W1 washing (10 mM imidazole); W2, washing (20 mM imidazole); E1 to E4, elution (240 mM imidazole)). (C) Optical and fluorescent images of different cells after the addition of EGFP-SA13_CBD. Scale bars, 10 um.

Table III-10. Binding spectrum of SA13_CBD

Species	Strain number[a]	SA13_CBD
Staphylococcus aureus	RN4220	+
Staphylococcus aureus	ATCC 6538	+
Staphylococcus aureus	ATCC 29213	+
Staphylococcus aureus	ATCC 33593	+
Staphylococcus aureus	ATCC 12100	+
Staphylococcus aureus	ATCC 33586	+
Staphylococcus aureus	Newman	+
Methicillin-resistant *Staphylococcus aureus*	CCARM 3089	+
Methicillin-resistant *Staphylococcus aureus*	CCARM 3090	+
Methicillin-resistant *Staphylococcus aureus*	CCARM 3793	+
Staphylococcus epidermidis	ATCC 35983	+
Staphylococcus saprophyticus	ATCC 15305	+
Staphylococcus haemolyticus	ATCC 29970	+
Staphylococcus hominis	ATCC 27844	+
Staphylococcus xylosus	ATCC 29971	+
Staphylococcus warneri	ATCC 10209	+
Staphylococcus captis	ATCC 35661	+
Staphylococcus intermedius	ATCC 29663	+
Staphylococcus cohini	ATCC 29974	-
Bacillus cereus	JCM 2504	-
Bacillus subtilis	ATCC 23857	-
Staphylococcus aureus	RN4220	-
Clostridium perfringens	ATCC 3624	-
Listeria monocytogenes	EGDe	-

[a] Source abbreviations: ATCC, American Type Culture Collection; JCM, Japan Collection of Microorganisms; CCARM, Culture Collection of Antimicrobial Resistant Microbes.

III-4. References

Altschul, S.F., Gish, W., Miller, W., Myers, E.W., Lipman, D.J., (1990) Basic local alignment search tool. J. Mol. Biol. 215, 403-410.

Anderson, I., Sorokin, A., Kapatral, V., Reznik, G., Bhattacharya, A., Mikhailova, N., Burd, H., Joukov, V., Kaznadzey, D., Walunas, T., Markd'Souza, Larsen, N., Pusch, G., Liolios, K., Grechkin, Y., Lapidus, A., Goltsman, E., Chu, L., Fonstein, M., Ehrlich, S.D., Overbeek, R., Kyrpides, N., Ivanova, N., (2005) Comparative genome analysis of Bacillus cereus group genomes with Bacillus subtilis. FEMS Microbiol. Lett. 250, 175-184.

Bagyan, I., Setlow, P., (2002) Localization of the cortex lytic enzyme CwlJ in spores of Bacillus subtilis. J. Bacteriol. 184, 1219-1224.

Beres, S.B., Sylva, G.L., Barbian, K.D., Lei, B., Hoff, J.S., Mammarella, N.D., Liu, M.Y., Smoot, J.C., Porcella, S.F., Parkins, L.D., Campbell, D.S., Smith, T.M., McCormick, J.K., Leung, D.Y., Schlievert, P.M., Musser, J.M., (2002) Genome sequence of a serotype M3 strain of group A Streptococcus: phage-encoded toxins, the high-virulence phenotype, and clone emergence. Proc. Natl. Acad. Sci. U. S. A. 99, 10078-10083.

Borysowski, J., Weber-Dabrowska, B., Gorski, A., (2006) Bacteriophage endolysins as a novel class of antibacterial agents. Exp. Biol. Med. 231, 366-377.

Brussow, H., Canchaya, C., Hardt, W.D., (2004) Phages and the evolution of bacterial pathogens: From genomic rearrangements to lysogenic conversion. Microbiol. Mol. Biol. Rev. 68, 560-602.

Callewaert, L., Walmagh, M., Michiels, C.W., Lavigne, R., (2011) Food applications of bacterial cell wall hydrolases. Curr. Opin. Biotechnol. 22, 164-171.

Canchaya, C., Fournous, G., Chibani-Chennoufi, S., Dillmann, M.L., Brussow, H., (2003) Phage as agents of lateral gene transfer. Curr. Opin. Microbiol. 6, 417-424.

Carlin, F., (2011) Origin of bacterial spores contaminating foods. Food microbiology 28, 177-182.

Chapot-Chartier, M.P., (2014) Interactions of the cell-wall glycopolymers of lactic acid bacteria with their bacteriophages. Frontiers in microbiology 5, 236.

Cheng, Q., Fischetti, V.A., (2007) Mutagenesis of a bacteriophage lytic enzyme PlyGBS significantly increases its antibacterial activity against group B streptococci. Appl. Microbiol. Biotechnol. 74, 1284-1291.

Chirakkal, H., O'Rourke, M., Atrih, A., Foster, S.J., Moir, A., (2002) Analysis of spore cortex lytic enzymes and related proteins in Bacillus subtilis endospore germination. Microbiology 148, 2383-2392.

Cladera-Olivera, F., Caron, G.R., Brandelli, A., (2004) Bacteriocin-like substance production by Bacillus licheniformis strain P40. Lett. Appl. Microbiol. 38, 251-256.

Daniel, A., Euler, C., Collin, M., Chahales, P., Gorelick, K.J., Fischetti, V.A., (2010) Synergism between a Novel Chimeric Lysin and Oxacillin Protects against Infection by Methicillin-Resistant Staphylococcus aureus. Antimicrob. Agents Chemother. 54, 1603-1612.

DeLano, W.L., (2005) The case for open-source software in drug discovery. Drug discovery today 10, 213-217.

Doherty, G.P., Bailey, K., Lewis, P.J., (2010) Stage-specific fluorescence intensity of GFP and mCherry during sporulation In Bacillus Subtilis. BMC Res. Notes 3, 303.

Fazzini, M.M., Schuch, R., Fischetti, V.A., (2010) A novel spore protein, ExsM, regulates formation of the exosporium in Bacillus cereus and Bacillus anthracis and affects spore size and shape. J. Bacteriol. 192, 4012-4021.

Fenton, M., Ross, P., McAuliffe, O., O'Mahony, J., Coffey, A., (2010) Recombinant bacteriophage lysins as antibacterials. Bioengineered bugs 1, 9-16.

Fischetti, V.A., (2008) Bacteriophage lysins as effective antibacterials. Curr.

Opin. Microbiol. 11, 393-400.

Ganz, H.H., Law, C., Schmuki, M., Eichenseher, F., Calendar, R., Loessner, M.J., Getz, W.M., Korlach, J., Beyer, W., Klumpp, J., (2014a) Novel Giant Siphovirus from Bacillus anthracis Features Unusual Genome Characteristics. PLoS One 9.

Ganz, H.H., Law, C., Schmuki, M., Eichenseher, F., Calendar, R., Loessner, M.J., Getz, W.M., Korlach, J., Beyer, W., Klumpp, J., (2014b) Novel giant siphovirus from Bacillus anthracis features unusual genome characteristics. PLoS One 9, e85972.

Grose, J.H., Belnap, D.M., Jensen, J.D., Mathis, A.D., Prince, J.T., Merrill, B.D., Burnett, S.H., Breakwell, D.P., (2014) The genomes, proteomes, and structures of three novel phages that infect the Bacillus cereus group and carry putative virulence factors. J. Virol. 88, 11846-11860.

Hayashi, T., Makino, K., Ohnishi, M., Kurokawa, K., Ishii, K., Yokoyama, K., Han, C.G., Ohtsubo, E., Nakayama, K., Murata, T., Tanaka, M., Tobe, T., Iida, T., Takami, H., Honda, T., Sasakawa, C., Ogasawara, N., Yasunaga, T., Kuhara, S., Shiba, T., Hattori, M., Shinagawa, H., (2001) Complete genome sequence of enterohemorrhagic Escherichia coli O157:H7 and genomic comparison with a laboratory strain K-12. DNA Res. 8, 11-22.

Haupts, U., Maiti, S., Schwille, P., Webb, W.W., (1998) Dynamics of fluorescence fluctuations in green fluorescent protein observed by fluorescence correlation spectroscopy. Proc. Natl. Acad. Sci. U. S. A. 95, 13573-13578.

Hendrix, R.W., (2002) Bacteriophages: evolution of the majority. Theor. Popul. Biol. 61, 471-480.

Hermoso, J.A., Garcia, J.L., Garcia, P., (2007) Taking aim on bacterial pathogens: from phage therapy to enzybiotics. Curr. Opin. Microbiol. 10, 461-472.

Imamura, D., Kuwana, R., Takamatsu, H., Watabe, K., (2011) Proteins involved in formation of the outermost layer of Bacillus subtilis spores. J. Bacteriol. 193, 4075-4080.

Kelley, L.A., Sternberg, M.J., (2009) Protein structure prediction on the Web: a case study using the Phyre server. Nat. Protoc. 4, 363-371.

Kikkawa, H.S., Ueda, T., Suzuki, S., Yasuda, J., (2008) Characterization of the catalytic activity of the gamma-phage lysin, PlyG, specific for Bacillus anthracis. FEMS Microbiol. Lett. 286, 236-240.

Kneen, M., Farinas, J., Li, Y.X., Verkman, A.S., (1998) Green fluorescent protein as a noninvasive intracellular pH indicator. Biophys. J. 74, 1591-1599.

Korndorfer, I.P., Danzer, J., Schmelcher, M., Zimmer, M., Skerra, A., Loessner, M.J., (2006) The crystal structure of the bacteriophage PSA endolysin reveals a unique fold responsible for specific recognition of Listeria cell walls. J. Mol. Biol. 364, 678-689.

Korndorfer, I.P., Kanitz, A., Danzer, J., Zimmer, M., Loessner, M.J., Skerra, A., (2008) Structural analysis of the L-alanoyl-D-glutamate endopeptidase domain of Listeria bacteriophage endolysin Ply500 reveals a new member of the LAS peptidase family. Acta Crystallogr. D Biol. Crystallogr. 64, 644-650.

Lambert, C., Leonard, N., De Bolle, X., Depiereux, E., (2002) ESyPred3D: Prediction of proteins 3D structures. Bioinformatics 18, 1250-1256.

Larkin, M.A., Blackshields, G., Brown, N.P., Chenna, R., McGettigan, P.A., McWilliam, H., Valentin, F., Wallace, I.M., Wilm, A., Lopez, R., Thompson, J.D., Gibson, T.J., Higgins, D.G., (2007) Clustal W and Clustal X version 2.0. Bioinformatics 23, 2947-2948.

Lee, J., Shin, H., Son, B., Ryu, S., (2012) Complete genome sequence of Bacillus cereus bacteriophage BCP78. J. Virol. 86, 637 - 638.

Leoff, C., Choudhury, B., Saile, E., Quinn, C.P., Carlson, R.W., Kannenberg, E.L., (2008) Structural elucidation of the nonclassical secondary cell wall polysaccharide from Bacillus cereus ATCC 10987. Comparison with the polysaccharides from Bacillus anthracis and B. cereus type strain ATCC 14579 reveals both unique and common structural features. J. Biol. Chem. 283, 29812-29821.

Loessner, M.J., (2005) Bacteriophage endolysins--current state of research and applications. Curr. Opin. Microbiol. 8, 480-487.

Loessner, M.J., Kramer, K., Ebel, F., Scherer, S., (2002) C-terminal domains of Listeria monocytogenes bacteriophage murein hydrolases determine specific recognition and high-affinity binding to bacterial cell wall carbohydrates. Mol. Microbiol. 44, 335-349.

Loessner, M.J., Maier, S.K., Daubek-Puza, H., Wendlinger, G., Scherer, S., (1997) Three Bacillus cereus bacteriophage endolysins are unrelated but reveal high homology to cell wall hydrolases from different bacilli. J. Bacteriol. 179, 2845-2851.

Low, L.Y., Yang, C., Perego, M., Osterman, A., Liddington, R., (2011) Role of net charge on catalytic domain and influence of cell wall binding domain on bactericidal activity, specificity, and host range of phage lysins. J. Biol. Chem. 286, 34391-34403.

Low, L.Y., Yang, C., Perego, M., Osterman, A., Liddington, R.C., (2005) Structure and lytic activity of a Bacillus anthracis prophage endolysin. J. Biol. Chem. 280, 35433-35439.

Marchler-Bauer, A., Anderson, J.B., Derbyshire, M.K., DeWeese-Scott, C., Gonzales, N.R., Gwadz, M., Hao, L., He, S., Hurwitz, D.I., Jackson, J.D., Ke, Z., Krylov, D., Lanczycki, C.J., Liebert, C.A., Liu, C., Lu, F., Lu, S., Marchler, G.H., Mullokandov, M., Song, J.S., Thanki, N., Yamashita, R.A., Yin, J.J., Zhang, D., Bryant, S.H., (2007) CDD: a conserved domain database for interactive domain family analysis. Nucleic Acids Res. 35, D237-240.

Matarante, A., Baruzzi, F., Cocconcelli, P.S., Morea, M., (2004) Genotyping and toxigenic potential of Bacillus subtilis and Bacillus pumilus strains occurring in industrial and artisanal cured sausages. Appl. Environ. Microbiol. 70, 5168-5176.

Mayer, M.J., Garefalaki, V., Spoerl, R., Narbad, A., Meijers, R., (2011) Structure-based modification of a Clostridium difficile-targeting endolysin affects activity and host range. J. Bacteriol. 193, 5477-5486.

Mayer, M.J., Gasson, M.J., Narbad, A., (2012) Genomic sequence of

bacteriophage ATCC 8074-B1 and activity of its endolysin and engineered variants against Clostridium sporogenes. Appl. Environ. Microbiol. 78, 3685-3692.

Mayer, M.J., Narbad, A., Gasson, M.J., (2008) Molecular characterization of a Clostridium difficile bacteriophage and its cloned biologically active endolysin. J. Bacteriol. 190, 6734-6740.

Mo, K.F., Li, X., Li, H., Low, L.Y., Quinn, C.P., Boons, G.J., (2012) Endolysins of Bacillus anthracis bacteriophages recognize unique carbohydrate epitopes of vegetative cell wall polysaccharides with high affinity and selectivity. J. Am. Chem. Soc. 134, 15556-15562.

Moriyama, R., Fukuoka, H., Miyata, S., Kudoh, S., Hattori, A., Kozuka, S., Yasuda, Y., Tochikubo, K., Makino, S., (1999) Expression of a germination-specific amidase, SleB, of Bacilli in the forespore compartment of sporulating cells and its localization on the exterior side of the cortex in dormant spores. J. Bacteriol. 181, 2373-2378.

Mukhopadhyay, S., Akmal, A., Stewart, A.C., Hsia, R.C., Read, T.D., (2009) Identification of Bacillus anthracis spore component antigens conserved across diverse Bacillus cereus sensu lato strains. Mol. Cell. Proteomics 8, 1174-1191.

Myers, G.S., Rasko, D.A., Cheung, J.K., Ravel, J., Seshadri, R., DeBoy, R.T., Ren, Q., Varga, J., Awad, M.M., Brinkac, L.M., Daugherty, S.C., Haft, D.H., Dodson, R.J., Madupu, R., Nelson, W.C., Rosovitz, M.J., Sullivan, S.A., Khouri, H., Dimitrov, G.I., Watkins, K.L., Mulligan, S., Benton, J., Radune, D., Fisher, D.J., Atkins, H.S., Hiscox, T., Jost, B.H., Billington, S.J., Songer, J.G., McClane, B.A., Titball, R.W., Rood, J.I., Melville, S.B., Paulsen, I.T., (2006) Skewed genomic variability in strains of the toxigenic bacterial pathogen, Clostridium perfringens. Genome Res. 16, 1031-1040.

Nicholson, W.L. and Setlow, P. (1990) Sporulation, germination, and outgrowth. In Molecular Biological Methods for Bacillus ed. Harwood, C.R. and Cutting, S.M. pp. 391–450. Chichester: John Wiley.

Nicholson, W.L., Munakata, N., Horneck, G., Melosh, H.J., Setlow, P., (2000) Resistance of Bacillus endospores to extreme terrestrial and extraterrestrial

environments. Microbiol. Mol. Biol. Rev. 64, 548-572.

Oliveira, H., Azeredo, J., Lavigne, R., Kluskens, L.D., (2012) Bacteriophage endolysins as a response to emerging foodborne pathogens. Trends in Food Science & Technology 28, 103-115.

Oliveira, H., Melo, L.D., Santos, S.B., Nobrega, F.L., Ferreira, E.C., Cerca, N., Azeredo, J., Kluskens, L.D., (2013) Molecular aspects and comparative genomics of bacteriophage endolysins. J. Virol. 87, 4558-4570.

Oliveira, H., Thiagarajan, V., Walmagh, M., Sillankorva, S., Lavigne, R., Neves-Petersen, M.T., Kluskens, L.D., Azeredo, J., (2014) A thermostable Salmonella phage endolysin, Lys68, with broad bactericidal properties against gram-negative pathogens in presence of weak acids. PLoS One 9, e108376.

Park, J., Yun, J., Lim, J.A., Kang, D.H., Ryu, S., (2012) Characterization of an endolysin, LysBPS13, from a Bacillus cereus bacteriophage. FEMS Microbiol. Lett. 332, 76-83.

Pohane, A.A., Joshi, H., Jain, V., (2014) Molecular dissection of phage endolysin: an interdomain interaction confers host specificity in Lysin A of Mycobacterium phage D29. J. Biol. Chem. 289, 12085-12095.

Porter, C.J., Schuch, R., Pelzek, A.J., Buckle, A.M., McGowan, S., Wilce, M.C., Rossjohn, J., Russell, R., Nelson, D., Fischetti, V.A., Whisstock, J.C., (2007) The 1.6 A crystal structure of the catalytic domain of PlyB, a bacteriophage lysin active against Bacillus anthracis. J. Mol. Biol. 366, 540-550.

Reynolds, E.S., (1981) Citation Classic - the Use of Lead Citrate at High Ph as an Electron-Opaque Stain in Electron-Microscopy. Cc/Life Sci, 16-16.

Rodriguez-Rubio, L., Martinez, B., Rodriguez, A., Donovan, D.M., Gotz, F., Garcia, P., (2013) The Phage Lytic Proteins from the Staphylococcus aureus Bacteriophage vB_SauS-phiIPLA88 Display Multiple Active Catalytic Domains and Do Not Trigger Staphylococcal Resistance. PLoS One 8.

Sanz, J.M., Diaz, E., Garcia, J.L., (1992) Studies on the structure and

function of the N-terminal domain of the pneumococcal murein hydrolases. Mol. Microbiol. 6, 921-931.

Sass, P., Bierbaum, G., (2007) Lytic activity of recombinant bacteriophage phi11 and phi12 endolysins on whole cells and biofilms of Staphylococcus aureus. Appl. Environ. Microbiol. 73, 347-352.

Schleife.Kh, Kandler, O., (1972) Peptidoglycan Types of Bacterial Cell-Walls and Their Taxonomic Implications. Bacteriol. Rev. 36, 407-477.

Schmelcher, M., Powell, A.M., Becker, S.C., Camp, M.J., Donovan, D.M., (2012) Chimeric phage lysins act synergistically with lysostaphin to kill mastitis-causing Staphylococcus aureus in murine mammary glands. Appl. Environ. Microbiol. 78, 2297-2305.

Schmelcher, M., Shabarova, T., Eugster, M.R., Eichenseher, F., Tchang, V.S., Banz, M., Loessner, M.J., (2010) Rapid multiplex detection and differentiation of Listeria cells by use of fluorescent phage endolysin cell wall binding domains. Appl. Environ. Microbiol. 76, 5745-5756.

Schmelcher, M., Tchang, V.S., Loessner, M.J., (2011) Domain shuffling and module engineering of Listeria phage endolysins for enhanced lytic activity and binding affinity. Microbial biotechnology 4, 651-662.

Schmitz, J., Schuch, R., Fischetti, V., (2010) Identifying active phage lysins through functional viral metagenomics. Appl. Environ. Microbiol. 76, 7181 - 7187.

Schmitz, J.E., Ossiprandi, M.C., Rumah, K.R., Fischetti, V.A., (2011) Lytic enzyme discovery through multigenomic sequence analysis in Clostridium perfringens. Appl. Microbiol. Biotechnol. 89, 1783-1795.

Son, B., Yun, J., Lim, J.A., Shin, H., Heu, S., Ryu, S., (2012) Characterization of LysB4, an endolysin from the Bacillus cereus-infecting bacteriophage B4. BMC Microbiol. 12, 33.

Son, J.S., Jun, S.Y., Kim, E.B., Park, J.E., Paik, H.R., Yoon, S.J., Kang, S.H., Choi, Y.J., (2010) Complete genome sequence of a newly isolated lytic bacteriophage, EFAP-1 of Enterococcus faecalis, and antibacterial activity of

its endolysin EFAL-1. J. Appl. Microbiol. 108, 1769-1779.

Tamai, E., Yoshida, H., Sekiya, H., Nariya, H., Miyata, S., Okabe, A., Kuwahara, T., Maki, J., Kamitori, S., (2014) X-ray structure of a novel endolysin encoded by episomal phage phiSM101 of Clostridium perfringens. Mol. Microbiol. 92, 326-337.

Tamura, K., Peterson, D., Peterson, N., Stecher, G., Nei, M., Kumar, S., (2011) MEGA5: molecular evolutionary genetics analysis using maximum likelihood, evolutionary distance, and maximum parsimony methods. Mol. Biol. Evol. 28, 2731-2739.

Thompson, B.M., Binkley, J.M., Stewart, G.C., (2011) Current physical and SDS extraction methods do not efficiently remove exosporium proteins from Bacillus anthracis spores. J. Microbiol. Methods 85, 143-148.

Wang, D.B., Yang, R., Zhang, Z.P., Bi, L.J., You, X.Y., Wei, H.P., Zhou, Y.F., Yu, Z., Zhang, X.E., (2009) Detection of B. anthracis spores and vegetative cells with the same monoclonal antibodies. PLoS One 4, e7810.

Weidenmaier, C., Peschel, A., (2008) Teichoic acids and related cell-wall glycopolymers in Gram-positive physiology and host interactions. Nat Rev Microbiol 6, 276-287.

Xu, Q., Sudek, S., McMullan, D., Miller, M.D., Geierstanger, B., Jones, D.H., Krishna, S.S., Spraggon, G., Bursalay, B., Abdubek, P., Acosta, C., Ambing, E., Astakhova, T., Axelrod, H.L., Carlton, D., Caruthers, J., Chiu, H.J., Clayton, T., Deller, M.C., Duan, L., Elias, Y., Elsliger, M.A., Feuerhelm, J., Grzechnik, S.K., Hale, J., Han, G.W., Haugen, J., Jaroszewski, L., Jin, K.K., Klock, H.E., Knuth, M.W., Kozbial, P., Kumar, A., Marciano, D., Morse, A.T., Nigoghossian, E., Okach, L., Oommachen, S., Paulsen, J., Reyes, R., Rife, C.L., Trout, C.V., van den Bedem, H., Weekes, D., White, A., Wolf, G., Zubieta, C., Hodgson, K.O., Wooley, J., Deacon, A.M., Godzik, A., Lesley, S.A., Wilson, I.A., (2009) Structural basis of murein peptide specificity of a gamma-D-glutamyl-l-diamino acid endopeptidase. Structure 17, 303-313.

Yang, H., Wang, D.B., Dong, Q., Zhang, Z., Cui, Z., Deng, J., Yu, J., Zhang, X.E., Wei, H., (2012) Existence of separate domains in lysin PlyG for recognizing Bacillus anthracis spores and vegetative cells. Antimicrob.

Agents Chemother. 56, 5031-5039.

Yang, H., Zhang, Y., Yu, J.P., Huang, Y.L., Zhang, X.E., Wei, H.P., (2014) Novel Chimeric Lysin with High-Level Antimicrobial Activity against Methicillin-Resistant Staphylococcus aureus In Vitro and In Vivo. Antimicrob. Agents Chemother. 58, 536-542.

Yuan, Y., Peng, Q., Gao, M., (2012) Characteristics of a broad lytic spectrum endolysin from phage BtCS33 of Bacillus thuringiensis. BMC Microbiol. 12, 297.

Zdobnov, E.M., Apweiler, R., (2001) InterProScan--an integration platform for the signature-recognition methods in InterPro. Bioinformatics 17, 847-848.

Zhang, W.H., Mi, Z.Q., Yin, X.Y., Fan, H., An, X.P., Zhang, Z.Y., Chen, J.K., Tong, Y.G., (2013) Characterization of Enterococcus faecalis Phage IME-EF1 and Its Endolysin. PLoS One 8.

Zimmer, M., Vukov, N., Scherer, S., Loessner, M.J., (2002) The murein hydrolase of the bacteriophage phi3626 dual lysis system is active against all tested Clostridium perfringens strains. Appl. Environ. Microbiol. 68, 5311-5317.

Chapter IV.

CBD-based engineering of novel detection agents

IV-1. Introduction

Antibodies are the most widely used biological probes for the detection of pathogenic bacteria (Lazcka et al., 2007). The sensitivity and specificity of techniques for bacterial detection are primarily dependent on the intrinsic properties of the antibodies. Production of specific antibodies, however, involves immunization of animals and maintenance of hybridoma cells, which are difficult, expensive, and time-consuming (Singh et al., 2012; Skottrup et al., 2008). Moreover, antibodies can lose their activity by changing temperature or pH and are prone to aggregation (Petrenko and Vodyanoy, 2003; Wang et al., 2007). Accordingly, it is necessary to explore robust and specific biological probes.

Bacteriophages have been used as alternative probes for pathogenic bacteria sensing due to their extreme host specificity, strong resistance to heat, pH, and chemicals, and relatively lower cost of production (Arya et al., 2011; Mahony et al., 2011; Tawil et al., 2014). Recently, bacteriophage-derived proteins have received more attention than whole bacteriophages since it is easy to modify the affinity and binding properties of these proteins (Brzozowska et al., 2015; Chibli et al., 2014; Javed et al., 2013; Poshtiban et al., 2013; Singh et al., 2011; Singh et al., 2010). Endolysin is a

peptidoglycan hydrolase of bacteriophage that lyses its bacterial host at the end of the phage life cycle (Fischetti, 2010; Loessner, 2005). Endolysins from Gram-positive bacteria-infecting phages consist of modular proteins including C-terminal cell wall binding domain (CBD) and N-terminal catalytic domain (Callewaert et al., 2011; Loessner et al., 2002). CBDs feature high specificity and strong binding affinity (K_D values of pico- to nanomolar range) to bacteria (Schmelcher et al., 2010; Schmelcher et al., 2011). In addition, they are small (10 ~ 15 kDa), act as a monomer, and have no lytic activity. Furthermore, these superior features of CBDs can be improved by genetic engineering. Therefore, several recent studies have exploited CBDs as novel probes for the detection of bacteria (Kretzer et al., 2007; Tolba et al., 2012).

However, there are two issues that must be addressed for the effective use of CBDs as detection agents. First one is that many CBDs show high affinity to its target cells in a strain-specific manner, which is not capable of detecting diverse environmental strains. Another issue is that randomly oriented immobilization of CBDs onto detection platforms causes loss of functionality of the immobilized CBDs.

In this chapter, a CBD cocktail with different fluorescent makers

was developed for the detection of multiple pathogens. In addition, dual CBD hybrid proteins were created by combinations of CBDs with complementary specificities to extend the binding range. Lastly, CBD-coated magnetic nanoclusters allowed efficient capture and recovery of *B. cereus* or *C. perfringens* cells from suspensions. These comprehensive and multidisciplinary studies may pave the way for the development of efficient CBD-based detection tools.

IV-2. Materials and Methods

IV-2-1. Reagents and materials

Gold(III) chloride trihydrate, sodium citrate dihydrate, sodium borohydride, 3-aminopropyltriethoxysilane (APTES), glutaldehyde, L-glutathione reduced, Nickel(II) chloride hexahydrate, and Nα ,Nα-Bis(carboxymethyl)-L-lysine hydrate were purchased from Sima-Aldrich (St. Louis, MO). Methoxy poly(ethylene glycol) functionalized with a thiol group (mPEG-SH, Mw: 5,000) was purchased from SunBio (Anyang, Korea). All of the solutions were prepared using Milli-Q purified water (Millipore, Molsheim, France). Magnetic nanoparticle clusters (MNCs) were kindly given by Dr. Sangmin Jeon at Postech. Dynabeads® His-tag isolation and pulldown (product no. 10103D) were purchased Life Technologies (Oslo, Norway). Anti-*Clostridium perfringes* antibody (ab35023) was purchased from Abcam (Cambridge, UK).

IV-2-2. Bacterial strains and growth conditions

Clostridium strains were grown in reinforced clostridial medium (RCM) broth at 37℃ under anaerobic condition. *Listeria*, *Staphylococcus*, and *Enterococcus* strains were grown in brain-heart infusion broth at 37℃ under shaking. All of the *Bacillus* strains and Gram-negative bacteria were grown in Luria-Bertani (LB) broth at 37℃. To create agar medium, the broth medium was supplemented with 1.5% agar All of the media used in this study were purchased from Difco and used according to the manufacturer's instructions.

IV-2-3. Production and purification of recombinant proteins

All synthetic oligonucleotide and plasmids used in this work are listed in **Table IV-1** and **Table IV-2** respectively.

Table IV-1. Oligonucleotides used in Chapter IV

Oligonucleotide	Sequence (5'-3')[a]
fNde_GST	gcg cat ATGTCCCCTATACTAGGTTATTGGAAAATTA AGG
rBamH_Link-GST	gcg ggatcc actacctgatccactacc TTTTGGAGGATGGTCGCCACCA
fSacI_FL_PBC1_CBD	gcg gagctc c ggtggcggtggctcc ggtggcggtggctcc ggtggcggtggctcc ggtggcggtggctcc GGCAAAGCAGTAAATGTTGATCCG
fSacI_HL_PBC1_CBD	gcg gagctc c gaagctgcggcaaaa gaagctgcggcaaaa gaagctgcggcaaaa gaagctgcggcaaaa GGCAAAGCAGTAAATGTTGATCCG
rSacI_PBC1_CBD_nostop	gcg gagctc cc ATACTCAATCACTTCTTCTTGATACCACCA
fSacI_FL_PBC4_CBD	gcg gagctc c ggtggcggtggctcc ggtggcggtggctcc ggtggcggtggctcc ggtggcggtggctcc GGACAAGAAACAAGTGGAGGTTCTAACA
fSacI_HL_PBC4_CBD	gcg gagctc c gaagctgcggcaaaa gaagctgcggcaaaa gaagctgcggcaaaa gaagctgcggcaaaa GGACAAGAAACAAGTGGAGGTTCTAACA
rSacI_PBC4_CBD_nostop	gcg gagctc cc AACTTCGTATAACTCAACGAACCAACCTT

[a] Restriction sites for cloning are underlined. Capital letters delineate regions homologous to the respective template DNA.

Table IV-2. Plasmids used in Chapter IV

Plasmid	Relevant characteristics	Source
pGSTparallel 1	*Glutathione S-transferase* (GST) gene cloned into Amp^R expressing vector	Sheffield et al. 1999
pEYFP-C1	Kan^R *eyfp* cassette vector	Clontech
pET28a-EYFP	EYFP gene cloned into NdeI-BamHI site of pET28a	This work
10His-pET28a	pET28a expression vector containing 10xHis-tag	This work
pET28a-GST	GST gene with 'GSGSGS' linker cloned into NdeI-BamHI site of pET28a	This work
10His-pET28a-mCherry-PBC1_CBD	The mCherry-PBC1_CBD fragment cloned into NdeI-HindIII site of 10His-pET28a	This work
pET28a-EYFP-CPF369_CBD	The CBD fragment (Val203-Ile342) of a gene (Gene ID: CPF_0369) from *C. perfringens* ATCC 13124 cloned into BamHI-HindIII site of pET28a-EYFP	This work
pET28a-GST-PBC1_CBD	The CBD fragment (Gly170-Tyr254) of LysPBC1 cloned into BamHI-HindIII site of pET28a-GST	This work
pET28a-GST-B4_CBD	The CBD fragment (Val156-Lys262) of LysB4 cloned into BamHI-HindIII site of pET28a-GST	This work
10His-pET28a-GST-CPF369_CBD	The CBD fragment (Val203-Ile342) of a CPF_0369	This work

	gene cloned into BamHI-HindIII site of 10His-pET28a-GST	
pET28a-EGFP-PBC4_CBD_FL_PBC1_CBD	PBC4_CBD and PBC1_CBD, fused via flexible linker region, cloned into BamHI-HindIII site of pET28a-EGFP	This work
pET28a-EGFP-PBC4_CBD_HL_PBC1_CBD	PBC4_CBD and PBC1_CBD, fused via helical linker region, cloned into BamHI-HindIII site of pET28a-EGFP	This work
pET28a-EGFP-PBC1_CBD_FL_PBC4_CBD	PBC1_CBD and PBC4_CBD, fused via flexible linker region, cloned into BamHI-HindIII site of pET28a-EGFP	This work
pET28a-EGFP-PBC1_CBD_HL_PBC4_CBD	PBC1_CBD and PBC4_CBD, fused via helical linker region, cloned into BamHI-HindIII site of pET28a-EGFP	This work

IV-2-3-1. Hybrid CBD between CBDs from PBC1 and PBC4

The CBD constructs (PBC1_CBD, PBC4_CBD) for hybrid CBD were introduced in Chapter III. The intrinsic stop codon of the C-terminal-fused CBD was omitted for translational fusion. Helical linker $(EAAAK)_4$ and flexible linker $(GGGGS)_4$ were used to link CBD-CBD hybrids. The nucleotide sequences encoding above linkers were derived from a previous study (Lu and Feng, 2008). The first upstream CBD gene (e.g. CBD1) was inserted into BamHI/SacI sites of pET28a-EGFP. Then, the downstream CBD gene including corresponding linker region was inserted into SacI/HindIII sites of pET28a-EGFP-CBD1. All constructs were verified by nucleotide sequencing. The resulting recombinant plasmids were transformed into BL21 (DE3). Overproduction and purification of hybrid proteins were carried out as described previously (Kong and Ryu, 2015).

IV-2-3-2. GST-CBD fusion protein

The GST coding gene was amplified by PCR using pGST Parallel 1 as a template (Sheffield et al., 1999). A flexible linker region encoding six Gly and Ser residues was added between the GST and CBD genes to enable efficient protein folding. The GST-CBD fusion protein was also produced by

the same method as the GFP-CBD fusion proteins.

IV-2-4. Cell binding assay with fluorescence microscopy, microplate reader,

and confocal microscopy

Binding assays of EGFP-CBD fusion proteins were performed as described before (Loessner et al., 2002). Briefly, exponentially growing bacterial cells in Dulbecco's phosphate buffered saline (DPBS, GenDepot) were incubated with 0.4 μM EGFP-CBD fusion proteins for 5 min at room temperature. The cells were washed twice with DPBS buffer and observed by epifluorescence microscopy using a DE/Axio Imager A1 microscope (Carl Zeiss) and a filter set (excitation 470/40; emission 525/50) for EGFP. Quantitative fluorescence assays were conducted using a using an SpectraMax i3 multimode microplate reader (Molecular Devices, Sunnyvale, CA) with excitation at 485 nm and emission at 535 nm. Confocal multi-fluorescence imaging was performed with a SP8-STED (Leica Microsystems, GmbH, Germany) in NICEM, Seoul National University.

IV-2-5. Synthesis of colloidal gold preparations

Colloidal gold nano-seed particles (mean diameter, 5 nm) were prepared according to the procedure in the literature (Wang et al., 2008). In brief, 2 ml of 1% sodium citrate and 100 ml of deionized water were mixed and stirred for 3 min. Then 1 ml of 1% $HAuCl_4$ solution was added, and the solution was stirred for another 5 min. Then, 1 ml of 0.1% $NaBH_4$, prepared by dissolving $NaBH_4$ into 1% sodium citrate solution, was rapidly injected under rapid stirring over 10 min. For gold nanoparticles (mean diameter,15 nm), 2.5 ml of 1% sodium citrate was added to 100 ml of boiling deionized water. With constant stirring, 1 ml of 1% HAuCl4 was added rapidly, and boiled for 12 min. Thereafter, the heating source was removed and the colloidal gold solution was stirred for another 5 min. The obtained gold colloids were stored in a dark bottle at 4℃.

IV-2-6. Characterization of nanoparticles

The size distributions and surface charge of nanoparticles were determined with a dynamic light scattering (DLS) experiments, performed at 25 °C using a Wyatt Dynapro Titan instrument (Wyatt Technology, Santa Barbara, CA) or a Zetasizer (Malvern Instruments, Malvern, UK). The TEM

images were taken with energy-filtering transmission electron microscope (LIBRA 120, Carl Zeiss) at NICEM, Seoul National University. The operation voltage was kept at 120 kV. The SEM images were taken with field emission scanning electron microscopy (FE-SEM, MERLIN Compact, Zeiss) at Center for Materials Analysis in Seoul National University. The operation voltage was kept at 1 kV. The UV-vis absorption spectra were measured by multimode plate reader (infinite M200, TECAN, Austria).

IV-2-7. Immobilization of CBD on the magnetic nanoparticle clusters (MNCs)

One mg of MNCs (dispersed in absolute ethanol) was treated with 1% APTES to form self-assembled monolayer of amine groups on the surface. After washing with absolute ethanol and water several times, the APTES-coated MNCs were functionalized with 0.05% glutaldehyde to form amine-reactive crosslinkers on the surface. The resulting amine-reactive MNCs were magnetically separated and rinsed a few times with water, and 1 mM of Nα ,Nα-Bis(carboxymethyl)-L-lysine hydrate was added and incubated for 30 min. The electrophilic carbon atoms of aldehydes in MNCs react with

primary amines of Nα ,Nα-Bis(carboxymethyl)-L-lysine hydrate (aminobutyl NTA) forming Schiff bases on the surface. Excessive NTA was removed by several washing with water, and the functionalized MNCs were treated with 1 mM of nickel chloride for 30 min to produce Ni-NTA functionalized MNCs. After washing with 5 mM Tris-Cl (pH 7.5) buffer several times, His-tagged mCherry-CBD fusion proteins (10 μg) were immobilized onto the Ni-NTA functionalized MNCs for 30 min at room temperature. The free surfaces of the nanoparticles were blocked with 100 μl of a 1% BSA overnight at 4℃. The CBD-conjugated MNCs were magnetically separated from unbound proteins and stored at 4℃ until use.

To immobilized GST-CBD fusion proteins, the citrate-stabilized gold nanoparticles (mean diameter, 5 nm) were attached to the APTES-coated MNCs by electrostatic interaction. The resulting 1 ml of gold nanoparticle-coated MNCs (Au-MNCs, 1 mg) were then incubated with 1 mM of reduced L-glutathione (GSH) for 1 h. The resulting GSH-coated Au-MNCs were washed with 5 mM of Tris-Cl (pH 7.5) several times, and then mixed with GST-tagged CBD (10 μg) for 1 h at room temperature. To block and stabilize the CBD-conjugated Au-MNCs, 20 μl of 1 mM thiol-terminated PEG (5 kDa) was added and incubated for another 2 h. The unbound proteins and PEGs

were removed by magnetic separation, and the final conjugate was stored in dark bottle at 4℃.

IV-2-8. Magnetic separation and enumeration of bacterial cells

CBD coated magnetic nanoclusters (5 to 40 ug) were mixed with the bacterial suspensions and the tubes were gently rotated for 10 to 40 min at room temperature. Total reaction volumes were adjusted to 1 ml by addition of buffer (5 mM Tris-Cl, pH 7.5). After magnetic separation (5 min), appropriate dilutions of supernatants were plated on LB agar (*B. cereus*) or BHI agar containing 0.2% sheep blood (*C. perfringens*) and incubated for 12 h at 37℃. Viable cell counts were determined by duplicate plating. To avoid the underestimated capture capacity due to the possible aggregation or compromised growth in the presence of nanocomposites (Chatterjee et al., 2011; Niemirowicz et al., 2014; Qu et al., 2005; Varshney et al., 2005), the capture efficiencies were calculated based on the number of residual cells in the supernatant after magnetic separation as described earlier (Fu et al., 2005; Kretzer et al., 2007; Sung et al., 2013) .

IV-3. Results and Discussion

IV-3-1. CBD cocktail for multiple fluorescence labeling of three different bacteria

Due to the complex nature of environmental samples, it is highly desirable to develop a method that capable of simultaneous detection of multiple pathogens. Because the CBDs can be fused with differently colored fluorescent proteins, I aimed to test whether simultaneous identification and differentiation of three different pathogens (*B. cereus*, *S. aureus*, and *C. perfringens*) in cell suspensions would be possible using a CBD cocktail. To provide proof of concept for application of this method, I produced three CBD fusion proteins with different fluorescent proteins: EGFP for *S. aureus* (EGFP-SA13_CBD), mCherry for *B. cereus* (mCherry-PBC1_CBD), and enhanced yellow fluorescent protein (EYFP) for *C. perfringens* (EYFP-CPF369_CBD) (**Fig. IV-1A)**. Confocal laser scanning micrographs revealed that the three different pathogens were clearly identified and distinguished by its colors **(Fig. IV-1B)**. *S. aureus* cells were colored in green and readily differentiated by their round and sphere forms (cocci), whereas *B. cereus* (red) and *C. perfringens* (yellow) cells showed round-ended cylinder forms. These results indicate that the presence of non-target bacteria did not

interfere with the target-specific binding property of each CBD. Furthermore, the results demonstrated here present the potential of a CBD cocktail as tools for multiplex pathogenic bacterial detection in naturally contaminated samples, especially with an unknown bacterial load.

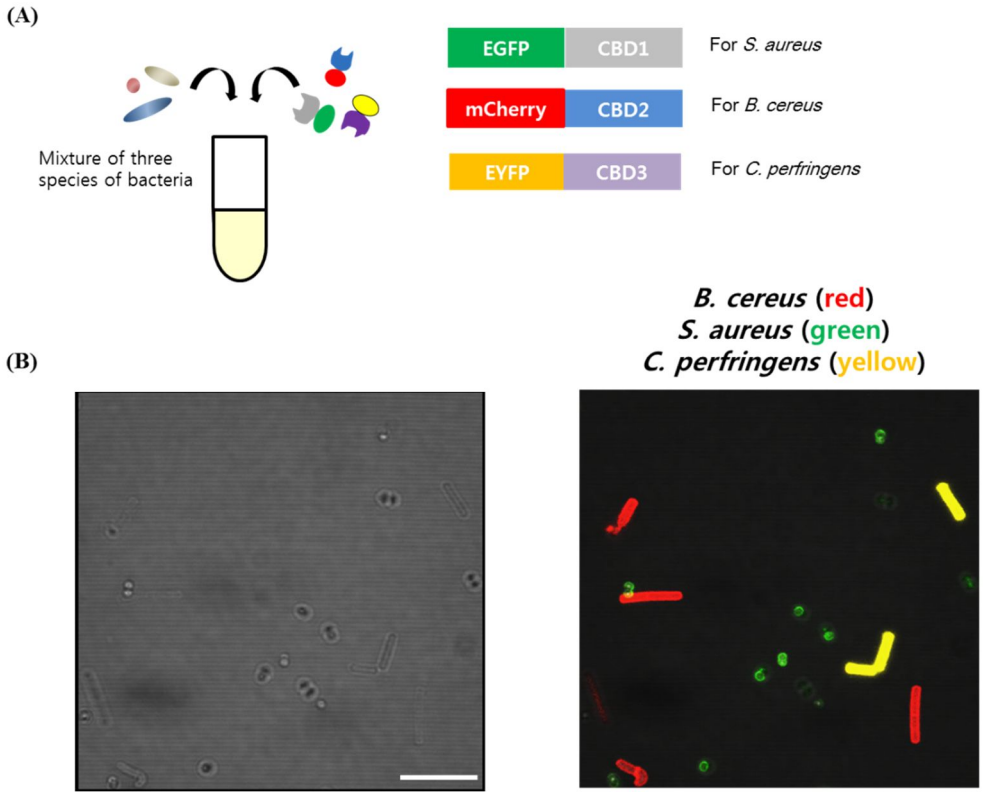

Fig. IV-1. Multiple fluorescence labeling of three different bacterial species by a CBD cocktail. (A) Schematic representation of use of a CBD cocktail for simultaneous detection of multiple pathogens. (B) Cells of *B. cereus, S. aureus,* and *C. perfringens* were incubated with mCherry-PBC1_CBD (red) and EGFP-SA13_CBD (green), and EYFP-CPF369_CBD (yellow), respectively, resulting in species-specific cell wall decoration. Scale bar, 10 um.

IV-3-2. CBD engineering for broad binding spectrum

For the practical application of using CBDs as detection agents, it would be desirable to have CBDs that recognize broad strains of target bacteria. Since the PBC1_CBD and PBC4_CBD showed complementary specificities towards *B. cereus* group strains, I created the dual CBD hybrid proteins with combination of both CBDs to extend the binding range. Two factors were considered when combining the two CBDs: a linker between two CBDs and orientation of the CBDs. Previous studies have shown that proper linker peptide should be inserted to make a fusion protein with heterofunctional domains to reduce folding interference and to make the domains work independently (Arai et al., 2001; Crasto and Feng, 2000). Not only is the composition of the linker but also its length critical for the desired function of the chimeric protein (George and Heringa, 2002). Although numerous peptides have been used as linkers, two types of linkers have been mainly used: flexible linkers and helical linkers (Lu and Feng, 2008). The repeated peptapeptides consisting of Gly and Ser (usually $(GGGGS)_n$, $n \leq 6$) are considered to be universal linkers due to their flexibility and resistance to proteases (Arai et al., 2004; Wen et al., 2013). Another popular type of linker is helical linkers $(EAAAK)_n$ (n = 2–5), which were expected to form

hydrophilic α-helices bundle and stabilized by Glu^{-}-Lys^{+} salt bridges (Arai et al., 2001).

A previous report showed that orientation of double *Listeria* CBD fusions was also important for the proper function of domains (Schmelcher et al., 2011). In their study, the CBD118 function was largely dependent on domain location, whereas the partner CBD500 appeared to be less affected by these constraints. Schematic representations of dual CBD hybrids created in this study are shown in **Fig. IV-2A**. PBC1_CBD and PBC4_CBD are fused via flexible $(GGGGS)_4$ or helical $(EAAAK)_4$ linkers in both orientations and all constructs were labeled by EGFP at the N-terminus. I inserted long enough linkers (20 amino acids) to separate the two domains at a reasonable distance, which allows minimization of steric hindrance. In addition, short helical linkers $(EAAAK)_n$ (n=2, 3) have been known to cause multimerization (Arai et al., 2004).

PBC1_CBD exhibited binding to *B. cereus* ATCC 10987, but not to *B. cereus* ATCC 14579 **(Fig. IV-2B)**. On the other hand, PBC4_CBD showed specific binding properties towards *B. cereus* ATCC 14579, but not *B. cerues* ATCC 10987. The Dual CBD hybrid proteins could bind to both strains, regardless of their domain orientation or linker peptides. However, in

the case of when the PBC4_CBD was located in a central position (4F1, 4H1), weak labeling was observed by fluorescence microscopy. Quantitative fluorescence assay confirmed these observations that dual CBD 1F4 and 1H4, both of which have PBC4_CBD at the C-termini, showed stronger fluorescence intensity than hybrid 4F1 and 4H1, featuring PBC4_CBD in a central place **(Fig. IV-2C)**. These results indicate that the importance of orientation when making dual CBD hybrids. The fusion of foreign protein to the C-terminal of PBC4_CBD adversely affected its natural binding activity towards the target cell (*B. cereus* ATCC 14579). In contrast, PBC1_CBD retained the binding activity toward its natural target cell (*B. cereus* ATCC 10987) when fused with C-terminal region. Taken together, PBC4_CBD functionality is greatly influenced by its orientation, whereas PBC1_CBD seemed to be less affected by spatial location.

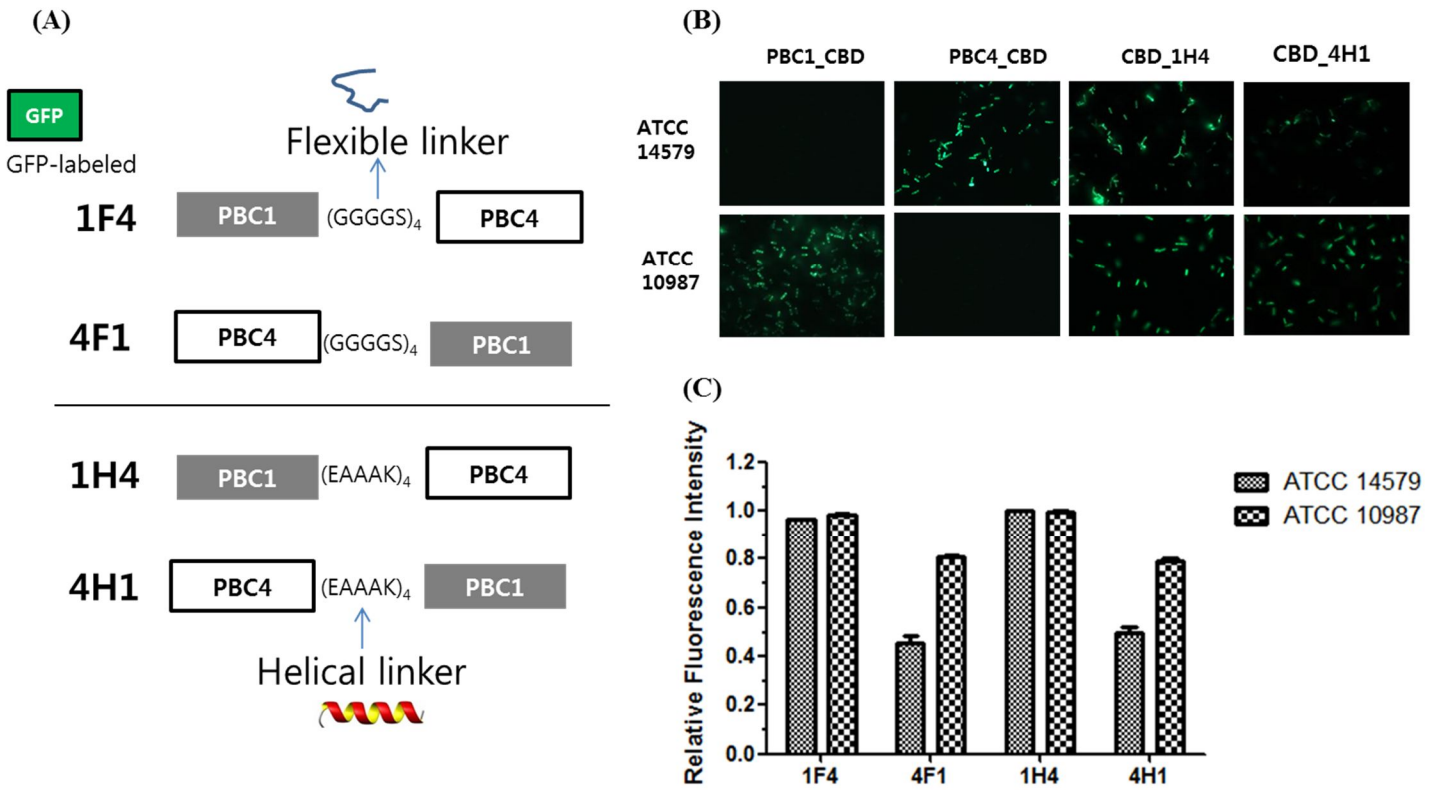
(A)
GFP
GFP-labeled
Flexible linker
1F4
PBC1
(GGGGS)4
PBC4
4F1
PBC4
(GGGGS)4
PBC1
1H4
PBC1
(EAAAK)4
PBC4
4H1
PBC4
(EAAAK)4
PBC1
Helical linker
(B)
PBC1_CBD
PBC4_CBD
CBD_1H4
CBD_4H1
ATCC 14579
ATCC 10987
(C)
Relative Fluorescence Intensity
1.2
1.0
0.8
0.6
0.4
0.2
0.0
1F4
4F1
1H4
4H1
ATCC 14579
ATCC 10987

Fig. IV-2. Schematic representation of CBD hybrids and cell binding activity of fluorescently tagged CBD hybrids. (A) Schematic diagram of CBD hybrid proteins used in this study. Note that all constructs were tagged with EGFP at their N-terminus. (B) Binding of *B. cereus* cells by fluorescently tagged CBD hybrids (CBD_1H4, CBD_4H1) and its parental CBDs (PBC1_CBD, PBC4_CBD). (C) Relative fluorescence intensities of *B. cereus* cells after staining with each CBD hybrid.

Since endolysins from phages infecting Gram-positive bacteria generally feature N-terminal EAD(s) and a C-terminal CBD, most CBDs may show full functionality when they are located at the C-terminus. PBC4_CBD appeared to follow this hypothesis as they showed diminished binding activity with its C-terminal fusion. PBC1_CBD, however, resulted in opposite consequences since it showed better binding properties when fused to C-terminus than to N-terminus. This suggests that overall conformation of the dual CBD constructs is more essential for the binding activities of each CBD. The types of linker region appeared to be less important than the orientation because both 1F4_CBD and 1H4_CBD showed quite good binding properties. However, the dual CBDs with flexible linker region exhibited the formation of inclusion bodies during purification, which led to much less protein yield than those with helical linker (data not shown). A possible explanation of these results is that the helical linker stabilized the folding or enhanced the protein solubility. Several reports that the rigidity of the α-helical linkers works better than flexible ones by keeping reasonable distances and causing less overall interference between the linked domains could support this explanation (Arai et al., 2004; Bai and Shen, 2006; Lu and Feng, 2008). For these reasons, I chose the 1H4_CBD, which possesses

helical linker region, for further characterization.

The dual CBD hybrid 1H4_CBD showed combined binding range of the each CBD, PBC1_CBD and PBC4_CBD **(Table IV-3)**. The 1H4_CBD decorated only *B. cereus* group strains, while other bacterial species did not be labeled by the 1H4_CBD. Comparison of cell binding activities among the 1H4_CBD and its parental CBDs disclosed that the 1H4 showed superior binding activity to its parental CBDs **(Fig. IV-3A)**. The 1H4_CBD demonstrated stronger fluorescent intensity than PBC4_CBD against three *B. cereus* strains (ATCC 27348, KCTC 1094, ATCC 10876), which could be originally labeled by PBC4_CBD. The other *B. cereus* strains (ATCC 11313, ATCC13061, ATCC 21768), which could be bound by PBC1_CBD, also showed similar patterns. These results suggest the synergistic binding effect of the dual CBD hybrid 1H4. To rule out the possibility that the increased binding properties of 1H4 CBD was not due to the enhanced fluorescence by EGFP-1H4_CBD fusion protein, the fluorescence of the same molar concentrations of each protein in PBS was measured. As shown in **Fig. IV-3B**, the fluorescence intensity of the hybrid CBD fusion protein was not higher, but rather lower than those from the parental CBD fusion proteins. Although further work (e.g. calculation of the binding constant) should be

needed to prove the increased binding activity of the hybrid 1H4_CBD towards the cell wall of *B. cereus*, these results propose that the physical proximity of the two CBDs may contribute to the observed synergistic binding effect of the hybrid CBD protein. It is also possible that the inserted helical linker region between the two functional domains could stabilize the each CBD, or may help the each CBD recognize and bind to its ligand more efficiently. Altogether, the tailored hybrid 1H4_CBD could be used as an efficient detection agent for diverse environmental strains of *B. cereus*. In addition, the results presented here demonstrate that the binding activity of CBD can be engineered to recognize additional targets by adding other binding modules with suitable linkers.

Table IV-3. Comparison of binding spectrum among hybrid CBD 1H4 and its parental CBDs

Species	Strain number	PBC1_CBD	PBC4_CBD	CBD_1H4
Bacillus cereus	ATCC 21768	+	-	+
Bacillus cereus	ATCC 13061	+	-	+
Bacillus cereus	ATCC 10987	+	-	+
Bacillus cereus	NCCP 10624	+	-	+
Bacillus cereus	ATCC 53522	+	-	+
Bacillus cereus	ATCC 21366	+	-	+
Bacillus cereus	ATCC 27348	-	+	+
Bacillus cereus	ATCC 14579	-	+	+
Bacillus cereus	ATCC 10876	-	+	+
Bacillus cereus	KCTC 1094	-	+	+
Bacillus cereus	NCCP 10634	-	+	+
Bacillus cereus	NCCP 10715	-	+	+
Bacillus cereus	NCCP 10856	-	+	+
Bacillus cereus	ATCC 4342	-	+	+
Bacillus cereus	NCCP 14043	-	+	+
Bacillus thuringiensis	ATCC 10792	-	+	+
Bacillus mycoides	ATCC 6462	-	+	+
Bacillus subtilis	ATCC 23857	-	-	-
Bacillus megaterium	JCM 2506	-	-	-
Bacillus circulans	JCM 2504	-	-	-
Staphylococcus aureus	RN4220	-	-	-
Clostridium perfringens	FD-1	-	-	-
Listeria monocytogenes	EGDe	-	-	-

* The black box indicates the *B. cereus* group strains.

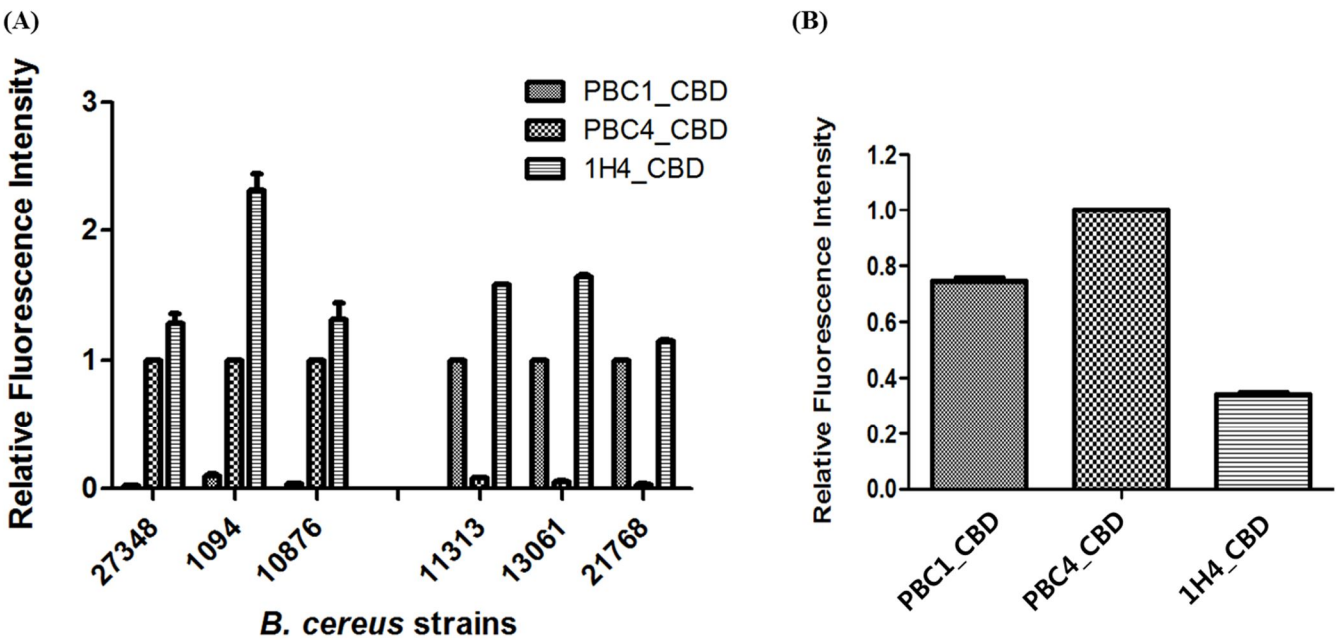

Fig. IV-3. Synergistic binding activity of CBD hybrid 1H4. (A) Relative fluorescence intensities of different *B. cereus* cells after staining with the 1H4_CBD, and its parental CBDs, PBC1_CBD and PBC4_CBD. (B) Relative fluorescence of the same molar concentrations of each protein in PBS was measured.

IV-3-3. Confirmation and capture efficiencies of CBD-MNCs

Since the pathogens are usually present in low numbers in food samples, enrichment culture steps or concentration processes are necessary before the detection can be accomplished. In addition, most foods are composed of complex materials, including proteins, polysaccharides, fats and oils, and even high numbers of background microflora. For these reasons, separation and concentration of small numbers of target cells from food matrices are an essential part of microbial diagnostics. Several techniques have been exploited as means of separating and concentrating bacterial cells from food suspensions: membrane filtration (Besse et al., 2004; Suttle et al., 1991), density gradient centrifugation (Fukushima et al., 2007), and immunomagnetic separation (IMS). Among them, IMS has been widely used in rapid detection method due to its simplicity and high capture efficiency (Dwivedi and Jaykus, 2011; Setterington and Alocilja, 2011). Furthermore, the magnetic carriers can be readily integrated in various diagnostic methods, such as PCR (Amagliani et al., 2006; Chung et al., 2013; Zhang et al., 2008), microfluidic devices (Lee et al., 2009b; Lee et al., 2014; Lee et al., 2015), and immunoassays (Afonso et al., 2013; Bruls et al., 2009; Cho and Irudayaraj, 2013a, b; Wang et al., 2013). Magnetic nanomaterials have been

applied in recent IMS technology because of their high surface-to-volume ratio and faster kinetics in solution, which are unique advantages of nano-sized materials over large micrometer-sized bead (Gu et al., 2006; Varshney et al., 2005).

Immobilization of biorecognition elements (e.g. antibody) to magnetic carriers forms the basis of IMS. In principle, proteins could be covalently or non-covalently immobilized on magnetic carriers (Wang et al., 2011). Despite of its stable and steady performance, covalent attachment, usually occurred with random orientation, is more likely to result in loss of functionality of immobilized proteins (Kausaite-Minkstimiene et al., 2010; Rusmini et al., 2007). Non-covalently immobilization is based on physical adsorption through hydrophobic interactions or salt bridges, but the relatively weak binding forces could cause the leakage of attached proteins after several washing steps (Lee et al., 2009a). In this respect, affinity immobilization is a promising alternative method that provides both relatively strong binding affinity and controlled protein orientation (Kim et al., 2009; Lee et al., 2009c).

Here, I suggest a novel strategy for affinity immobilization of CBD fusion protein to magnetic nanoclusters (MNCs). Schematic diagram of

immobilization of his-tagged mCherry_CBD protein onto the MNCs was shown in **Fig. IV-4A**. The surface hydroxyl groups of iron oxide MNCs were reacted with APTES, resulting in self-assembled monolayer (SAM) of the NH2-terminated silane onto the surface. The reactive amine groups of MNCs were then reacted with glutaldehyde, a homo-bifunctional crosslinker, and formed Schiff bases (imines) through nucleophilic addition of the amine to the carbonyl group of the aldehyde. The addition of aminobutyl NTA, which has a reactive primary amine and four chelation sites for nickel ions, and subsequent nickel chloride, produced Ni-NTA functionalized MNCs. The CBD-MNCs conjugation was based on the coordinate bonding between Ni-NTA of MNCs and the electron donor groups on imidazole rings of hexahistidine tagged CBD fusion protein. Since several studies revealed that deca-histidine tag binds more tightly to Ni-NTA beads than hexa-histidine tag (Fischer et al., 2011; Gaberc-Porekar and Menart, 2005), the recombinant decahistidine-tagged mCherry-CBD fusion protein was produced and used for the conjugation. The immobilization of the fusion protein was verified by fluorescence microscopy, showing that red fluorescent magnetic nanoparticles were attached onto the surface of *B. cereus* cells (**Fig. IV-4B)**. Dynamic light scattering (DLS) analysis revealed that the resulting CBD-

coated MNCs had a zeta potential of -36 mV, indicating moderate stable behavior of the colloid.

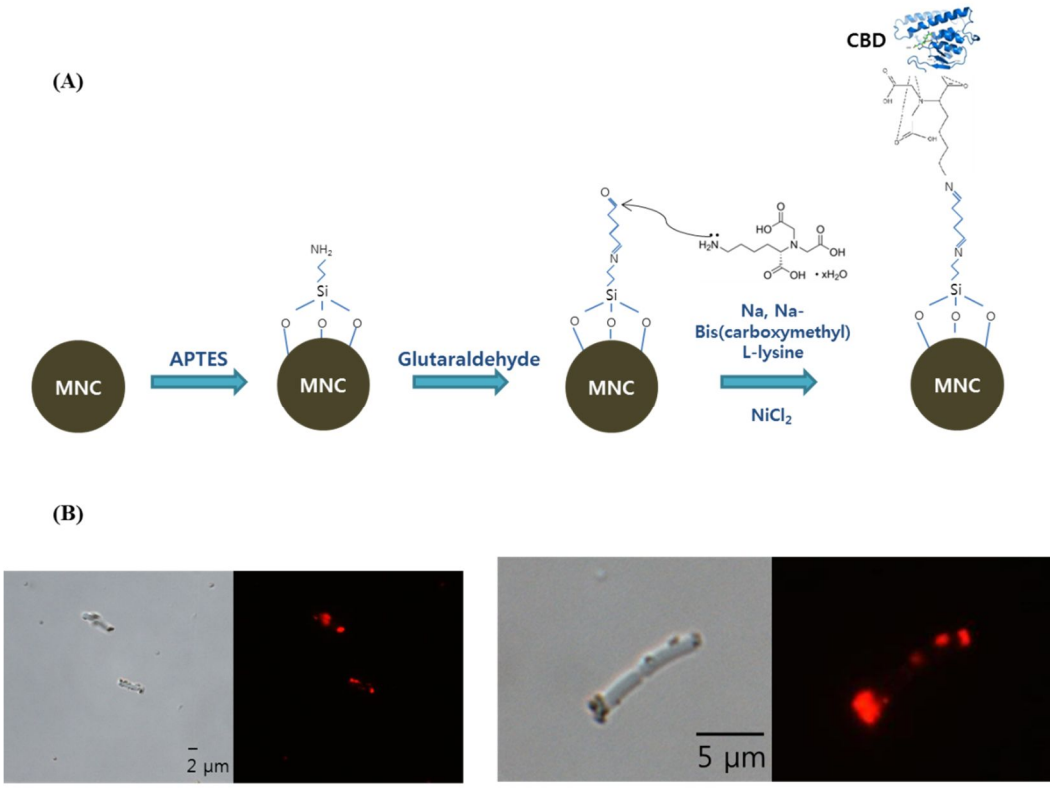

Fig. IV-4. Schematic representation of oriented affinity immobilization of His-mCherry-CBD fusion protein on Ni-NTA functionalized magnetic nanoparticle clusters (MNCs). (A) Schematic representation of oriented affinity immobilization of His-mCherry-CBD fusion protein onto the surface of Ni-NTA functionalized MNCs. (B) Fluorescence microscopic images of *B. cereus* captured and identified by His-mCherry-CBD conjugated MNCs.

To determine the capture efficiencies of the CBD-MNCs complex, different concentrations of bacterial suspensions were mixed with 5 ug of CBD-MNCs, and the mixtures were incubated for 10 min at room temperature. As shown in **Fig. IV-5A**, significant proportions of *B. cereus* cells (85% to 50%) were magnetically separated from bacterial suspensions. Also, an increasing amount of cells (from 10^3 to 10^8 CFU/ml) gradually decreased the capture efficiencies of the CBD-MNCs, indicating that the treated amounts of CBD-MNCs (5 ug, estimated to contain about 1 x 10^7 clusters) were not enough to capture high concentrations of *B. cereus* cells (e.g. > 10^7 CFU/ml) within 10 min. Indeed, the addition of increased amounts of CBD-MNCs (40 ug) to samples with longer incubation time (30 min) improved the cell capture efficiencies (90% to 82%) **(Fig. IV-5B)**. When comparing the capture efficiencies between CBD-MNCs and CBD-coated Dynabeads, a better performance was obtained with CBD-MNCs. Note that because the CBD-MNCs were based on the oriented affinity immobilization of His-tagged fusion proteins, I used cobalt-coated Dynabeads (magnetic beads used for His-tag pulldown) to apply the same immobilization strategy, which could allow more reliable comparison. The superior properties of MNCs (~200 nm in diameter) over Dynabeads (~1 um

in diameter) could be explained by the use of small nano-sized materials. The surface/volume ratio of MNCs is about five times higher than Dynabeads, which offers more contact surface area for capturing bacteria. Furthermore, as the size of CBD-MNCs is more than one order of magnitude smaller than a bacterium, multiple magnetic clusters could be attached onto a bacterial cell, which may render easy magnet-mediated separation (Zhang et al., 2012). Several previous studies reporting the advantages of using magnetic nanoparticles in separating bacterial cells support this explanation (Lin et al., 2006; Varshney et al., 2005; Yang et al., 2007). Considering the low cost and relatively easy synthesis of iron oxide MNCs as well as the better capture efficiency, all of the further experiments were performed with CBD-coated MNCs only.

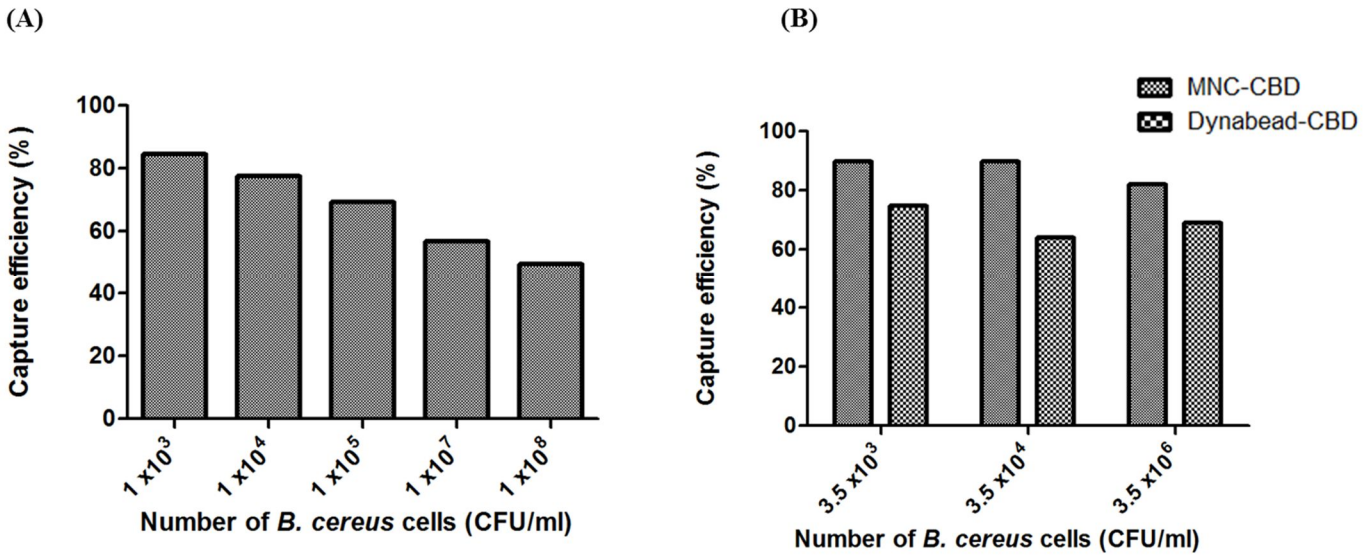

Fig. IV-5. Magnetic capture efficiencies of His-mCherry-CBD conjugated MNCs. (A) Capture efficiencies of His-mCherry-PBC1_CBD-coated MNCs (5 ug) with different concentrations of *B. cereus* suspensions within 10 min. (B) Comparative capture efficiencies of both CBD-coated magnetic carriers (MNCs, Dynabeads, 40 ug) with different concentrations of *B. cereus* suspensions for 30 min.

IV-3-4. Confirmation of CBD-conjugated Au-MNCs and comparison of cell capture efficiencies between CBD and antibody

For more accurate comparison of the cell capture capacities between the CBD and antibody, there are two issues that should be considered. First, choosing a proper bacterial strain that can be recognized both CBD and antibody is of great importance because most antibodies showed reduced or even no reactivity to certain strains of target bacteria (Charni et al., 2000; Jaradat and Zawistowski, 1996). Due to the limited availability and information of the commercial *B. cereus* antibodies, I chose an anti-*C. perfringens* polyclonal antibody (ab35023, Abcam) raised against native *C. perfringens* ATCC 13124 as immunogens. The counterpart CBD was *C. perfringens*-specific CPF369_CBD, which was identified from the genome of *C. perfringens* ATCC 13124. Second, I used gold-coated magnetic nanoclusters (Au-MNCs) for the affinity immobilization of the proteins because the Ni-NTA functionalized MNCs are not appropriate for conjugation of the antibody. Instead, well-established thiol chemistry enabled oriented immobilization of both CBD and antibody onto the surface of Au-MNCs. For antibody conjugation, the gold surface was pretreated with the cysteine-tagged protein G to form semi-covalent bonds between gold and the

thiol group of the cysteine tag (Dubois and Nuzzo, 1992; Lee et al., 2007). Since the protein G specifically binds to nonantigenic (Fc) regions of antibody, the antigen binding sites of the conjugated antibodies are available to their target antigens.

For conjugation of the CBD to the Au-MNCs, glutathione-functionalized Au-MNCs were used for oriented immobilization. The reduced glutathione (GSH), a tripepetide consisting of γ-Glu-Cys-Gly, has been used as a stabilizing linker to bind with gold nanoparticles (Chen et al., 2009). Additionally, the ligand–receptor interaction between GSH and glutathione S-transferase (GST) allows the proper orientation of the GST fusion proteins on the surfaces of nanoparticles (Pan et al., 2011). To immobilize the CBDs onto a GSH-coated gold nanoparticles, I genetically engineered the CPF369_CBD by adding GST genes to the N-terminal of the CBD. The fusion of GST protein offers several advantages. First, with the reasonable affinity and specificity of GSH-GST interaction (Sagermann et al., 2009; Singh et al., 2011; Tessema et al., 2006), the recombinant GST-CBD fusion protein could be immobilized on the GSH-functionalized Au-MNCs in an oriented manner. Second, the GST moiety (25 kDa) could act as a spacer and keep the CBD away from the Au-MNCs thereby minimizing

possible steric hindrance and ensuring full functionality of the CBD (Kim and Herr, 2013). Lastly, GST-tag has been known to increase the recombinant protein solubility and to stabilize the protein by protecting the intracellular protease cleavage (Terpe, 2003; Zhou and Wagner, 2010).

To prepare Au-MNCs, 5 nm of gold nanoseeds were synthesized by the addition of sodium citrate and sodium borohydride ($NaBH_4$) as a capping agent and a strong reducing agent, respectively. DLS measurement revealed that the average diameter of the synthesized gold nanoseeds were 5.3 nm (data not shown). Citrate-stabilized gold nanoseeds were then attached onto the APTES-modified MNCs occurred by stable amide bond between carboxyl groups of citrate and primary amine groups of APTES. **Fig. IV-6A** and **B** showed SEM images of MNCs and Au-MNCs, respectively. Note that each MNC consists of a few hundreds of small Fe_3O_4 magnetic nanoparticles (Chun et al., 2011). The average sizes of the MNCs and Au-MNCs were 171 nm and 189 nm, respectively, and both particles have narrow size distributions. As shown in **Fig. IV-6B**, the gold nanoseeds successfully adhered to the surface of Fe_3O_4 MNCs. The UV-vis absorption spectra demonstrated that greater absorption emerged after 520 nm for the Au-MNCs, whereas bare MNCs did not have any apparent absorption pattern **(Fig. IV-**

6C). This change in the absorption spectrum could be attributed to the deposition of gold nanoseeds onto MNCs, which again confirmed the formation of the Au-MNCs. The TEM image showed that many CBD-conjugated Au-MNCs bound to the surface of a *C. perfringens* bacterium, indicating the feasibility of magnetic separation from sample solutions using the CBD-coated MNCs (**Fig. IV-6D)**.

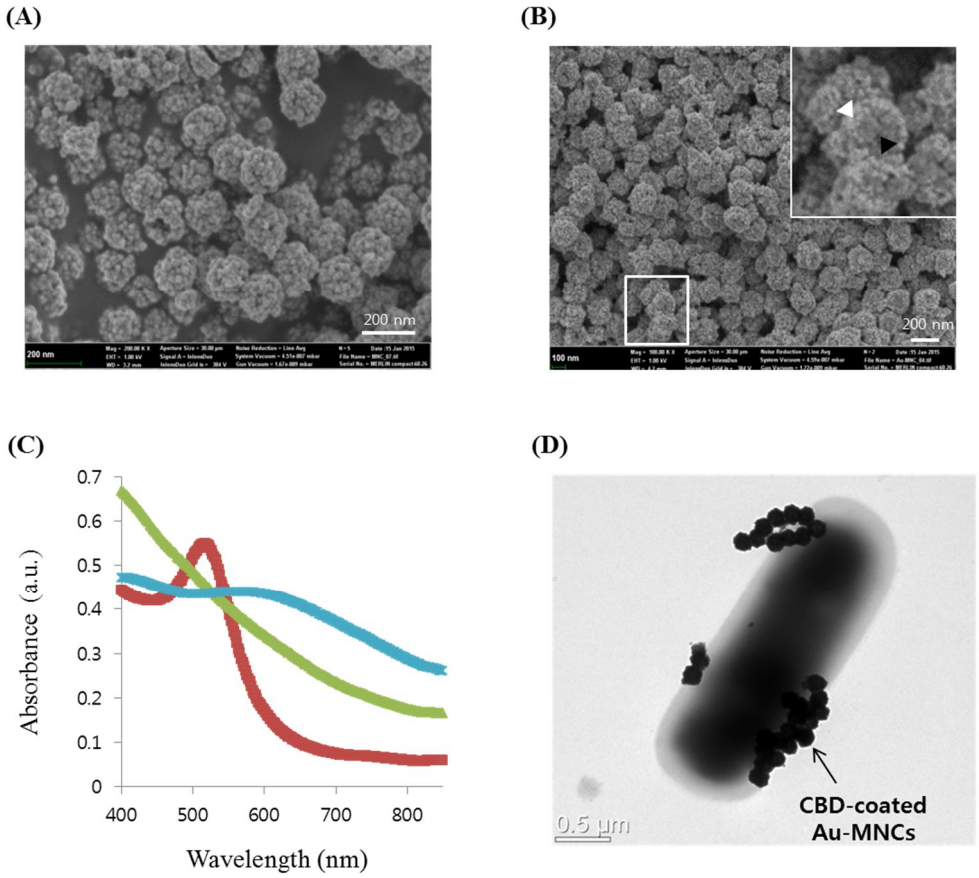

Fig. IV-6. Schematic representation of oriented affinity immobilization of GST-CBD fusion protein on glutathione (GSH) functionalized gold-coated magnetic nanoparticle clusters (Au-MNCs). (A, B) Scanning electron microscopy images of MNCs (A) and Au-MNCs (B). Inset shows attached gold nanoseeds (white arrowhead) and uncovered MNCs (black arrowhead). (C) The absorption spectra of MNCs (green), Au-MNCs (blue),

and 5 nm gold nanoseed (red). (D) TEM images of *C. perfringes* captured and identified with GST-CPF369_CBD conjugated Au-MNCs.

Fig. IV-7A showed schematic representation of affinity immobilization of CBD and antibody onto the surface of Au-MNCs. When the CBD-coated MNCs were applied to a buffer containing different concentrations of *C. perfringens* cells (10^3 to 10^5 CFU/ml), the capture efficiencies ranged from 72% to 60%, gradually decreasing as target cells decreased **(Fig. IV-7B)**. On the other hand, the antibody-coated MNCs exhibited cell capture efficiencies of about 40%, regardless of treated cell concentrations. One possible reason for this superior performance of CBD-coated MNCs is that the smaller sizes of the linker (GSH) and GST-CBD may increase their amounts anchored onto the MNCs surface, which in turn translate to higher cell capture efficiencies (Jin et al., 2014; Kell et al., 2008; Lin et al., 2005). Another probable explanation is that antibody-coated MNCs may lead to agglutination of cell-MNCs mixtures, which is often seen with many antibody-coated magnetic beads (Kretzer et al., 2007). Further work is under progress to improve the sensitivity, stability, and specificity of the CBD-conjugated MNCs. Also, I aim to extend this work into real food samples in the future.

In conclusion, the CBD-coated Au-MNCs showed cell capture performance better than a paralleled antibody approach, providing a

significant potential as an alternative to a conventional antibody-based IMS. These CBD-based magnetic separation methods would be useful for pre-analytical sample processing steps to improve the detection of target pathogens. In addition, the concept of affinity immobilization of CBDs onto MNCs can be easily incorporated to other rapid biosensing platforms (e.g. PCR, electrochemical, and optical sensors) and thus offers the great potential in developing CBD-based biosensors.

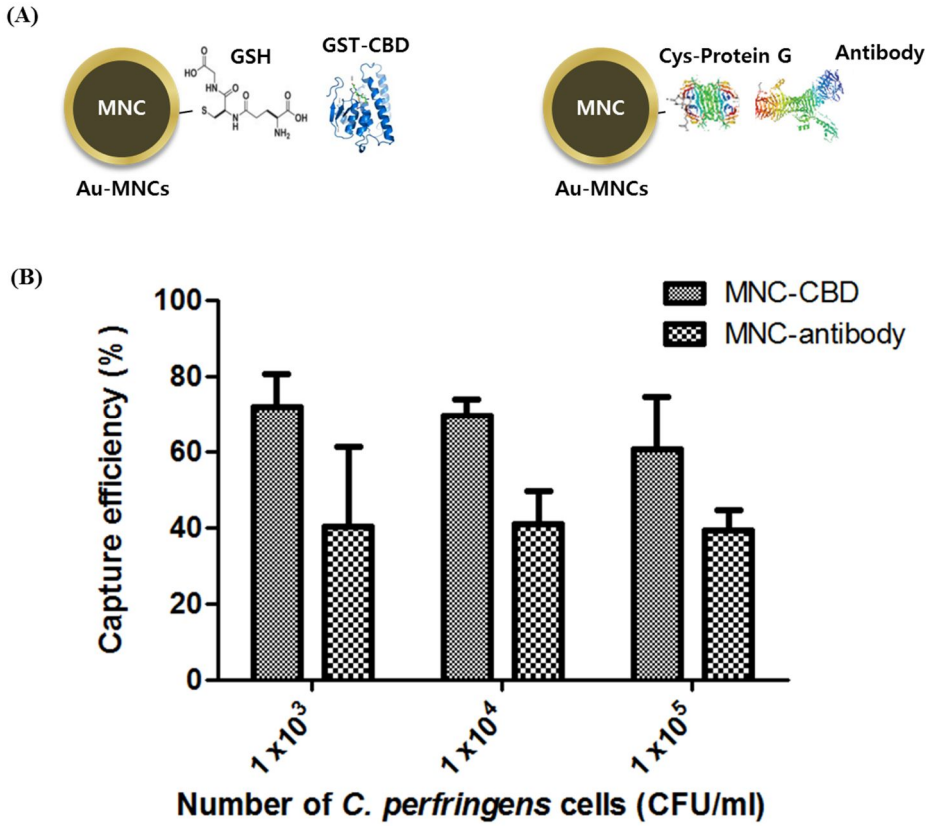

Fig. IV-7. Comparison of capture efficiencies between GST-CBD conjugated Au-MNCs and anti-*Clostridium* conjugated Au-MNCs. (A) Schematic representation of GST-CBD coated Au-MNCs and antibody-coated Au-MNCs used in this study. (B) Capture efficiencies of CBD-coated Au-MNCs and antibody-coated Au-MNCs for *C. perfringens* cells with varying concentrations within 20 min. Same amounts of both protein-conjugated Au-MNCs (20 ug) were used for comparison.

IV-4. References

Afonso, A.S., Perez-Lopez, B., Faria, R.C., Mattoso, L.H.C., Hernandez-Herrero, M., Roig-Sagues, A.X., Maltez-da Costa, M., Merkoci, A., (2013) Electrochemical detection of Salmonella using gold nanoparticles. Biosens. Bioelectron. 40, 121-126.

Amagliani, G., Omiccioli, E., Campo, A., Bruce, I.J., Brandi, G., Magnani, M., (2006) Development of a magnetic capture hybridization-PCR assay for Listeria monocytogenes direct detection in milk samples. J. Appl. Microbiol. 100, 375-383.

Arai, R., Ueda, H., Kitayama, A., Kamiya, N., Nagamune, T., (2001) Design of the linkers which effectively separate domains of a bifunctional fusion protein. Protein Eng. 14, 529-532.

Arai, R., Wriggers, W., Nishikawa, Y., Nagamune, T., Fujisawa, T., (2004) Conformations of variably linked chimeric proteins evaluated by synchrotron X-ray small-angle scattering. Proteins 57, 829-838.

Arya, S.K., Singh, A., Naidoo, R., Wu, P., McDermott, M.T., Evoy, S., (2011) Chemically immobilized T4-bacteriophage for specific Escherichia coli detection using surface plasmon resonance. Analyst 136, 486-492.

Bai, Y., Shen, W.C., (2006) Improving the oral efficacy of recombinant granulocyte colony-stimulating factor and transferrin fusion protein by spacer optimization. Pharm. Res. 23, 2116-2121.

Besse, N.G., Audinet, N., Beaufort, A., Colin, P., Cornu, M., Lombard, B., (2004) A contribution to the improvement of Listeria monocytogenes enumeration in cold-smoked salmon. Int. J. Food Microbiol. 91, 119-127.

Bruls, D.M., Evers, T.H., Kahlman, J.A., van Lankvelt, P.J., Ovsyanko, M., Pelssers, E.G., Schleipen, J.J., de Theije, F.K., Verschuren, C.A., van der Wijk, T., van Zon, J.B., Dittmer, W.U., Immink, A.H., Nieuwenhuis, J.H., Prins, M.W., (2009) Rapid integrated biosensor for multiplexed immunoassays based on actuated magnetic nanoparticles. Lab on a chip 9, 3504-3510.

Brzozowska, E., Smietana, M., Koba, M., Gorska, S., Pawlik, K., Gamian, A., Bock, W.J., (2015) Recognition of bacterial lipopolysaccharide using bacteriophage-adhesin-coated long-period gratings. Biosens. Bioelectron. 67, 93-99.

Callewaert, L., Walmagh, M., Michiels, C.W., Lavigne, R., (2011) Food applications of bacterial cell wall hydrolases. Curr. Opin. Biotechnol. 22, 164-171.

Charni, N., Perissol, C., Le Petit, J., Rugani, N., (2000) Production and characterization of monoclonal antibodies against vegetative cells of Bacillus cereus. Appl. Environ. Microbiol. 66, 2278-2281.

Chatterjee, S., Bandyopadhyay, A., Sarkar, K., (2011) Effect of iron oxide and gold nanoparticles on bacterial growth leading towards biological application. Journal of nanobiotechnology 9, 34.

Chen, C.T., Chen, W.J., Liu, C.Z., Chang, L.Y., Chen, Y.C., (2009) Glutathione-bound gold nanoclusters for selective-binding and detection of glutathione S-transferase-fusion proteins from cell lysates. Chem. Commun. (Camb.), 7515-7517.

Chibli, H., Ghali, H., Park, S., Peter, Y.A., Nadeau, J.L., (2014) Immobilized phage proteins for specific detection of staphylococci. Analyst 139, 179-186.

Cho, I.H., Irudayaraj, J., (2013a) In-situ immuno-gold nanoparticle network ELISA biosensors for pathogen detection. Int. J. Food Microbiol. 164, 70-75.

Cho, I.H., Irudayaraj, J., (2013b) Lateral-flow enzyme immunoconcentration for rapid detection of Listeria monocytogenes. Anal. Bioanal. Chem. 405, 3313-3319.

Chun, C., Joo, J., Kwon, D., Kim, C.S., Cha, H.J., Chung, M.S., Jeon, S., (2011) A facile and sensitive immunoassay for the detection of alpha-fetoprotein using gold-coated magnetic nanoparticle clusters and dynamic light scattering. Chem. Commun. (Camb.) 47, 11047-11049.

Chung, H.J., Castro, C.M., Im, H., Lee, H., Weissleder, R., (2013) A magneto-DNA nanoparticle system for rapid detection and phenotyping of

bacteria. Nature nanotechnology 8, 369-375.

Crasto, C.J., Feng, J.A., (2000) LINKER: a program to generate linker sequences for fusion proteins. Protein Eng. 13, 309-312.

DeLano, W.L., (2002) Unraveling hot spots in binding interfaces: progress and challenges. Curr. Opin. Struct. Biol. 12, 14-20.

Dubois, L.H., Nuzzo, R.G., (1992) Synthesis, Structure, and Properties of Model Organic-Surfaces. Annu. Rev. Phys. Chem. 43, 437-463.

Dwivedi, H.P., Jaykus, L.A., (2011) Detection of pathogens in foods: the current state-of-the-art and future directions. Crit. Rev. Microbiol. 37, 40-63.

Fischer, M., Leech, A.P., Hubbard, R.E., (2011) Comparative assessment of different histidine-tags for immobilization of protein onto surface plasmon resonance sensorchips. Anal. Chem. 83, 1800-1807.

Fischetti, V.A., (2010) Bacteriophage endolysins: a novel anti-infective to control Gram-positive pathogens. Int. J. Med. Microbiol. 300, 357-362.

Fu, Z., Rogelj, S., Kieft, T.L., (2005) Rapid detection of Escherichia coli O157:H7 by immunomagnetic separation and real-time PCR. Int. J. Food Microbiol. 99, 47-57.

Fukushima, H., Katsube, K., Hata, Y., Kishi, R., Fujiwara, S., (2007) Rapid separation and concentration of food-borne pathogens in food samples prior to quantification by viable-cell counting and real-time PCR. Appl. Environ. Microbiol. 73, 92-100.

Gaberc-Porekar, V., Menart, V., (2005) Potential for using histidine tags in purification of proteins at large scale. Chem Eng Technol 28, 1306-1314.

George, R.A., Heringa, J., (2002) An analysis of protein domain linkers: their classification and role in protein folding. Protein Eng. 15, 871-879.

Gu, H., Xu, K., Xu, C., Xu, B., (2006) Biofunctional magnetic nanoparticles for protein separation and pathogen detection. Chem. Commun. (Camb.), 941-949.

Jaradat, Z.W., Zawistowski, J., (1996) Production and characterization of monoclonal antibodies against the O-5 antigen of Salmonella typhimurium lipopolysaccharide. Appl. Environ. Microbiol. 62, 1-5.

Javed, M.A., Poshtiban, S., Arutyunov, D., Evoy, S., Szymanski, C.M., (2013) Bacteriophage Receptor Binding Protein Based Assays for the Simultaneous Detection of Campylobacter jejuni and Campylobacter coli. PLoS One 8.

Jin, Y., Liu, F., Shan, C., Tong, M., Hou, Y., (2014) Efficient bacterial capture with amino acid modified magnetic nanoparticles. Water research 50, 124-134.

Kausaite-Minkstimiene, A., Ramanaviciene, A., Kirlyte, J., Ramanavicius, A., (2010) Comparative study of random and oriented antibody immobilization techniques on the binding capacity of immunosensor. Anal. Chem. 82, 6401-6408.

Kell, A.J., Stewart, G., Ryan, S., Peytavi, R., Boissinot, M., Huletsky, A., Bergeron, M.G., Simard, B., (2008) Vancomycin-modified nanoparticles for efficient targeting and preconcentration of Gram-positive and Gram-negative bacteria. ACS nano 2, 1777-1788.

Kelley, L.A., Sternberg, M.J., (2009) Protein structure prediction on the Web: a case study using the Phyre server. Nat. Protoc. 4, 363-371.

Kim, D., Herr, A.E., (2013) Protein immobilization techniques for microfluidic assays. Biomicrofluidics 7, 41501.

Kim, H., Kwon, H.S., Ahn, J., Lee, C.H., Ahn, I.S., (2009) Evaluation of a silica-coated magnetic nanoparticle for the immobilization of a His-tagged lipase. Biocatal Biotransfor 27, 246-253.

Kong, M., Ryu, S., (2015) Bacteriophage PBC1 and Its Endolysin as an Antimicrobial Agent against Bacillus cereus. Appl. Environ. Microbiol. 81, 2274-2283.

Kretzer, J.W., Lehmann, R., Schmelcher, M., Banz, M., Kim, K.P., Korn, C., Loessner, M.J., (2007) Use of high-affinity cell wall-binding domains of bacteriophage endolysins for immobilization and separation of bacterial cells.

Appl. Environ. Microbiol. 73, 1992-2000.

Larkin, M.A., Blackshields, G., Brown, N.P., Chenna, R., McGettigan, P.A., McWilliam, H., Valentin, F., Wallace, I.M., Wilm, A., Lopez, R., Thompson, J.D., Gibson, T.J., Higgins, D.G., (2007) Clustal W and Clustal X version 2.0. Bioinformatics 23, 2947-2948.

Lazcka, O., Del Campo, F.J., Munoz, F.X., (2007) Pathogen detection: a perspective of traditional methods and biosensors. Biosens. Bioelectron. 22, 1205-1217.

Lee, D.G., Ponvel, K.M., Kim, M., Hwang, S., Ahn, I.S., Lee, C.H., (2009a) Immobilization of lipase on hydrophobic nano-sized magnetite particles. J Mol Catal B-Enzym 57, 62-66.

Lee, H., Yoon, T.J., Weissleder, R., (2009b) Ultrasensitive Detection of Bacteria Using Core-Shell Nanoparticles and an NMR-Filter System. Angew Chem Int Edit 48, 5657-5660.

Lee, J.J., Jeong, K.J., Hashimoto, M., Kwon, A.H., Rwei, A., Shankarappa, S.A., Tsui, J.H., Kohane, D.S., (2014) Synthetic ligand-coated magnetic nanoparticles for microfluidic bacterial separation from blood. Nano letters 14, 1-5.

Lee, J.M., Park, H.K., Jung, Y., Kim, J.K., Jung, S.O., Chung, B.H., (2007) Direct immobilization of protein G variants with various numbers of cysteine residues on a gold surface. Anal. Chem. 79, 2680-2687.

Lee, K.S., Woo, M.H., Kim, H.S., Lee, E.Y., Lee, I.S., (2009c) Synthesis of hybrid Fe3O4-silica-NiO superstructures and their application as magnetically separable high-performance biocatalysts. Chem Commun, 3780-3782.

Lee, W., Kwon, D., Choi, W., Jung, G.Y., Jeon, S., (2015) 3D-printed microfluidic device for the detection of pathogenic bacteria using size-based separation in helical channel with trapezoid cross-section. Sci. Rep. 5, 7717.

Lin, Y., Jiang, X., Elkin, T., Fernando, K.A., Gu, L., Taylor, S., Yang, H., Jones, E., Wang, W., Sunl, Y.P., (2006) Carbon nanotubes for

immunomagnetic separation of Escherichia coli O157: H7. Journal of nanoscience and nanotechnology 6, 868-871.

Lin, Y.S., Tsai, P.J., Weng, M.F., Chen, Y.C., (2005) Affinity capture using vancomycin-bound magnetic nanoparticles for the MALDI-MS analysis of bacteria. Anal. Chem. 77, 1753-1760.

Loessner, M.J., (2005) Bacteriophage endolysins--current state of research and applications. Curr. Opin. Microbiol. 8, 480-487.

Loessner, M.J., Kramer, K., Ebel, F., Scherer, S., (2002) C-terminal domains of Listeria monocytogenes bacteriophage murein hydrolases determine specific recognition and high-affinity binding to bacterial cell wall carbohydrates. Mol. Microbiol. 44, 335-349.

Loessner, M.J., Maier, S.K., Daubek-Puza, H., Wendlinger, G., Scherer, S., (1997) Three Bacillus cereus bacteriophage endolysins are unrelated but reveal high homology to cell wall hydrolases from different bacilli. J. Bacteriol. 179, 2845-2851.

Lu, P., Feng, M.G., (2008) Bifunctional enhancement of a beta-glucanase-xylanase fusion enzyme by optimization of peptide linkers. Appl. Microbiol. Biotechnol. 79, 579-587.

Mahony, J., McAuliffe, O., Ross, R.P., van Sinderen, D., (2011) Bacteriophages as biocontrol agents of food pathogens. Curr. Opin. Biotechnol. 22, 157-163.

Marchler-Bauer, A., Anderson, J.B., Derbyshire, M.K., DeWeese-Scott, C., Gonzales, N.R., Gwadz, M., Hao, L., He, S., Hurwitz, D.I., Jackson, J.D., Ke, Z., Krylov, D., Lanczycki, C.J., Liebert, C.A., Liu, C., Lu, F., Lu, S., Marchler, G.H., Mullokandov, M., Song, J.S., Thanki, N., Yamashita, R.A., Yin, J.J., Zhang, D., Bryant, S.H., (2007) CDD: a conserved domain database for interactive domain family analysis. Nucleic Acids Res. 35, D237-240.

Nariya, H., Miyata, S., Tamai, E., Sekiya, H., Maki, J., Okabe, A., (2011) Identification and characterization of a putative endolysin encoded by episomal phage phiSM101 of Clostridium perfringens. Appl. Microbiol. Biotechnol. 90, 1973-1979.

Niemirowicz, K., Swiecicka, I., Wilczewska, A.Z., Misztalewska, I., Kalska-Szostko, B., Bienias, K., Bucki, R., Car, H., (2014) Gold-functionalized magnetic nanoparticles restrict growth of Pseudomonas aeruginosa. International journal of nanomedicine 9, 2217-2224.

Pan, Y., Long, M.J.C., Li, X.M., Shi, J.f., Hedstrom, L., Xu, B., (2011) Glutathione (GSH)-decorated magnetic nanoparticles for binding glutathione-S-transferase (GST) fusion protein and manipulating live cells. Chemical Science 2, 945-948.

Petrenko, V.A., Vodyanoy, V.J., (2003) Phage display for detection of biological threat agents. J. Microbiol. Methods 53, 253-262.

Poshtiban, S., Javed, M.A., Arutyunov, D., Singh, A., Banting, G., Szymanski, C.M., Evoy, S., (2013) Phage receptor binding protein-based magnetic enrichment method as an aid for real time PCR detection of foodborne bacteria. Analyst 138, 5619-5626.

Qu, L., Luo, P.G., Taylor, S., Lin, Y., Huang, W., Anyadike, N., Tzeng, T.R., Stutzenberger, F., Latour, R.A., Sun, Y.P., (2005) Visualizing adhesion-induced agglutination of Escherichia coli with mannosylated nanoparticles. Journal of nanoscience and nanotechnology 5, 319-322.

Rusmini, F., Zhong, Z., Feijen, J., (2007) Protein immobilization strategies for protein biochips. Biomacromolecules 8, 1775-1789.

Sagermann, M., Chapleau, R.R., DeLorimier, E., Lei, M., (2009) Using affinity chromatography to engineer and characterize pH-dependent protein switches. Protein Sci. 18, 217-228.

Schmelcher, M., Shabarova, T., Eugster, M.R., Eichenseher, F., Tchang, V.S., Banz, M., Loessner, M.J., (2010) Rapid multiplex detection and differentiation of Listeria cells by use of fluorescent phage endolysin cell wall binding domains. Appl. Environ. Microbiol. 76, 5745-5756.

Schmelcher, M., Tchang, V.S., Loessner, M.J., (2011) Domain shuffling and module engineering of Listeria phage endolysins for enhanced lytic activity and binding affinity. Microbial biotechnology 4, 651-662.

Setterington, E.B., Alocilja, E.C., (2011) Rapid electrochemical detection of polyaniline-labeled Escherichia coli O157:H7. Biosens. Bioelectron. 26, 2208-2214.

Sheffield, P., Garrard, S., Derewenda, Z., (1999) Overcoming expression and purification problems of RhoGDI using a family of "parallel" expression vectors. Protein Expr. Purif. 15, 34-39.

Singh, A., Arutyunov, D., McDermott, M.T., Szymanski, C.M., Evoy, S., (2011) Specific detection of Campylobacter jejuni using the bacteriophage NCTC 12673 receptor binding protein as a probe. Analyst 136, 4780-4786.

Singh, A., Arutyunov, D., Szymanski, C.M., Evoy, S., (2012) Bacteriophage based probes for pathogen detection. Analyst 137, 3405-3421.

Singh, A., Arya, S.K., Glass, N., Hanifi-Moghaddam, P., Naidoo, R., Szymanski, C.M., Tanha, J., Evoy, S., (2010) Bacteriophage tailspike proteins as molecular probes for sensitive and selective bacterial detection. Biosens. Bioelectron. 26, 131-138.

Skottrup, P.D., Nicolaisen, M., Justesen, A.F., (2008) Towards on-site pathogen detection using antibody-based sensors. Biosens. Bioelectron. 24, 339-348.

Sung, Y.J., Suk, H.J., Sung, H.Y., Li, T., Poo, H., Kim, M.G., (2013) Novel antibody/gold nanoparticle/magnetic nanoparticle nanocomposites for immunomagnetic separation and rapid colorimetric detection of Staphylococcus aureus in milk. Biosens. Bioelectron. 43, 432-439.

Suttle, C.A., Chan, A.M., Cottrell, M.T., (1991) Use of Ultrafiltration to Isolate Viruses from Seawater Which Are Pathogens of Marine-Phytoplankton. Appl. Environ. Microbiol. 57, 721-726.

Tamai, E., Yoshida, H., Sekiya, H., Nariya, H., Miyata, S., Okabe, A., Kuwahara, T., Maki, J., Kamitori, S., (2014) X-ray structure of a novel endolysin encoded by episomal phage phiSM101 of Clostridium perfringens. Mol. Microbiol. 92, 326-337.

Tawil, N., Sacher, E., Mandeville, R., Meunier, M., (2014) Bacteriophages:

biosensing tools for multi-drug resistant pathogens. Analyst 139, 1224-1236.

Terpe, K., (2003) Overview of tag protein fusions: from molecular and biochemical fundamentals to commercial systems. Appl. Microbiol. Biotechnol. 60, 523-533.

Tessema, M., Simons, P.C., Cimino, D.F., Sanchez, L., Waller, A., Posner, R.G., Wandinger-Ness, A., Prossnitz, E.R., Sklar, L.A., (2006) Glutathione-S-transferase-green fluorescent protein fusion protein reveals slow dissociation from high site densiy beads and measures free GSH. Cytom Part A 69A, 326-334.

Tolba, M., Ahmed, M.U., Tlili, C., Eichenseher, F., Loessner, M.J., Zourob, M., (2012) A bacteriophage endolysin-based electrochemical impedance biosensor for the rapid detection of Listeria cells. Analyst 137, 5749-5756.

Varshney, M., Yang, L., Su, X.L., Li, Y., (2005) Magnetic nanoparticle-antibody conjugates for the separation of Escherichia coli O157:H7 in ground beef. J. Food Prot. 68, 1804-1811.

Wang, D.B., Tian, B., Zhang, Z.P., Deng, J.Y., Cui, Z.Q., Yang, R.F., Wang, X.Y., Wei, H.P., Zhang, X.E., (2013) Rapid detection of Bacillus anthracis spores using a super-paramagnetic lateral-flow immunological detection system. Biosens. Bioelectron. 42, 661-667.

Wang, L., Bai, J., Li, Y., Huang, Y., (2008) Multifunctional nanoparticles displaying magnetization and near-IR absorption. Angew. Chem. Int. Ed. Engl. 47, 2439-2442.

Wang, W., Singh, S., Zeng, D.L., King, K., Nema, S., (2007) Antibody structure, instability, and formulation. J. Pharm. Sci. 96, 1-26.

Wang, W., Wang, D.I., Li, Z., (2011) Facile fabrication of recyclable and active nanobiocatalyst: purification and immobilization of enzyme in one pot with Ni-NTA functionalized magnetic nanoparticle. Chem. Commun. (Camb.) 47, 8115-8117.

Wen, D., Foley, S.F., Hronowski, X.L., Gu, S., Meier, W., (2013) Discovery and investigation of O-xylosylation in engineered proteins containing a

(GGGGS)n linker. Anal. Chem. 85, 4805-4812.

Yang, H., Qu, L., Wimbrow, A.N., Jiang, X., Sun, Y., (2007) Rapid detection of Listeria monocytogenes by nanoparticle-based immunomagnetic separation and real-time PCR. Int. J. Food Microbiol. 118, 132-138.

Zdobnov, E.M., Apweiler, R., (2001) InterProScan--an integration platform for the signature-recognition methods in InterPro. Bioinformatics 17, 847-848.

Zhang, L., Luo, Q., Zhang, F., Zhang, D.M., Wang, Y.S., Sun, Y.L., Dong, W.F., Liu, J.Q., Huo, Q.S., Sun, H.B., (2012) High-performance magnetic antimicrobial Janus nanorods decorated with Ag nanoparticles. J. Mater. Chem. 22, 23741-23744.

Zhang, M., Cushing, B.L., O'Connor, C.J., (2008) Synthesis and characterization of monodisperse ultra-thin silica-coated magnetic nanoparticles. Nanotechnology 19, 085601.

Zhou, P., Wagner, G., (2010) Overcoming the solubility limit with solubility-enhancement tags: successful applications in biomolecular NMR studies. J. Biomol. NMR 46, 23-31.

Zimmer, M., Vukov, N., Scherer, S., Loessner, M.J., (2002) The murein hydrolase of the bacteriophage phi3626 dual lysis system is active against all tested Clostridium perfringens strains. Appl. Environ. Microbiol. 68, 5311-5317.

Chapter V.

Overall conclusions and future perspectives

V-1. *B. cereus* bacteriophages and its genome

Six *B. cereus* phages were isolated and characterized. TEM analysis revealed that isolated phages were classified into the *Siphoviridae* (PBC1, PBC2, PBC4, PBC5) and *Myoviridae* (PBC6, PBC9) families. All of the isolated *B. cereus* phages have high host specificity to the *B. cereus* group species. Genomic analysis revealed that the *B. cereus* phages contain double-stranded DNA genomes of between 41.2 kb and 168.7 kb. All phage genomes are organized into function-specific gene clusters, which is typical characteristics of tailed phages. This study could broaden our knowledge of *B. cereus* phages, and be useful for developing efficient biocontrol agents against the notorious human pathogen *B. cereus*.

1. PBC1 showed a very narrow host range, infecting only 2 of 14 *B. cereus* strains. This result indicates that PBC1 alone would not be an efficient biocontrol agent against diverse strains of *B. cereus*. However, since the host strain (ATCC 21768) is resistant to all other isolated phages and PBC1 is very effective in preventing the growth of the *B. cereus* strain in both liquid cultures and boiled rice, I think that PBC1 could be a useful component for the development of a phage cocktail against *B.*

cereus.

2. Because PBC1 forms clear plaques, rapidly kills the *B. cereus* host bacteria and does not contain any lysogeny-related genes in its genome, PBC1 is considered to be a virulent phage. To the best of my knowledge, PBC1 is the only naturally isolated virulent *Siphoviridae* phage among the reported *B. cereus* phages.

3. PBC1 is a unique siphovirus and features a 41.2-bk genome. Phylogenetic analysis based on the MCP demonstrated that PBC1 is more closely related to the *B. clarkii* phage BCJA1c and lactic acid bacteria phages than to the phages infecting *B. cereus.* Whole genome comparison showed that the late gene region, including the terminase, structural genes, and holin of PBC1 are similar to those from *B. cereus* temperate phage 250, whereas their endolysins are different.

4. Both siphoviruses PBC2 and PBC4 feature 168.7 kb (PBC2) and 80.6 kb (PBC4), respectively. Both PBC2 and PBC4 have integrases or recombinase enzymes in their genomes, indicating temperate life styles. Comparative genomics revealed that PBC2

has similar genomic structure and high nucleotide identity with the *B. anthracis* phage Tsamsa. The genomes between PBC4 and *B. cereus* phage Basilisk also showed close relatedness as they share a 83.3% average nucleotide identity over the entire genome. However, their differences in putative tail fiber proteins imply that the two phages may have distinct host specificities.

5. The genome sequence of PBC5 is 56,332 bp in length. The TerL and MCP of PBC5 showed a low degree of homology to those from other reported *B. cereus* phages, suggesting that PBC5 is a novel *B. cereus* phage. Two myoviruses PBC6 and PBC9 are highly similar phages (94.9% of nucleotide identity), and feature 157.1 kb and 156.2 kb, respectively. Their morphological and genetic properties suggest that both PBC6 and PBC9 are the members of the newly proposed Bastille group within the *Spounavirinae* subfamily.

V-2. Characterization of endolysins and their various domains

In this chapter, I characterized several endolysins from the isolated *B. cereus* phages and identified their functional domains, including EADs, CBDs, and a SBD. The *B. cereus* phage endolysins generally showed much broader lytic activity than phages, suggesting that they could be alternative biocontrol agents against *B. cereus*. Also, CBDs from *B. cereus* phage endolysins showed specific binding properties towards the *B. cereus* group species. Lastly, a facile and efficient method for identifying a novel CBD from a sequenced bacterial genome was presented. The molecular and biochemical studies of the endolysins would be the basis for the development of effective therapeutics and novel diagnostic tools.

1. *B. cereus* phage endolysins are between 250 and 350 amino acids in length. Most endolysins have distinct modular structure, consisting of an N-terminal enzymatic active domain (EAD) and a C-terminal CBD, whereas LysPBC5 and LysPBC10 are devoid of recognizable CBDs. While the EADs of the *B. cereus* phage endolysins are generally conserved across the bacterial autolysins and phage endolysins, the CBDs are variable, which may explain the great specificity of the endolysins, allowing

them to bind specifically to a unique component of the host cell wall.

2. Most endolysins were highly expressed in soluble form in *E. coli.* Compared to the extreme host specificity of phages, their endolysins showed a much broader lytic spectrum, albeit limited to the genus *Bacillus*. LysPBC2 can more efficiently lyse *B. subtilis* group strains than the *B. cereus* group strains. On the other hand, LysPBC4 showed specific lytic activity against the *B. cereus* group strains, whereas other *Bacillus* species were insensitive to the LysPBC4.

3. LysPBC1 showed stronger lytic activity against *B. cereus* cells compared with the truncated endolysin LysPBC1_EAD. However, LysPBC1_EAD showed higher lytic activity than LysPBC1 against non-native targets such as the *B. subtilis* group strains. The LysPBC1_EAD did not lyse bacteria other than *Bacilli,* indicating that the catalytic domain alone maintains the host specificity and the removal of the cell wall binding domain rarely affects the lytic spectrum of LysPBC1.

4. The CBDs from LysPBC2 and LysB4 showed broad binding spectrum towards the *B. cereus* group strains. On the other hand, CBDs from LysPBC1 and LysPBC4 bound to certain strains of the *B. cereus* group species, and their binding ranges are complementary to each other. Both PBC5_CBD and PBC10_CBD are found to be unidentified, novel cell wall binding domains of *B. cereus* phage endolysins.

5. LysPBC2 has a spore binding domain (PBC2_SBD) located mainly within its catalytic domain. PBC2_SBD specifically binds to *B. cereus* spores but not to vegetative forms of *B. cereus*. Spores with disrupted exosporium hair-like nap displayed much higher binding of the PBC2_SBD, suggesting that the exosporium nap layer may not be the binding target of the PBC2_SBD.

6. I described a simple method for identifying CBD from a sequenced bacterial genome employing homology search for phage lysin genes. A putative CBD (CPF369_CBD) was identified from a genome of *C. perfringens* type strain ATCC 13124 and its function was studied with the GFP-CPF369_CBD

fusion protein recombinantly expressed in *Escherichia coli*. Fluorescence microscopy showed the specific binding of the fusion protein to *C. perfringens* cells, which demonstrates the potential of this method for the identification of novel bioprobes for specific detection of pathogenic bacteria.

V-3. CBD-based engineering of novel detection agents

In this chapter, a CBD cocktail with different fluorescent makers was developed for the detection of multiple pathogens. In addition, I created dual CBD hybrid proteins by combinations of CBDs with complementary specificities to extend the binding range. Lastly, I demonstrated that CBD-coated magnetic nanoclusters (CBD-MNCs) allowed efficient capture and recovery of *B. cereus* or *C. perfringens* cells from suspensions. These comprehensive and multidisciplinary studies may pave the way for the development of efficient CBD-based detection tools.

1. It is highly desirable to develop a method that capable of simultaneous detection of multiple pathogens. I produced three CBD fusion proteins with different fluorescent proteins: EGFP-SA13_CBD for *S. aureus*, mCherry-PBC1_CBD for *B. cereus*, and EYFP-CPF369_CBD for *C. perfringens*. Confocal laser scanning micrographs revealed that the three different pathogens were clearly identified by its colors and the presence of non-target bacteria did not interfere with the target-specific binding property of each CBD. This result presents the potential of a CBD cocktail as tools for multiplex pathogenic bacterial

detection in naturally contaminated samples.

2. PBC1_CBD and PBC4_CBD are fused via flexible or helical linkers in both orientations. PBC4_CBD functionality is greatly influenced by its orientation, whereas PBC1_CBD seemed to be less affected by spatial location. The dual CBDs with a flexible linker formed inclusion bodies during purification. The best dual CBD hybrid 1H4_CBD showed combined binding range of the each CBD and superior binding activity to its parental CBDs. I expect the tailored hybrid 1H4_CBD could be used as an efficient detection agent for diverse environmental strains of *B. cereus*.

3. Separation and concentration of small numbers of target cells from food matrices are an essential part of microbial diagnostics. I presented novel strategies for affinity immobilization of CBD fusion protein to magnetic nanoclusters (MNCs). The resulting CBD-coated MNCs showed better cell capture performance than a commercial antibody-based approach. These CBD-based magnetic separation methods would be useful for pre-analytical sample processing steps to improve the detection of target

pathogens. In addition, the concept of affinity immobilization of CBDs onto MNCs could be incorporated to other rapid biosensing platforms and thus offers the great potential in developing CBD-based biosensors.

V-4. Suggestions for future study

Several studies can be suggested for future work. For example, optimizing conditions for CBD-coated MNCs to enhance the cell capture efficiency, stability, and specificity could be performed. Validation of cell capture capacity of the CBD-MNCs in real food samples could also be involved. Furthermore, integration of CBD-MNCs with other rapid detection method (e.g. quantitative PCR) could be another interesting study. Collaborations are already in place with Dr. Je-kyun Park at KAIST to apply CBD-conjugated gold nanoparticles in the paper-based analytical device for the detection of diverse pathogens and with Dr. Bong Hyun Chung at KRIBB to use CBD-modified surface plasmon resonance (SPR) chips to detect *B. cereus*.

Another planned experiment includes biophysical characterization of the CBDs. The apparent association and dissociation constants of CBDs or hybrid CBDs towards their cognate cell walls could be calculated from SPR. A similar study could be performed with PBC2_SBD and purified *B. cereus* spores. These kinetic data would provide a framework for further development of CBD- or SBD-based biosensors.

I will also focus on identifying the binding target of the PBC2_SBD by employing immunogold electron microscopy. Determining the location of PBC2_SBD within the *B. cereus* spores could be useful for elucidating the biological role of this unusual domain.

국문 초록

바실러스 세레우스(*Bacillus cereus*)는 식중독, 또는 비장관성 병을 일으키는 기회감염성 세균이다. 다제내성 바실러스 세레우스균의 등장 및 항생제 내성 문제로 인하여 박테리오파지 기반의 생물 제제(biocontrol agent)가 주목 받고 있다. 또한, 박테리오파지 그 자체뿐만 아니라 파지가 가지고 있는 수많은 신규 단백질 역시 의료, 분자, 생물공학적으로 큰 활용 가능성을 가지고 있다. 본 연구에서는 파지의 유전학적 다양성을 이해하고 파지 기반 방제용 생물 제제 및 검출용 제제를 개발하기 위하여 토양, 하수 등 환경 샘플로부터 바실러스 세레우스 균을 특이적으로 감염시키는 파지를 분리하고, 그들의 유전체를 분석하였다. 투과 전자 현미경을 통한 형태학적 분석 결과 4 종의 파지 (PBC1, PBC2, PBC4, PBC5)는

Siphoviridae family에 속하고, 2 종의 파지 (PBC6, PBC9)는 *Myoviridae* family에 속함을 알 수 있었다. 분리된 6 종의 파지는 대체적으로 바실러스 세레우스 그룹에 속한다고 알려진 종 내에서 제한된 범위의 숙주 특이성을 가지고 있었다. 유전체 분석 결과, *Siphoviridae*에 속하는 파지들은 상대적으로 다양한 크기의 게놈을 보유하고 있었으며, PBC1이 41.2 kb로 가장 작고, 그 뒤를 PBC5 (56.3 kb), PBC4 (80.6 kb), PBC2 (168.7 kb)가 이었다. *Myoviridae* 에 속하는 PBC6과 PBC9는 매우 유사한 유전체를 가지고 있었으며, 그 크기는 각각 157.1 kb와 157.2 kb 였다. Siphovirus인 PBC2는 바실러스 안트라시스 (*B. anthracis*) 파지인 Tsamsa와 유전체, 형태학적으로 유사함을 보였고, PBC4는 바실러스 세레우스 파지인 Basilisk와 전체 게놈 수준에서 높은 유사도를 보였다. 이에 반해 PBC1 파지와 PBC5 파지는 기존에 보고된 파지들과 유전체 수준에서 매우

낮은 유사도를 보이기 때문에 신규 바실러스 세레우스 파지로 보여진다. 특히 PBC1은 게놈 분석 결과, 분리된 파지 중 유일하게 항생제 저항성이나 독성 유전자를 지니고 있지 않은 용균성 파지(virulent phage)임이 밝혀졌다. 배양액과 끓인 밥 샘플에서의 바실러스 세레우스 균 성장 저해실험을 통해 PBC1의 강한 용균 능력을 확인하였다. 이러한 결과들은 비록 PBC1이 매우 좁은 숙주 범위를 갖지만, 다른 파지들이 죽이지 못하는 바실러스 세레우스 균주를 죽일 수 있다는 점과 더불어 바실러스 세레우스를 제어할 수 있는 파지 칵테일의 구성 성분으로 이용될 수 있음을 시사한다. 항균능력을 보이는 다양한 파지의 단백질 또한 유용한 생물 제제로 보고되고 있다. 그 중 파지의 엔도라이신(endolysin)은 파지가 숙주 내에서 복제되어 나오는 과정에서 숙주 세포벽을 깰 때 필요한 효소로서, 강한 용균 능력과 높은 특이성으로 인해 항균제로서의 가능

성이 많이 연구되고 있다. 또한 엔도라이신이 일반적으로 효소적 활성 도메인(enzymatic active domain, EAD)과 세포 벽 결합 도메인(cell wall binding domain, CBD)의 모듈 구조로 구성되어 있다는 점에서 독특한 기능을 갖는 다양한 도메인의 생물학적 응용 가능성 또한 제시되고 있다. 본 연구에서는 분리된 바실러스 세레우스 파지들로부터 나온 엔도라이신의 특성 분석 및 그들의 EAD, CBD, 포자 결합 도메인(spore binding domain, SBD)와 같은 기능적 도메인을 동정하였다. 높은 숙주 특이성을 보이는 파지와 달리 그들의 엔도라이신은 일반적으로 넓은 범위의 바실러스 속에 용균 범위를 보였다. PBC1 엔도라이신의 EAD만 발현 시, 바실러스 속 특이적인 용균 활성을 보였으며, CBD가 포함되어 있는 전체 길이 엔도라이신에 비해 바실러스 세레우스 그룹 종에는 약한 활성을, 반면 바실러스 서브틸리스 그룹 종에는 더 강한 활성을 보였다. 바실러스 세

레우스 파지의 엔도라이신에서 분리한 CBD는 바실러스 세레우스 그룹에 특이적으로 결합하는 특성을 보여주었기 때문에 바실러스 세레우스 검출을 위한 신규 프로브로서 활용 가능성을 있음을 암시하였다. PBC2 엔도라이신에서 분리한 SBD는 바실러스 세레우스 포자에만 특이적으로 결합하였고, 생장 세포 (vegetative cell)에는 결합하지 않았다. SBD가 포자외막 (Exosporium) nap 층이 파괴된 포자와 강한 결합을 하는 것으로 보아, 포자외막 nap 층은 SBD의 결합 타겟 부위가 아닌 것으로 추측된다. 파지 엔도라이신으로부터 CBD를 획득하는 과정은 시간이 많이 걸리고, 노동 집약적이다. 이 문제를 해결하기 위해, 본 연구에서는 세균 전체 게놈과 파지 엔도라이신 유전자와의 상동성 검색을 이용해, 보다 간단하게 CBD를 동정하는 방법을 제시하였다. 이 방법을 통해 클로스트리디움 퍼프린젠스 (*Clostridium perfringens*) 게놈으로부터 CBD를 동정하고, 이

CBD가 클로스트리디움 퍼프린젠스에 특이적으로 결합함을 확인하였다. 이 방법은 파지의 분리 및 게놈 시퀀싱이 필요 없고, 데이터베이스에 나와있는 세균 게놈만 이용하면 되므로, CBD를 동정하는 일반적인 접근 방법이 될 수 있을 것이라 생각된다. 본 연구에서는 다양한 세균을 검출하기 위해 타겟-특이적인 결합을 보이는 엔도라이신의 CBD를 engineering 하였다. 효과적인 CBD 기반의 검출 도구 개발을 위해 몇 가지 고려해야 할 사항이 있다. 첫째, 본 연구에서 발굴한 바실러스 세레우스, 클로스트리디움 퍼프린젠스 및 스타필로코커스 아우레우스 (*Staphylococcus aureus*)를 인식하는 CBD를 다양한 색깔을 가진 형광 단백질과 조합하여 CBD 칵테일을 제작하고, 이를 이용하여 3 가지 다른 종류의 세균을 동시에 검출할 수 있음을 확인하였다. 둘째, 많은 CBD가 타겟 세균 내에서도 특정 균주에만 붙기 때문에 다양한 환경 균주들을 검출하기에는 한계가

있었다. 본 연구에서는 CBD의 검출 범위를 넓히기 위해, 서로 상보적인 결합 범위를 갖는 두 가지 종류의 CBD를 조합한 듀얼 CBD 하이브리드를 제작하였다. 이렇게 해서 만들어진 1H4_CBD는 PBC1_CBD와 PBC4_CBD가 나선 링커 (helical linker)로 연결되어 있는 하이브리드로, 대부분의 바실러스 세레우스 균주와 결합할 수 있었으며, 모체 CBD보다 뛰어난 결합능을 보여주었다. 이러한 결과는 기존 CBD에 다른 결합 모듈을 적절한 링커와 함께 붙임으로써 추가적인 타겟에 결합할 수 있도록 조절하는 것이 가능함을 보여준다. 마지막으로 CBD가 고정되어 있는 자성 나노클러스터(CBD-MNCs)를 이용하여 상당 수의 생균이 30분 안에 현탁액으로부터 분리됨을 확인하였다. 또한, CBD를 이용한 자성분리가 기존 항체를 이용한 자성 분리 방법보다 우수한 성능을 보인 것은 본 연구가 CBD 기반 세균 검출 기술 개발에 이바지할 수 있음을 시사한다.

핵심어: 바실러스 세레우스, 박테리오파지, 엔도라이신, 생물 방제 (biocontrol), 세포벽 결합 도메인 (CBD), 검출

학번: 2012-30318